Final report for Phase I research sponsored by
NIAC – NASA Institute for Advanced Concepts

Spacecraft Formation-flying using Inter-vehicle Coulomb Forces

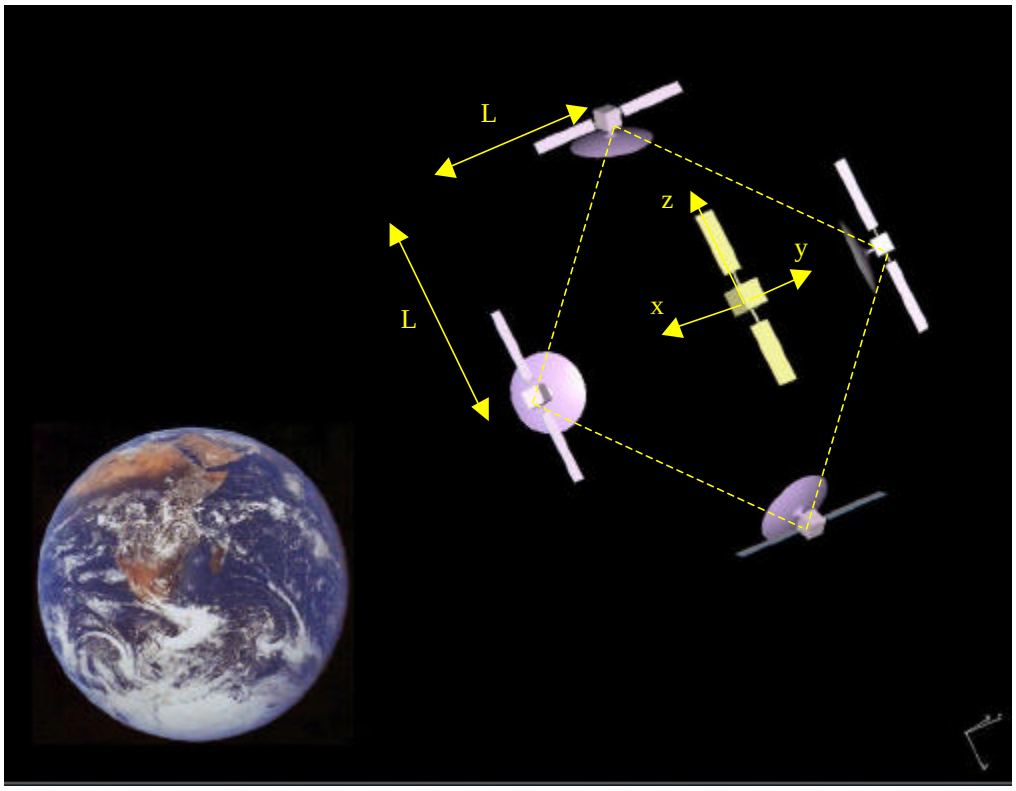

Lyon B. King
Gordon G. Parker
Satwik Deshmukh
Jer-Hong Chong

January 7, 2002

Michigan Technological University
Department of Mechanical Engineering-Engineering Mechanics
1400 Townsend Drive
Houghton, MI 49931

ABSTRACT

Swarms of microsatellites are envisioned as an attractive alternative to traditional large spacecraft. Such swarms, acting collectively as virtual satellites, benefit from the use of cluster orbits where the vehicles fly in coordinated formation. A class of missions that may benefit from formation flying is that of separated spacecraft interferometry for astronomical or Earth imaging. In such formations, vehicle spacing on the order of tens of meters is required. Constellations flying in close formation will need propulsion systems capable of producing micro-Newtons of thrust in a controllable manner. Candidate thruster technologies will emit caustic propellant exhaust that will contaminate neighboring vehicles.

The concept explored in this report involves controlling the potential of spacecraft in orbit by interacting with the ambient space plasma environment. It is shown that vehicle potentials on the order of a few kilovolts are sufficient to generate inter-spacecraft Coulomb forces of tens of micro- Newtons. The Coulomb control system can operate with a specific impulse as high as 10^{13} seconds and utilize a few hundred milliWatts of spacecraft power. Control forces can be adjusted in a timescale of milliseconds.

Representative formation geometries applicable to space-based interferometry are studied in the context of Coulomb control. Equilibrium solutions are found both in Earth orbit and interplanetary space for interacting Coulomb formations. Mission trade comparisons are performed between the Coulomb formations and those achievable with traditional electric propulsion thrusters. Significant propulsion system mass savings (up to 98%) are enabled by Coulomb control for all formations studied.

Table of Contents

1. Introduction

1.1. Formation Flying Background

Swarms of microsatellites are currently envisioned as an attractive alternative to traditional large spacecraft. Such swarms, acting collectively as virtual satellites, will benefit from the use of cluster orbits where the satellites fly in a close formation.[1] The formation concept, first explored in the 1980's to allow multiple geostationary satellites to share a common orbital slot,[2,3] has recently entered the era of application with many missions slated for flight in the near future. For example, EO-1 will formation fly with LandSat-7 to perform paired earth imagery, ST-3 will use precision formation flight to perform stellar optical interferometry, TechSat 21 will be launched in 2004 to perform sparse-aperture sensing with inter-vehicle spacing as close as 5 m, and the ION-F science mission will perform distributed ionospheric impedance measurements.[4,5] The promised payoff of formation-flying has recently inspired a large amount of research in an attempt to overcome the rich technical problems. A variety of papers can be found in the proceedings of the 1999 AAS/AIAA Space Flight Mechanics Meeting,[6,7,8] the 1998 Joint Air Force/MIT Workshop on Satellite Formation Flying and Micro-Propulsion,[9] a recent textbook on micropropulsion,[10] and numerous other sources.[11,12,13,14,15,16,17]

Relative positional control of multiple spacecraft is an enabling technology for missions seeking to exploit satellite formations. Of the many technologies that must be brought to maturity in order to realize routine formation flying, perhaps the most crucial is the spacecraft propulsion system. In fact, during his keynote address at the 1998 Joint Air Force/MIT Workshop on Satellite Formation Flying and Micro-Propulsion, Dr. David Miller of the Space Systems Laboratory at MIT delivered a "Top Ten List" of formation-flying technological obstacles. On this list, the two most important technologies were identified as (1) Micropropulsion; and (2) Payload contamination, arising from propellant exhausted from closely spaced satellites.[9]

Constellations of small satellites will require propulsion systems with micro- to milli-Newton thrust levels for deployment, orbit maintenance, disposal, and attitude control.[18,19] Formation-keeping thrusters must be capable of producing finely controlled, highly repeatable impulse bits. Although no suitable thruster has yet been proven in flight, recent research suggests that the best current technologies are micro-pulsed-plasma thrusters (micro PPT),[5] field-emission electric propulsion thrusters (FEEP),[20] and colloid thrusters.[21]

As identified in item (2) from Dr. Miller's technology list, current research-level thruster candidates pose significant contamination problems. In close proximity, the propellant emitted by such devices as micro-PPT's (vaporized Teflon), FEEP (ionized cesium), or colloid thrusters (liquid glycerol droplets doped with NaI) will impinge upon neighboring vehicles and damage payloads. To worsen the problem, orbital mechanics for many clusters of interest mandate continuous thruster firings pointed directly towards

other vehicles in the formation. The contamination problem will be amplified as the formation spacing is reduced.

1.2. Coulomb Control Concept

1.2.1. Objective of NIAC Project

All spacecraft propulsion systems flown to date operate according to the rocket principle: mass is ejected from a vehicle to affect momentum transfer and propulsive force. Varieties on this principle utilize chemical reactions to accelerate the mass as well as electromagnetic forces, however the thruster lifetime is fundamentally constrained by the amount of mass (propellant) available on board.

The goal of this proposal is to investigate the feasibility of achieving nearly propellantless control of satellites in a formation using Coulomb forces between vehicles. The proposed concept will rely on interaction with ambient space plasma and the active emission of electric charge from the vehicle to control spacecraft charging. Attractive and repulsive Coulomb forces between vehicles can be adjusted to maintain the relative cluster formation. This novel propulsive scheme may utilize a negligible amount consumables, enable high-precision close-formation flying superior to conventional thruster technology, eliminate thruster plume exhaust contamination of neighboring spacecraft, and provide a mechanism for configuring a formation into a "safe" collision-avoidance mode in the event of position uncertainty.

1.2.2. Existing Technology

Of the many technologies that must be brought to maturity in order to validate the satellite formation-flying concept, perhaps the most crucial is the propulsion system. Fine positioning and formation-keeping of low-mass vehicles in a swarm will require development of very low-thrust propulsion systems with finely controllable impulse bits. Even with the high-specific-impulse available from conventional electric propulsion (EP) thrusters, maintaining a formation by forcing individual satellites to occupy non-Keplerian orbit paths will require continuous thrusting over the lifetime of the mission. Over a five- to ten-year mission, such continuous thrust requirements will place heavy demands on thruster reliability and operational lifetime.

For widely spaced formations (inter-spacecraft separation on the order of 100 m or more) the fine-positioning requirements may be met with conventional EP thrusters. However, for very closely spaced swarms, current propulsive systems are not well suited to perform precision formation flying. For space interferometry, configurations are envisioned where the inter-satellite spacing is less than ten meters. In such a tight swarm, precision formation keeping will be extremely difficult. Existing thruster technologies that have been identified as the most promising tools for accomplishing such tight-formation flying include micro pulsed-plasma thrusters (micro PPT's), field-emission

electric propulsion (FEEP) thrusters, and colloid thrusters.[22] Although all of these thrusters are technologically immature, each device is capable, in principle, of generating controllable micro-Newton levels of thrust.

Propellant-emitting thrusters will pose a spacecraft integration/contamination problem for tight satellite formations. Each of the thruster technologies currently under development will exhaust damaging propellant. For many spacecraft operating in close proximity, the microthruster propellant (vaporized Teflon for PPT's, liquid cesium for FEEP, and NaI-doped liquid glycerine for colloid) has a high likelihood of contaminating sensitive spacecraft surfaces, optics, and other instruments on neighboring craft. Such contamination would be incompatible with high-resolution imaging systems. In addition to material contamination problems, the potential exists for exhaust plume impingement forces to be transmitted from one spacecraft in the constellation to another, greatly complicating the fine position control.

1.2.3. Overview of Coulomb Concept

The concept proposed in this document uses the principle of Coulomb attraction/repulsion between charged bodies to control the spacing between nodes of a microsatellite cluster. The Coulomb control principle is most easily conveyed by examining the interaction between two neighboring bodies capable of transferring electric charge. Much more detailed analysis of the physical processes will be presented in later chapters.

Consider, for instance, two vehicles separated a distance *d* in space. Initially, both spacecraft are electrically neutral, i.e., the amount of negative charge (electrons) is equal to the amount of positive charge producing a net vehicle charge of zero and no interaction between the craft. Now, allow one craft to change its charge state through the emission of electrons. This is a trivial process utilizing an electron-gun or similar cathode device. If the electron beam is used to transfer an amount of negative charge, q_{SC}, from spacecraft 1 (SC1) to spacecraft 2 (SC2), the net negative charge of SC2 will equal the net postive charge remaining on SC1, producing an attractive force between the spacecraft given by

Eqn. 1-1
$$F_0 = \frac{1}{4\pi\varepsilon_0}\frac{q_{SC}^2}{d^2}.$$

The charge required to produce a 10 μN attractive force at a spacecraft separation of d = 10 m is $q_{SC} = 3.3\times10^{-7}$ C. Thus, using a 1-mA electron beam current, this charge can be transferred in only 330 μsec.

For discussion purposes, consider 1-m spherical spacecraft (radius of 0.5 m). The potential of the charged-spacecraft surface can be evaluated from Gauss' law as:

Eqn. 1-2

$$V_{SC} = \frac{1}{4\pi\varepsilon_0}\frac{q_{SC}}{r_{SC}},$$

where V_{SC} is the spacecraft potential in volts and r_{SC} is the spacecraft radius. For a charge of $q_{SC} = 3.3\text{x}10^{-7}$ C and radius of r = 0.5 m, the surface of SC1 will assume a positive potential of 6 kV, while V_{SC2} = -6 kV. Thus, a 12-kV electron beam must be used in order to allow the charge from SC1 to "climb the hill" and reach the surface of SC2. The minimum power required to generate a 10 μN attractive force in 330 μsec between the spacecraft separated a distance *d* = 10 m is then only 12 Watts. This power can be reduced if longer charging time is acceptable.

It is perhaps more intuitive to discuss inter-spacecraft Coulomb forces in terms of the spacecraft potential in volts, V_{SC}. By combining the above equations, the Coulomb force between two spacecraft can be written as

Eqn. 1-3

$$F_0 = 4\pi\varepsilon_0 \frac{r_{SC1} r_{SC2} V_{SC1} V_{SC2}}{d^2}.$$

Spacecraft charging has historically been associated with negative impacts on satellite payloads. Arcs and other breakdown phenomena arising from such differential charging can wreak havoc on sensitive electronics. Differential charging results when some regions of a spacecraft assume electric potentials drastically different from other regions of the same vehicle. The induced intra-vehicle electric fields can cause spontaneous interruption of payload functions. In this proposal, *absolute* spacecraft charging is proposed as a formation controlling method. If adjusted uniformly over a vehicle, the spacecraft absolute potential with-respect-to space, V_{SC}, can be driven to large values (such as many kilo-volts) with no impact to spacecraft functions and no risk of arc or spontaneous failure.

1.2.4. Supporting Flight Heritage

A wealth of pertinent data and experience is available from the results of the SCATHA flight experiment. The SCATHA satellite was launched in January, 1979 with the goal of measuring the build-up and breakdown of charge on various spacecraft components and to characterize the natural environment at GEO altitudes.[23]

The satellite potential with respect to space plasma potential was monitored on the SCATHA craft. During passive operation of the satellite, the spacecraft potential was seen to vary from near ground to many kilovolts negative. This is a common occurrence. An isolated passive body immersed in plasma will accrue a net negative charge due to the higher mobility of electrons as compared to heavy ions. For hot plasma such as that found at MEO-GEO, this negative charge is substantial. One goal of the SCATHA

mission was to test the validity of actively controlling the spacecraft potential by emitting charge through an electron beam. To this end, an electron gun was used to transfer charge from SCATHA to the space plasma at various current and voltage levels up to 13 mA and 3 kV.

Due to the plasma environment, spacecraft routinely charge to negative voltages. However, a very important result, as reported by Gussenhoven, et al., was that, "*the electron beam can achieve large, steady-state changes in the vehicle potential and the returning ambient plasma*."[24] In fact, Gussenhoven found that when a 3 kV electron beam was operated, "*the satellite became positively charged to…a value approaching beam energy for 0.10 mA*" emission current. Similarly, Cohen, et al. report that "*spacecraft frame and surfaces on the spacecraft went positive with respect to points 50 meters from the satellite when the gun was operated. Depending upon ejected electron currents and energies, spacecraft frame-to-ambient-plasma potential differences between several volts and 3 kV were generated.*"[25]

For rough estimation, we can approximate the SCATHA spacecraft as a sphere with a diameter of 1.7 m.[26] If an identical SCATHA spacecraft had been in orbit simultaneously, the satellite potential control demonstrated on this 1979 mission would have been sufficient to actively generate attractive and repulsive forces between the vehicles with magnitudes up to almost 10 μN over 10 meters, at a power expense of only 3 Watts. In addition to the SCATHA data, during a separate flight-experiment the ATS-6 spacecraft demonstrated charging as high as 19 kV.[27,28] Assuming a spacecraft diameter on the order of 1 meter, findings hint at the possibility to generate and control forces of hundreds of μN.

1.3. Separated Spacecraft Interferometry

1.3.1. Space-based Imaging Problem

It has long been known that increased astronomical imaging capability could be realized if the optics for the imaging system were placed outside of the earth's atmosphere. Missions such as the current Hubble Space Telescope (HST) and planned Next Generation Space Telescope (NGST) exemplify this principle. The increased clarity offered by space-based astronomy is somewhat offset, however, by practical limits placed on angular resolution of the image. The angular resolution (resolving power) of an optic is related to the physical size of the collector by

Eqn. 1-4
$$q = \frac{l}{2d},$$

where θ is the minimum resolvable angular feature, λ is the wavelength to be imaged, and d is the physical size of the collecting aperture. Thus, to obtain fine angular resolution (small θ) requires a large aperture. Herein lies the problem for space-based

imaging systems: the physical size of the aperture is limited by launch vehicle fairing dimensions. The largest launch fairing currently available is that of the the Ariane V, which is approximately 5 meters in diameter. For space-based imaging in the optical wavelengths (400-700 nm) using a monolithic aperture, missions are limited to angular resolution no better than 4×10^{-8} radians (about 8 milli-arcseconds).

The ability to resolve an astronomical object is directly proportional to the size of the object and inversely proportional to the distance from the observer. At the Spaceborne Interferometry Conference, Ridgeway presented a graphical depiction of the apparent size of "interesting" astronomical objects.[29] Ridgeway's schematic is reproduced in Figure 1-1. In this figure, lines of constant apparent angular size (resolution) are shown. It is significant that most of the science topics begin with angular scales of about 1 milli-arcsecond, approximately a factor of 1000 smaller than the typical limit of optical imaging from the ground.

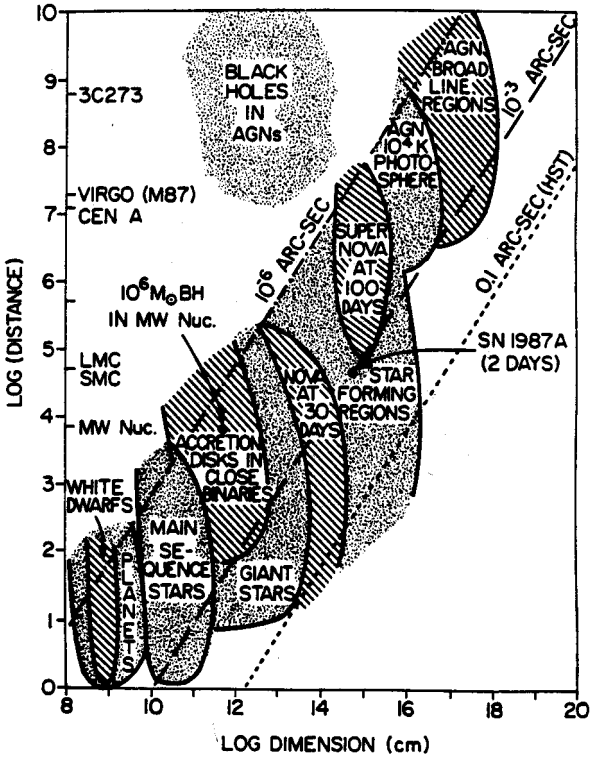

Figure 1-1. Depiction of apparent size of astronomical target objects. The distance to the objects is listed on the vertical axis, with the transverse dimension of the object on the horizontal axis. Diagonal lines denote the angular extent of the target and, thus, the resolution required for imaging. The 0.1 arc-sec line denotes Hubble Space Telescope (HST) capabilities. It is significant that most science topics begin with resolutions better than 1 milli-arcsecond.

1.3.2. Interferometry Fundamentals

There are two options for circumventing the aperture resolution restrictions created by launch vehicles. First, a deployable structure can be designed that can fold to stow into the size-limited fairing. The structure can then be deployed on-orbit to a final size greater than the fairing diameter. Although deployable structures avoid a direct physical size limitation, the stowed structure must still fit within the available launch volume and is thus constrained at some larger, but finite, dimension related to the launch vehicle size. The second method for overcoming vehicle size restrictions is separated spacecraft interferometry.

Separated spacecraft interferometry is a direct extension of an imaging technique that has been employed with ground-based systems for years. In ground-based interferometry, physically separated apertures collect incident radiation from the target at two or more discrete locations and direct this collected radiation to a common combiner station. Using principles of Fourier optics, the radiation can be interfered to produce image data. The power of interferometry arises from the increased angular resolution: the resolving power of the combined optical system is a function of the separation, or baseline, between individual collectors and not on the collector sizes themselves. Quantitatively, the resolving power is still given by Eqn. 1-4, however d is now the distance *between* the collectors, rather than the *size* of a given optic. In principle, the baseline, d, and thus the resolving power can be increased without limit. Detailed accounts of interferometry theory can be found in many textbooks[30] and descriptions of space-based interferometry can be found in previous research works.[14,15,16] A basic summary will be presented here.

Qualitatively, the information in an image can be represented in two different formats. The first mode, which is most intuitively familiar, is that of a spatial intensity map. For every location (x, y coordinate) in a spatial plane some value of radiant intensity is given. Mapping the intensity values produces an image in the same fashion that the human eye/retina records optical information. The same information contained in the intensity map can be presented in a second format relating to spatial frequencies.

The spatial frequency representation of an image can most easily be understood in the context of a checker-board tile floor. A spatial intensity map summarizes the floor image by assigning an amplitude to every x, y point on the floor corresponding to, say, the brightness of the floor. One can also recognize obvious patterns in the floor that repeat themselves on a regular spatial period. If the tiles in the floor are square, then the repeating pattern in the x direction has the same period, or spatial frequency, as the pattern in the y direction; if they are rectangular the x and y patterns will have different frequencies. Specification of the spatial frequencies then yields some of the image information. For each spatial frequency in the floor, one must also specify an amplitude to fully describe all of the image information. For the square-wave pattern of the checker-board floor, a large amplitude may correspond to black and white tiles, while a smaller amplitude may represent gray and white tiles.

Fourier mathematics extends the simple qualitative tile floor analogy to images of arbitrary complexity. Any function of intensity in the physical plane (x, y space) can be represented by an infinite series of Fourier terms. Each term of the Fourier series has a spatial frequency (u, v point for x and y spatial frequencies respectively) and an amplitude coefficient. Thus, if one knows the amplitude coefficient for every spatial frequency (u, v point), the Fourier representation of the image information can be transformed to produce the more familiar spatial intensity map of the target.

In interferometry, the u-v points in the Fourier plane are obtained by separated collector points in the x-y physical plane. When light of wavelength λ collected by two spacecraft at locations (x_1, y_1) and (x_2, y_2) is combined (interfered), the resulting interference pattern yields a single value. The single value is the complex amplitude of the Fourier term with spatial frequencies (u, v) denoted by

Eqn. 1-5

$$u = \frac{\pm (x_2 - x_1)}{l}$$
$$v = \frac{\pm (y_2 - y_1)}{l} \quad .$$

Thus, each unique spacecraft separation vector, or baseline, yields one term of the Fourier representation of the image. To reconstruct the image one must have information from many (theoretically an infinite number) of unique spacecraft baselines. For multiple spacecraft, the u-v coverage is represented by the correlation function of the physical coverage. For N spacecraft, each of the spacecraft has N-1 different position vectors to other vehicles in the array. Thus the total number of u-v points from an array of N spacecraft is N(N-1) plus a zero baseline point.

Judicious use of spacecraft collector assets mandates intelligent placement of the vehicles in physical space. For instance, redundant baselines (separation vectors) between vehicles in a formation produce redundant Fourier information and represent a "waste" of assets. Ideally, each of the N(N-1) u-v points should be unique. Numerous collector formation possibilities exist based upon optimization of various parameters. Golay performed a study of collector placement based upon optimization of the u-v compactness of the overall formation.[31] The resulting Golay formations are shown in Figure 1-2 for N=3, 6, 9, and 12 spacecraft. Similarly, Cornwell derived formations which were designed to optimize the uniformity of coverage in the u-v plane.[32] Representative configurations for N=3-12 spacecraft Cornwell configurations are shown in Figure 1-3.

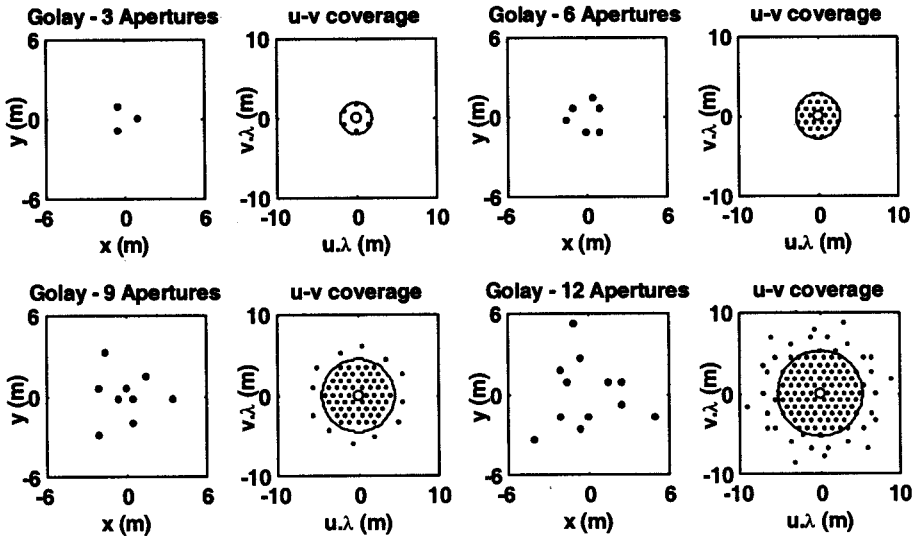

Figure 1-2. Golay interferometric formations based upon optimizing the compactness of the group in u-v space. The aperture locations in x-y space and the corresponding baselines in u-v space are plotted in adjacent diagrams. (Figure reproduced from Ref. 15)

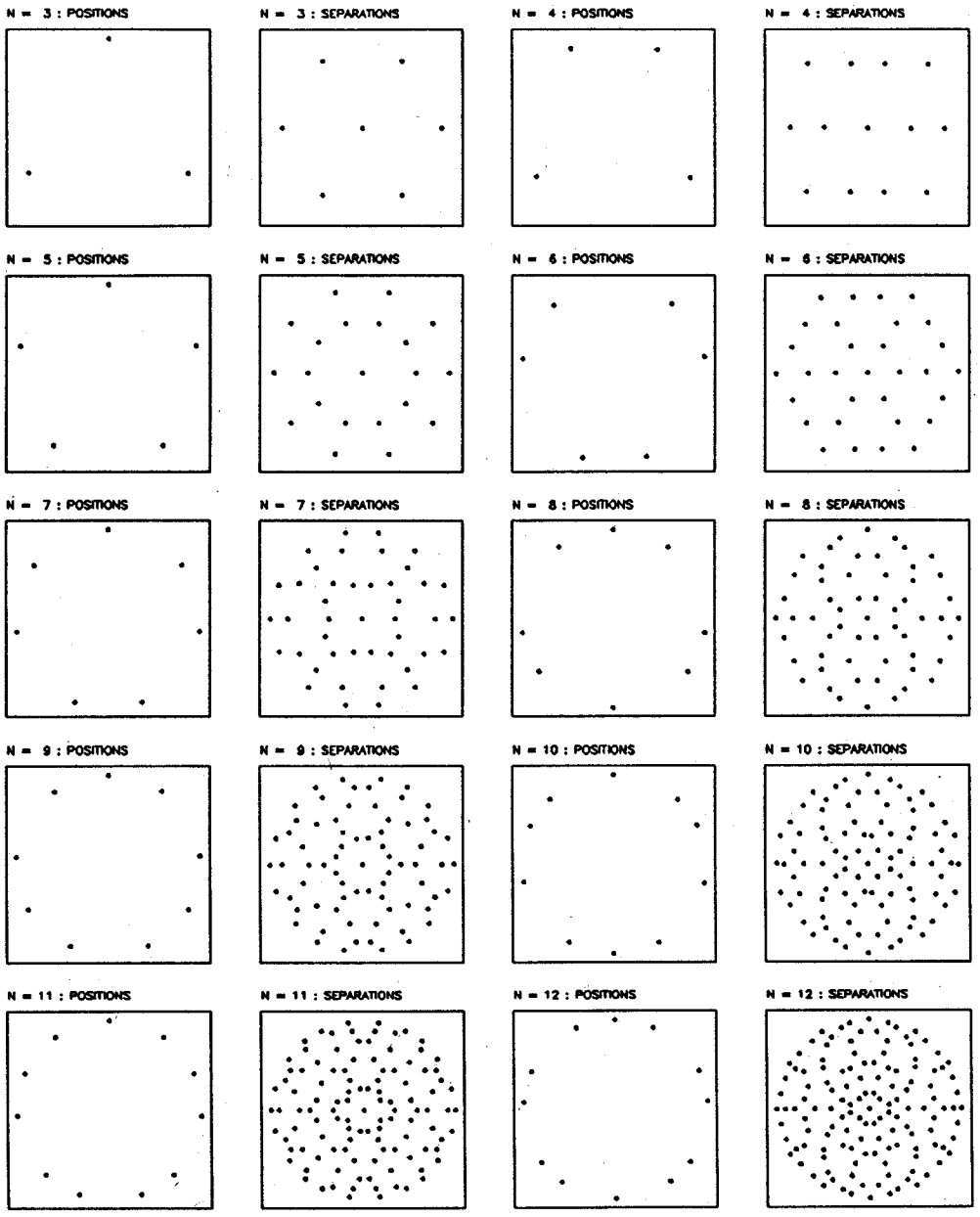

Figure 1-3. Cornwell optimized arrays for uniform u-v coverage for N=3-12. The positions of the apertures (spacecraft) are shown in x-y space, while the unique baselines (separations) show up as points in u-v space. Positions and corresponding separations are plotted in adjacent diagrams.

1.3.3. Practical Aspects of Space Interferometry

The method by which the u-v points are mapped out depends upon the nature of the target object. For static targets whose features are relatively constant (such as astronomical objects), the u-v points can be mapped out sequentially with as few as two collector spacecraft. The vehicles simply move to the specified x-y positions, record a data point, and move on to other locations. The image is then processed after a predefined number of u-v points have been recorded. Such is the method employed by missions such as Deep Space 3 and Terrestrial Planet Finder. For rapidly changing targets, such as those on the surface of the Earth, the image features must be recorded in a "snapshot" mode where all of the u-v points are obtained simultaneously. Such configurations are said to produce full, instantaneous u-v coverage. For such snapshots the number of independent collector spacecraft must be equal to the number of u-v points required to produce the image.

Inteferometric imaging in the optical regime poses a constraint on an imaging array. For lower frequencies, such as those in the radio spectrum for radar imaging, the incoming wavefront from each collector can be recorded and archived, with the actual interferometry between separate collectors performed later through post-processing. Optical signals, however, have frequencies too high to permit recording of the wavefront for post-processing. Instead, the incoming signals from two collectors must be interfered in real time at the combiner. In order to permit interference between the same wavefront from each collector, the light path length from each collector to the combiner must be equal to within a fraction of the radiation wavelength. It is clear from an examination of Figure 1-2 and Figure 1-3 that Cornwell arrays, with all of the collector apertures lying on the circumference of a circle, are ideally suited to a central combiner for optical path symmetry, while Golay arrays are not amenable to a single combiner vehicle.

For formation-flying spacecraft performing visible imagery, the requirement of equal optical path lengths seems to present an unobtainable formation tolerance between spacecraft of a few nanometers. In practice, however, this constraint is relaxed through the use of on-board delay lines for fine control. In such a delay-line configuration, the individual spacecraft need only keep formation tolerance errors within a few centimeters, while actively controlled movable optics compensate for the coarse position errors down to the interferometry requirement. A schematic is shown in Figure 1-4. By repositioning the optics on-board one or both of the vehicles, the light from one collector can be made to traverse the same distance as that from another collector.

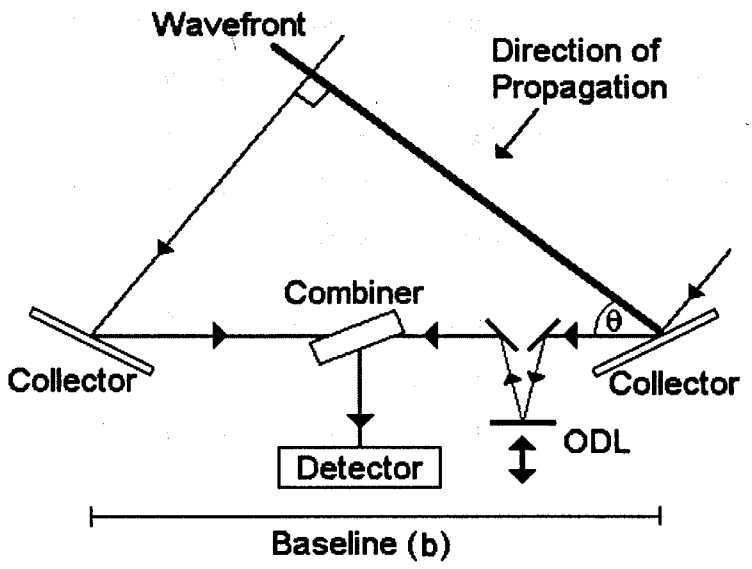

Figure 1-4. Illustration of optical delay line (ODL) for fine adjustment of science light path from collector to combiner in interferometry.

The need for full, instantaneous u-v coverage begs the question of mathematical completeness. To exactly invert the Fourier image information requires an infinite number of amplitude coefficients and, thus, an infinite number of collector locations. This is evidenced in the amount of white space representing missing u-v information in the plots of Figure 1-2 and Figure 1-3. One method for solving the completeness problem lies in post-processing techniques for image reconstruction. Another method relies on intelligent placement of finite-sized collector optics.

To extend the qualitative description of interferometry to finite-sized collectors, one can envision a single collector of diameter *d* as an assembly of sub-collector elements. Image information for u-v points represented by distances between sub-collector elements is then obtained from a single optic as shown in Figure 1-5. In fact, a single optic of diameter *d* yields an infinite number of u-v points for all baselines less than or equal to *d*. All baselines (u-v points) greater than *d* must then come from sub-elements on separated spacecraft. In terms of full, instantaneous u-v coverage, this implies that spacecraft must be separated by a distance comparable to their individual size, *d*, to avoid omission of u-v points. Thus, snapshot-style imaging requires very close formation flying.

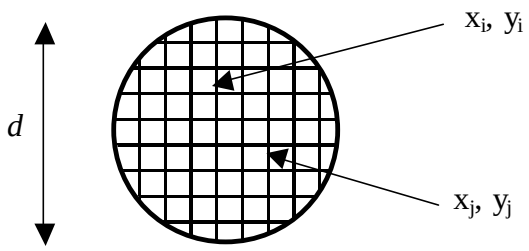

Figure 1-5. Conceptual image of single collector optic as array of sub-collectors. The elements i and j will yield interferometric information for the u-v point representing the baseline between the elements.

1.4. Formation Geometries Considered in Study

Although the Coulomb control concept explored in this report could conceptually be used for any mission requiring close formation flying, the strengths of the concept strongly coincide with the needs for interferometric imaging as outlined in the previous section. As such, the formation geometries studied in the reported work were slanted towards interferometry applications.

Based on discussions in Section 1.3.3, visible interferometry involving full, instantaneous u-v coverage can be said to have two overarching requirements: 1) the vehicles must fly in close formation, with spacing on the order of the vehicle dimension, and 2) the optical path length between any collector and the combiner must be equal. Based on these rough guidelines, four fundamental formation geometries of increasing sophistication were studied in the context of Coulomb control. The geometries will be summarized here, with more detail provided in Section 3.

1.4.1. Earth Orbiting 3-Satellite Formation

The first set of formations studied included only three spacecraft. Conceptually, the formation can be thought of as two collectors and a single combiner. The vehicles were constrained to a straight line, with the combiner located midway between the collectors, flying in formation in Earth orbit. Three variations on this formation, depending upon the relation between the formation axis and the orbital velocity vector, were studied to investigate the fundamental nature of Coulomb control on a simplified system. Schematics of the various three-spacecraft formations can be found in Section 3.

1.4.2. Earth Orbiting 5-Satellite Formation

In an incremental increase in the complexity of the formation, a geometry of four collector vehicles surrounding a single combiner satellite was considered within Earth orbit. A diagram of this formation is shown in Figure X. The 5-satellite formation maintained geometrical simplicity, while still retaining the two overarching constraints for full, instantaneous u-v coverage. The orientation of the formation was chosen to loosely represent a visible Earth observing array operating from geosynchronous orbit.

1.4.3. Earth Orbiting 6-Satellite Formation

The first step towards analyzing a sophisticated, yet practical, interferometry configuration was performed by analyzing the dynamics of a 6-Satellite formation. The geometry of the formation was chosen to represent the optimized five-aperture (pentagonal) Cornwell array of Figure 1-3, with a central combiner included in a free orbit. The entire formation was analyzed in an Earth orbital environment, representative of either a visible Earth imager or an astronomical platform.

1.4.4. Rotating 5-Spacecraft Formation

The final formation geometry analyzed was chosen in order to analyze the suitability of Coulomb control for the Terrestrial Planet Finder (TPF) mission under consideration by NASA. For the TPF mission, an array of four collectors and a single combiner are planned. The entire five-vehicle formation is constrained to a straight line, rotating rigidly about the center vehicle. Rather than operating within Earth orbit, the TPF mission has been designed to occupy one of the Earth-Sun Lagrange points, thus the formation local dynamics can ignore gravity. Design variations on the formation have previously been investigated for either structurally connected vehicles via a central truss, or separated spacecraft using electric propulsion thrusters to maintain uniform circular motion. In this study, we will add to the comparison by considering a Coulomb control system for formation keeping.

---

[1] Pollard, J.E., Chao, C.C., and Janson, S.W., "Populating and maintaining cluster constellations in low-earth orbit," AIAA-99-2878, AIAA Meeting Papers on Disk Vol. 4, No. 3, Proc. Of 35th AIAA/ASME/SAE/ASEE Joint Propulsion Conference, June 20-24, 1999, Los Angeles, CA.

[2] Walker, J.G., "The geometry of cluster orbits," J. Brit. Interplan. Soc., Vol. 35, 1982, p. 345.

[3] Murdoch, J. and Pocha, J.J., "The orbit dynamics of satellite clusters," Paper IAF-82-54, 33rd International Astronautical Congress, Sept. 27-Oct. 2, 1982, Paris, France.

[4] Micci, M.M. and Ketsdever, A.D., Micropropulsion for Small Spacecraft, Progress in Astronautics and Aeronautics Vol. 187, AIAA Press, Reston VA, 2000, pp. 3-22.

[5] Hoskins, W.A., Wilson, M.J., Willey, M.J., Meckel, N.J., Campell, M., and Chung, S., "PPT development efforts at Primex Aerospace Company," Paper AIAA-99-2291, AIAA Meeting Papers on Disk Vol. 4, No. 3, Proc. Of 35th AIAA/ASME/SAE/ASEE Joint Propulsion Conference, June 20-24, 1999, Los Angeles, CA.

[6] Chao, C.C., Pollard, J.E., and Janson, S.W., "Dynamics and control of cluster orbits for distributed space missions," Paper AAS-99-126, Space Flight Mechanics Meeting, Feb. 7-10 1999, Breckenridge, CO.

[7] Kong, E.M.C., Miller, D.W., and Sedwick, R.J., "Exploiting orbital dynamics for aperture synthesis using distributed satellite systems: Applications to a visible Earth imager system," Paper AAS-99-122, Space Flight Mechanics Meeting, Feb. 7-10 1999, Breckenridge, CO.

[8] Sedwick, R., Miller, D., and Kong, E., "Mitigation of differential perturbations in clusters of formation flying satellites," Paper AAS-99-124, Space Flight Mechanics Meeting, Feb. 7-10 1999, Breckenridge, CO.

[9] Miller, D.W. and Spores, R.A., "Proceedings of the Formation Flying and Micropropulsion Workshop," unpublished, Oct. 20-21 1998, available from Dr. Ronald Spores, Air Force Research Laboratory, Edwards AFB, CA.

[10] Micci, M.M. and Ketsdever, A.D., Micropropulsion for Small Spacecraft, Progress in Astronautics and Aeronautics, Vol. 187, AIAA Press, Reston, VA, 2000.

[11] Corazzini, T., Robertson, A., Adams, J.C., Hassibi, A., and How, J.P., "GPS sensing for spacecraft formation flying," Proceedings of the 10th International Technical Meeting, ION/GPS, Sept. 16-19 1997, Kansas City, MO.

[12] Vassar, R.H. and Sherwood, R.B., "Formationkeeping for a pair of satellites in a circular orbit," Journal of Guidance, Control, and Dynamics, Vol. 8, No. 2, 1985.

[13] Leonard, C.L., "Fuel penalty of using ballistic coefficient control for satellite formationkeeping," AAS 13th Annual Guidance and Control Conference, Keystone, CO, Feb. 1990.

[14] Jilla, Cyrus D., Separated Spacecraft Interferometry – System Architecture Design and Optimization, Master's Thesis, Dept. of Aeronautics and Astronautics, Massachusetts Institute of Technology, Feb. 1999.

[15] Kong, Edmund M., Optimal Trajectories and Orbit Design for Separated Spacecraft Interferometry, Master's Thesis, Dept. of Aeronautics and Astronautics, Massachusetts Institute of Technology, Nov. 1998.

[16] Yashko, Gregory, Ion Micro-Propulsion and Cost Modelling for Satellite Clusters, Master's Thesis, Dept. of Aeronautics and Astronautics, Massachusetts Institute of Technology, June 1998.

[17] Hacker, Troy L., Performance of a Space-based GMTI Radar System using Separated Spacecraft Interferometry, Master's Thesis, Dept. of Aeronautics and Astronautics, Massachusetts Institute of Technology, May 2000.

[18] Janson, S.W., Helvajian, H., Hansen, W.W., and Lodmell, J., "Microthrusters for nanosatellites," 2nd International Conference on Integraed Micro Nanotechnology for Space Applications (MNT99), Apr. 11-14 1999, Pasadena, CA.

[19] Janson, S.W., Helvajian, H., Hansen, W.W., and Lodmell, J., "Batch-fabricated CW microthrusters for kilogram-class spacecraft," Paper AIAA-99-2722, AIAA Meeting Papers on Disk Vol. 4, No. 3, Proc. Of 35th AIAA/ASME/SAE/ASEE Joint Propulsion Conference, June 20-24, 1999, Los Angeles, CA.

[20] Tajmar, M., Mitterauer, J., and Wang, J., "Field-emission-electric-propulsion (FEEP) plasma modeling: 3D full particle simulations," Paper AIAA-99-2298, AIAA Meeting Papers on Disk Vol. 4, No. 3, Proc. Of 35th AIAA/ASME/SAE/ASEE Joint Propulsion Conference, June 20-24, 1999, Los Angeles, CA.

[21] Martinez-Sanchez, M. and Pollard, J.E., "Spacecraft electric propulsion – An overview," Journal of Propulsion and Power, Vol. 14, No. 5, Sept-Oct 1998, pp. 688-699.

[22] Martinez-Sanchez, M., and Pollard, J.E., "Spacecraft Electric Propulsion – An Overview," Journal of Propulsion and Power, Vol. 14, No. 5, Sept.-Oct. 1998, pp. 688-699.

[23] Osgood, R.N., "Operational status of the space test program P78-2 spacecraft and payloads," reported in Proceedings of 3rd Spacecraft Charging Technology Conference, Nov. 12-14, 1980, NASA Conference Publication 2182, pp. 365-369.

[24] Gussenhoven, M.S., Cohen, H.A., Hardy, D.A., Burke, W.J., and Chesley, A., "Analysis of ambient and beam particle characteristics during the ejection of an electron beam from a satellite in near-geosynchronous orbit on March 30, 1979," reported in Proc. of 3rd Spacecraft Charging Technology Conference, No. 12-14, 1980, NASA Conference Publication 2182, pp. 642-664.

[25] Cohen, H.A., Adamo, R.C., Aggson, T., Chesley, A.L., Clark, D.M., Damron, S.A., Delorey, D.E., Fennell, J.F., Gussenhoven, M.S., Hanser, F.A., Hall, D., Hardy, D.A., Huber, W.B., Katz, I., Koons, H.C., Lau, S.T., Ledley, B., Mizera, P.F., Mullen, E.G., Nanevicz, J.E., Olsen, R.C., Rubin, A.G., Schnuelle, G.W., Saflekos, N.A., Tautz, M.F., and Whipple, E.C., "P78-2 Satellite and payload responses to electron beam operations on March 30, 1979," reported in Proc. of 3rd Spacecraft Charging Technology Conference, Nov. 12-14, 1980, NASA Conference Publication 2182, pp. 509-559.

[26] Osgood, R.N., "Operational status of the space test program P78-2 spacecraft and payloads," reported in Proc. of 3rd Spacecraft Charging Technology Conference, Nov. 12-14, 1980, NASA conference Publication 2182, pp. 412-432.

[27] Whipple, E.C., and Olsen, R.C., "Importance of differential charging for controlling both natural and induced vehicle potentials on ATS-5 and ATS-6," reported in Proc. of 3rd Spacecraft Charging Technology Conference, Nov. 12-14, 1980, NASA Conference Publication 2182, p. 887.

[28] Deininger, W.D., Aston, G., and Pless, L.C., "Hollow-cathode plasma source for active spacecraft charge control," Review of Scientific Instruments, Vol. 58, No. 6, June 1987, pp. 1053-1062.

[29] Ridgeway, S.T., "The scientific support for a space interferometry mission," SPIE Vol. 1947 Spaceborne Interferometry, 1993, pp. 2-11.

[30] See, for instance, Hecht, E., Optics, Addison-Wesley, 1998.

[31] Golay, M., "Point arrays having compact non-redundant autocorrelations, Journal of Optical Society of America, Vol. 61, pg. 272, 1971.

[32] Cornwell, T.J., "A Novel Principle for Optimization of the Instantaneous Fourier Plane Coverage of Correlation Arrays," IEEE Trans. On Antennas and Propagation, Vol. 36, No. 8, pp. 1165-1167.

2. Spacecraft Plasma Interactions

This chapter addresses the plasma conditions in low Earth orbit (LEO), Geosynchronous Earth orbit (GEO), and Interplanetary space. A spacecraft immersed in space plasma develops an absolute charge relative to this plasma. There also can be differential charging between various parts of the spacecraft. Both of these are compared here. The spacecraft and ambient plasma are represented by an equivalent electrical circuit to study the transient response of the system.

2.1. Plasma Environment

Near the Earth in LEO the cold, dense plasma is near equilibrium. Farther away from Earth its density drops significantly and mean energy increases out to GEO. Eventually it transmits into solar wind plasma outside the magnetosphere. Hastings has described these plasma environments in detail.[33] For convenience sake, we will summarize the plasma environment from LEO to interplanetary orbit in this section.

2.1.1. Low Earth Orbit

The Ionosphere is a transition region from a relatively un-ionized atmosphere to a fully ionized region called plasmasphere. It is divided into layers like F-Layer between 150 and 1000 km, E-Layer between 100 and 150 km, and D-layer between 60 and 100 km. Ionosphere has electron densities of 10^{10} m^{-3} to 10^{-11} m^{-3} at an altitude of 1000 km and then drops to about 10^{9} at its outer boundary called plasmapause. Plasmapause is characterized by a rapid drop in electron density to 10^{5} m^{-3} to 10^{6} m^{-3}. Plasma density profiles in LEO are shown in Figure 2-1 and Figure 2-2.

The ion densities reach 10^{12} m^{-3} at the peak in the F-region at about 300 km on the sunlit side. At night the peak ion density falls below 10^{11} m^{-3} and the composition changes from O^{+} to H^{+}. Temperatures follow roughly that of the neutral atmosphere, increasing exponentially from a few hundred Kelvin at 50-60 km to 2000 - 3000 K above 500 km.(i.e. a few tenths of an eV). The electron temperature tends to be a factor of two greater than that of the neutral, with the ion temperature falling in between.

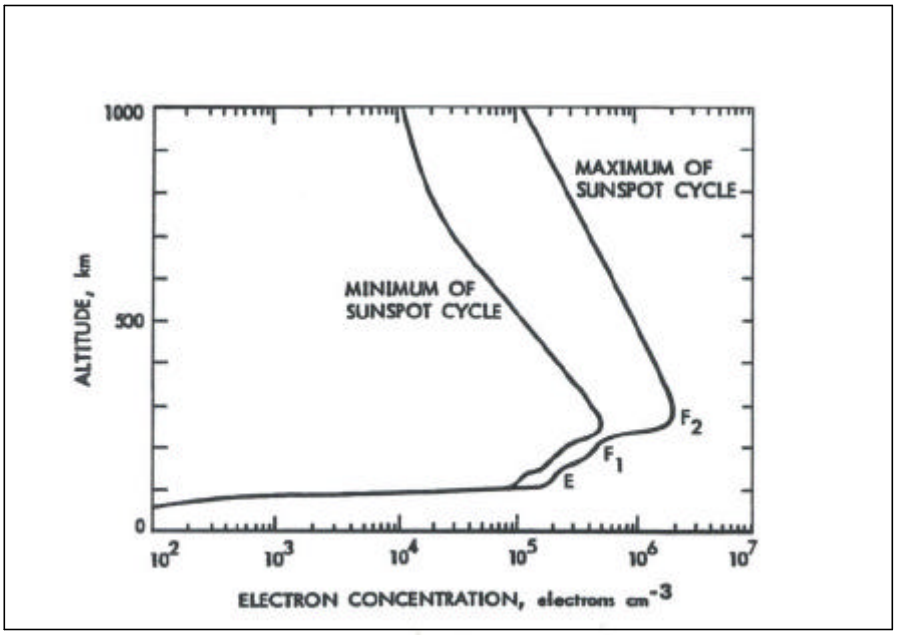

Figure 2-1. Plot of Altitude (km) Vs Electron Density (cm^{-3}) for The Ionosphere (LEO)[33]

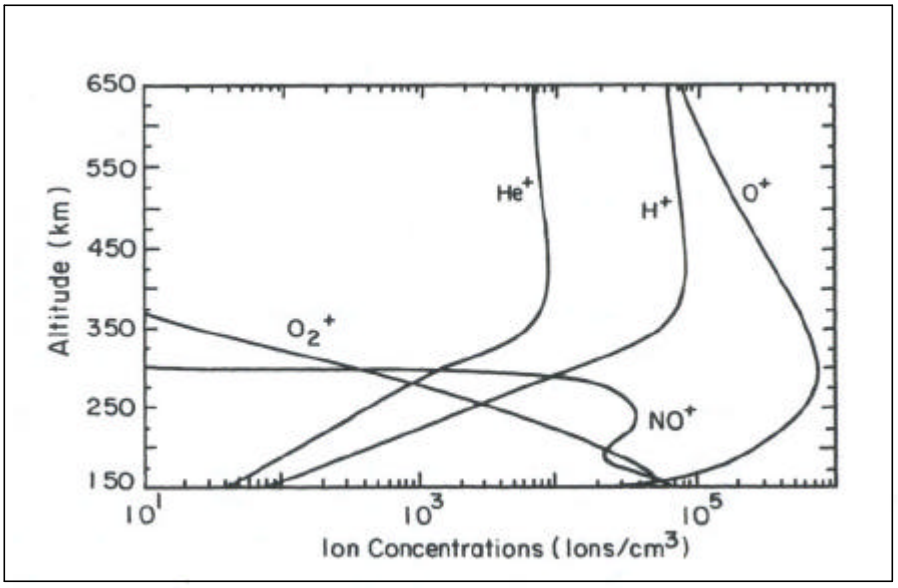

Figure 2-2. Plot of Altitude (km) Vs Ion Composition (cm^{-3}) for The Ionosphere (LEO)[33]

2.1.2. GEO Plasma Environment

A spacecraft at GEO is at the edge of plasmapause. GEO plasma is tenuous, and cool as compared to LEO plasma although sudden injections of high energy plasma (with mean energy of a few tens of keV) during substorms are observed. This collisionless plasma does not follow a single Maxwellian distribution. Instead, plasma parameters must be measured experimentally. The particle detectors on the ATS[34,35,36] and SCATHA[37] spacecraft have measured plasma variations between 5-10 eV and 50-80 eV approximately, for 50 complete days at 1 to 10 minute resolution from 1969 through 1980, bracketing one solar cycle.

Garrett and Deforest[34] fitted an analytical two-temperature model to data collected over 10 different days from ATS-5 spacecraft between 1969 and 1972. These data were selected in such a way to show a wide range of geomagnetic activity including plasma injection events (i.e. sudden appearance of dense, relatively high energy plasma at GEO occurring at local midnight). The model gives reasonable and consistent representation of the variations following a substorm injection event at GEO. The parameters for this model during average GEO conditions are shown in Table 2-1 with "Worst-case" GEO conditions given in Table 2-2.

Parameter	**Electrons**	**Ions**
Number density m^{-3}	$1.09 \pm 0.89 \times 10^6$	$0.58 \pm 0.35 \times 10^6$
Number density n_1 (1^{st} Maxwellian fit) m^{-3}	$0.78 \pm 0.7 \times 10^6$	$0.19 \pm 0.16 \times 10^6$
Temperature kT_1/e (1^{st} Maxwellian fit) eV	$0.55 \pm 0.32 \times 10^3$	$0.8 \pm 1.0 \times 10^3$
Number density n_2 (2^{nd} Maxwellian fit) m^{-3}	$0.31 \pm 0.37 \times 10^6$	$0.39 \pm 0.26 \times 10^6$
Temperature kT_2/e (2^{nd} Maxwellian fit) eV	$8.68 \pm 4.0 \times 10^3$	$15.8 \pm 5.0 \times 10^3$

Table 2-1. Average GEO Environment[37]

Parameter	**Electrons**	**Ions**
Number density m^{-3}	3.0×10^6	3.0×10^6
Number density n_1 (1^{st} Maxwellian fit) m^{-3}	1.0×10^6	1.1×10^6
Temperature kT_1/e (1^{st} Maxwellian fit) eV	600	400
Number density n_2 (2^{nd} Maxwellian fit) m^{-3}	1.4×10^6	1.7×10^6
Temperature kT_2/e (2^{nd} Maxwellian fit) eV	2.51×10^4	2.47×10^4

Table 2-2. Worst-case GEO Environment[37]

2.1.3. Interplanetary Plasma Environment

The sun is the dominant source for the space plasma environment in the solar system. The sun's main influence on the space environment is through its electromagnetic flux and emitted charged particles. The solar particle flux is basically composed of two components: The very sporadic, high energy (E > 1 MeV) plasma bursts associated with solar events (flares, coronal mass ejections, proton events, and so forth) and the variable, low-energy (E ≈ tens of eV) background plasma referred to as the solar wind. The solar wind, because of its density (tens of particles per cm^3) and velocity

(≈ 200-2000 km/s), energetically dominates the interplanetary environment and can directly reach the GEO environment on occasion.

2.1.4. Debye Length in Space Plasmas

It is easily shown[38] that an isolated charged body, when placed in plasma, attracts charges of the opposite sign such that the effect of its charge is limited in extent. Within the distance known as Debye length of a charge, the electrostatic potential field is essentially the same as that of the charge in vacuum. Far from the central charge, however, the long-range electrostatic force field is effectively shielded due to the enveloping plasma space charge.

On a large enough scale, plasma that is near equilibrium must be approximately charge neutral. If this were not the case, the strong Coulomb interactions would drive the particles apart and not allow an equilibrium state to exist. The length scale over which the charge neutrality is established in plasma is called Debye length.

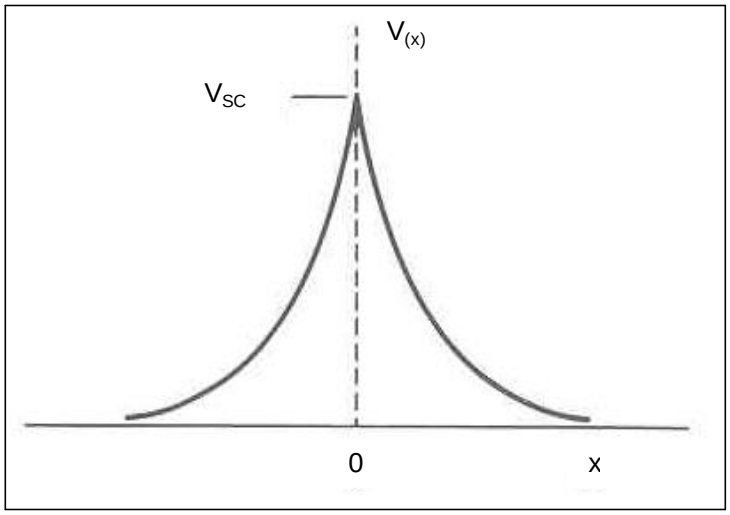

Figure 2-3. Potential Distribution Near a Grid in Plasma[39]

Consider a perfectly transparent grid as shown in Figure 2-3[39] in a plasma held at spacecraft potential V_{SC} in the plane x = 0. Let V_x be the potential due to charge on spacecraft at some x which is the distance from the spacecraft. For simplicity, we assume that the ion-electron mass ratio M/m is large enough that the inertia of ions prevents them from moving significantly on the time scale of the experiment. Poisson's equation in one dimension is

Eqn. 2-1
$$e_0 \frac{d^2V}{dx^2} = -e(n_i - n_e)$$

If the density far away is n_∞, we have

Eqn. 2-2 $$n_i = n_\infty$$

The electron density will be[39]

Eqn. 2-3 $$n_e = n_\infty \exp(eV/KT_e)$$

Substituting for n_i and n_e in Eqn. 2-1, we get

Eqn. 2-4 $$e_0 \frac{d^2V}{dx^2} = en_\infty \left\{ \left[\exp\left(\frac{eV}{KT_e} \right) \right] - 1 \right\}$$

In the region where $|e\phi/KT_e| << 1$, we can expand the exponential in Taylor Series as follows,

Eqn. 2-5 $$e_0 \frac{d^2V}{dx^2} = en_\infty \left\{ \frac{eV}{KT_e} + \frac{1}{2}\left(\frac{eV}{KT_e} \right)^2 + ... \right\}$$

Keeping only the linear terms in Eqn. 2-5, we get,

Eqn. 2-6 $$e_0 \frac{d^2V}{dx^2} = \frac{n_\infty e^2 V}{KT_e}$$

We can define Debye length, $?_d$ as,

Eqn. 2-7 $$?_d \equiv \left(\frac{e_0 KT_e}{ne^2} \right)^{1/2}$$

Where n stands for n_∞. Now we can write the solution of Eqn. 2-6 as

Eqn. 2-8 $$V = V_{SC} \exp(-|x|/?_d)$$

Debye length is the measure of the shielding distance or thickness of the sheath. Table 2-3 lists Debye lengths calculated by this formula using parameters from Table 2-1, Table 2-2, Section 2.1.1 and Section 2.1.3.

Plasma Environment	Lowest Debye Length m	Highest Debye length m
LEO plasma environment	0.02	0.4
GEO plasma environment	142	1,496
Interplanetary plasma	7.4	24

Table 2-3. Range of Debye Length in Various Plasma Environments

2.1.5. Spacecraft Charging

A spacecraft in ambient plasma behaves like an isolated probe (Langmuir Probe),[33] repelling or collecting free charges depending upon the vehicle potential as shown in figure Figure 2-4.

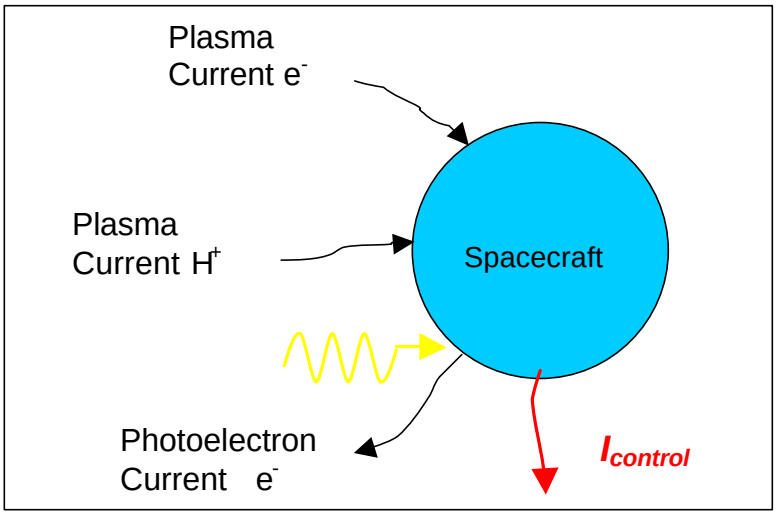

Figure 2-4. Currents Flowing To and From The Spacecraft

The current voltage characteristics of spacecraft (Langmuir probe) in the absence of external magnetic field is shown in Figure 2-5. In region 1, where Vsc is biased to a large negative value, almost all the electrons are repelled and the current to the vehicle is dominated by plasma ions. As the potential of the vehicle is increased, the ion current is reduced and a greater number of electrons are able to reach the spacecraft as a result of their kinetic energy. At a certain negative potential known as the floating potential, or V_f, the electron current will balance with the ion current, resulting in a zero net current to the vehicle. This floating potential is the value that an isolated spacecraft would assume in equilibrium and is given by (for $V_{SC}<0$)

Eqn. 2-9

$$V_f = -\frac{kT_e}{e}\ln\left[\sqrt{\frac{T_i m_i}{T_e m_e}}\left(1-\frac{eV_{sc}}{kT_i}\right)\right].$$

For a plasma consisting of protons and electrons at approximately the same temperatures,

Eqn. 2-10

$$V_f \approx -2.5\frac{kT_e}{e}.$$

The spacecraft floating potential is thus on the order of, and scales proportionally with, the electron temperature. As the vehicle potential increases above the floating potential, the number of plasma electrons reaching the surface keeps increasing, while the ion current is reduced further. The point at which most of the ions are prohibited from reaching the vehicle is known as the plasma potential, V_{plasma}, and is characterized by the "knee" in the I-V characteristic. For spacecraft potentials greater than the plasma potential, the current is composed entirely of plasma electrons.

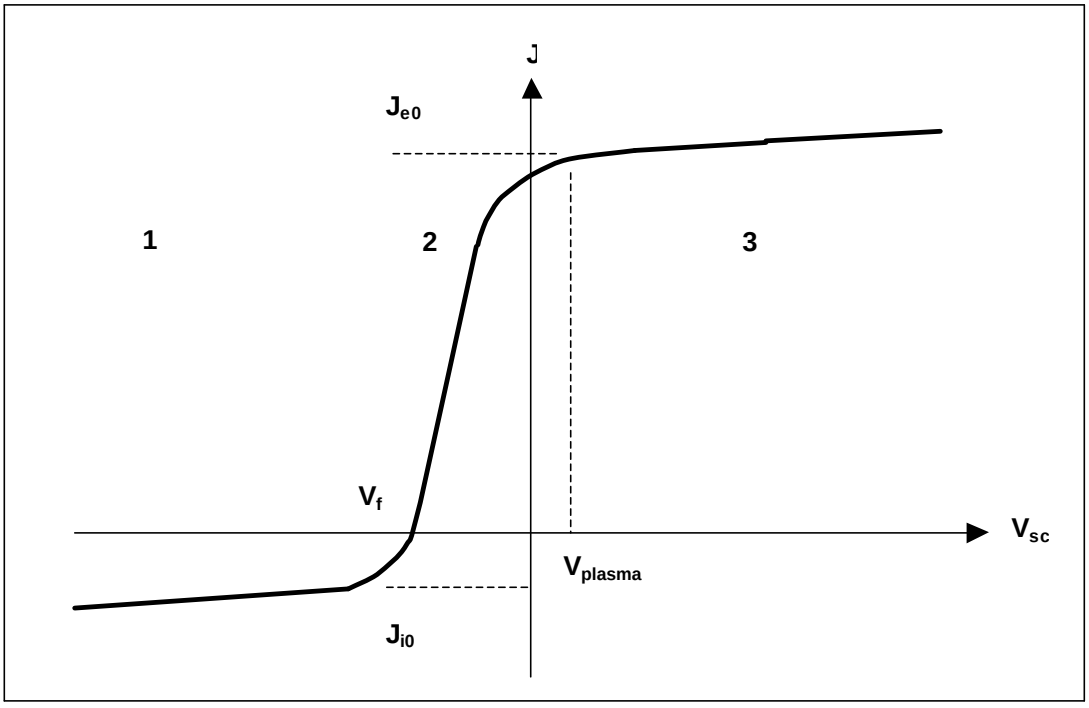

Figure 2-5. I Vs V Graph for Spacecraft. Vertical Axis Represents Net Current Collected by The Vehicle at a Given Spacecraft Potential (Horizontal Axis)

Considering a simple spherical geometry for the spacecraft, the entire I-V characteristic of the vehicle within a space plasma can be given as an expression for the plasma current density, J_p, as a function of spacecraft potential, V_{sc} in two parts:

Eqn. 2-11 For $V_{sc} < 0$

$$J_p = J_{e0} \exp\left(\frac{-e|V_{sc}|}{kT_e}\right) - J_{i0}\left(1 + \frac{e|V_{sc}|}{kT_i}\right)$$

Eqn. 2-12 For $V_{sc} > 0$

$$J_p = J_{e0}\left(1 + \frac{eV_{sc}}{kT_e}\right) - J_{i0}\exp\left(\frac{-eV_{sc}}{kT_i}\right)$$

where J_{e0} and J_{e0} are termed the electron and ion saturation currents, respectively, and are given by

Eqn. 2-13 $$J_{e0} = en_e\left[\frac{kT_e}{2p\,m_e}\right]^{1/2}$$

Eqn. 2-14 $$J_{i0} = -en_i\left[\frac{kT_i}{2pm_i}\right]^{1/2}$$

Where e is electron charge in C, $n_{i(e)}$ is ion (electron) density in m^{-3}, k is Boltzmann constant in J/K, $T_{i(e)}$ is ion/electron temperature and $m_{i/e}$ is mass of ion (electron) measured in kg. The behavior of the ion/electron saturation currents for plasma conditions of interest to this report are demonstrated in Figure 2-6 and Figure 2-7.

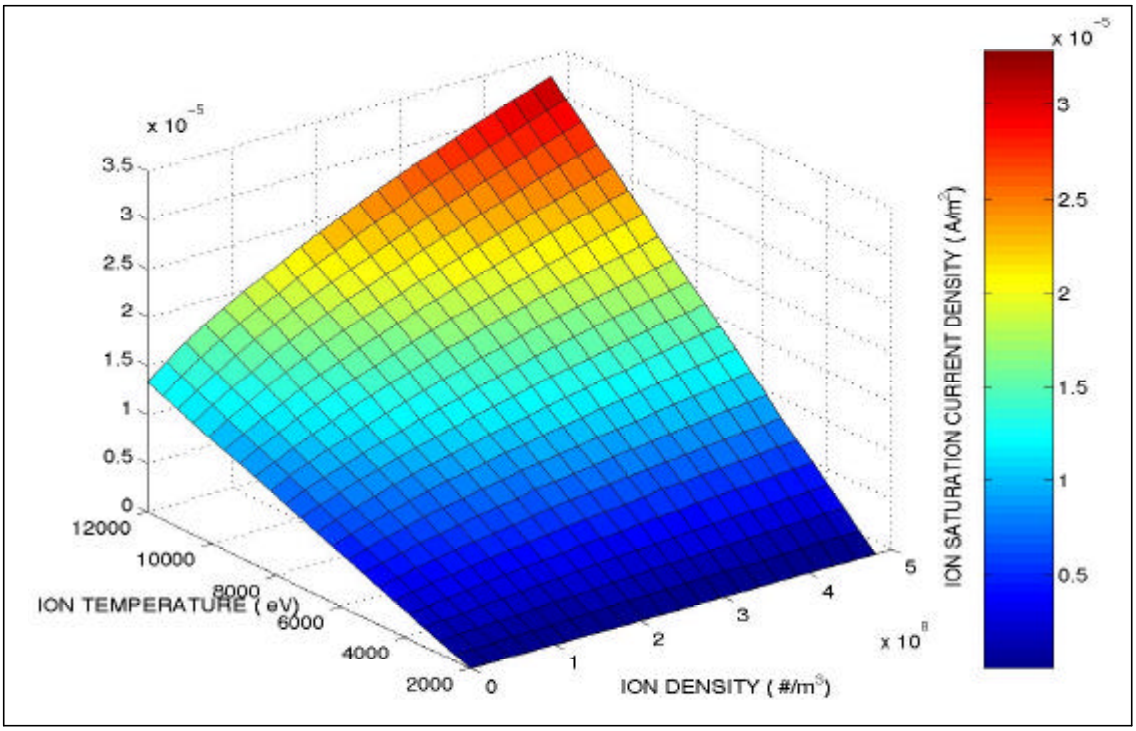

Figure 2-6. Plot of Ion Saturation Current Density as a Function of Ion Temperature and Ion Density

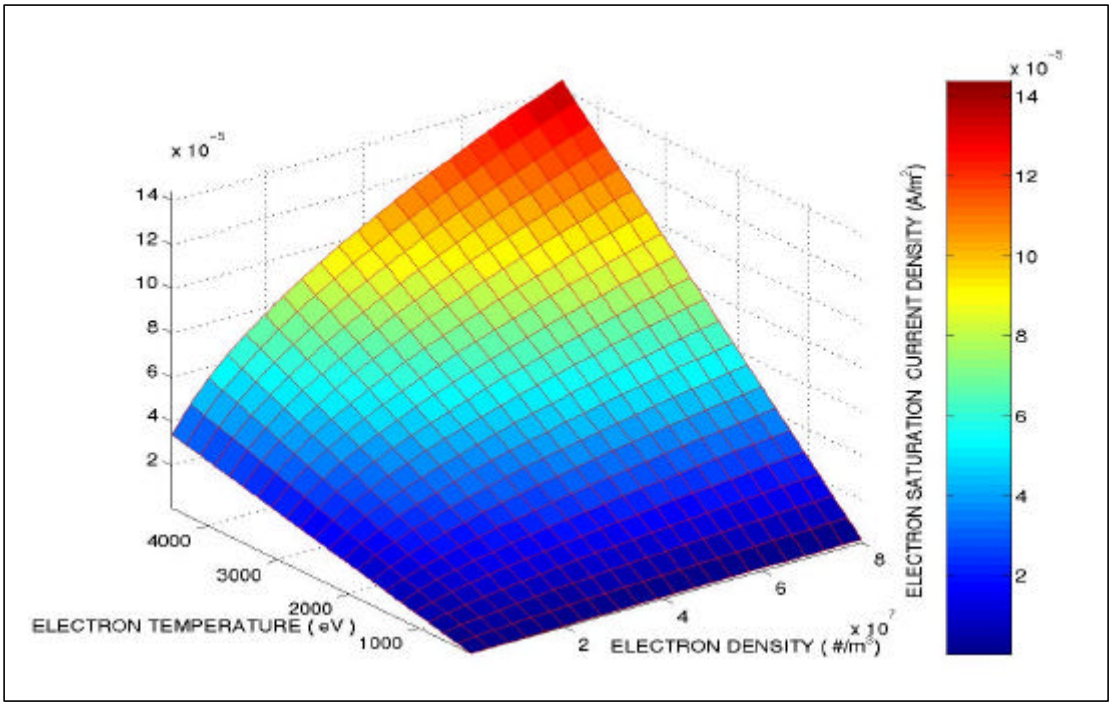

Figure 2-7. Plot of Electron Saturation Current Density as a Function of Electron Temperature and Electron Density

In addition to the plasma current to the vehicle, light absorption results in emission of photoelectrons during the day. The flux of electron emission is proportional to the flux of absorbed photons. For the sake of simplicity we assume that the emitted photoelectrons follow a Maxwellian velocity distribution characterized by an average temperature of T_{pe}. The photoelectron current density is

Eqn. 2-15 For $V_{sc} < 0$

$$J_{pe} = J_{pe0} = \text{const}$$

Eqn. 2-16 For $V_{sc} > 0$

$$J_{pe} = J_{pe0} \exp\left(\frac{-eV_{sc}}{kT_{pe}}\right)\left(1 + \frac{eV_{sc}}{kT_{pe}}\right)$$

Where T_{pe} is temperature of photoelectrons.

So total current density to the vehicle can be given by sum of electron plasma current, ion plasma current and photoelectron current as follows:

Eqn. 2-17 If $V_{sc} \leq 0$,

$$J_p = J_{e0} \exp\left(\frac{-e|V_{sc}|}{kT_e}\right) - J_{i0}\left(1 + \frac{e|V_{sc}|}{kT_i}\right) - J_{pe0}$$

Eqn. 2-18 If $V_{sc} > 0$,

$$J_p = J_{e0}\left(1 + \frac{eV_{sc}}{kT_e}\right) - J_{i0} \exp\left(\frac{-eV_{sc}}{kT_i}\right) - J_{pe0} \exp\left(\frac{-eV_{sc}}{kT_{pe}}\right)\left(1 + \frac{eV_{sc}}{kT_{pe}}\right)$$

2.1.6. Modeling Spacecraft Charging

Spacecraft charging, especially differential charging, has been of prime concern to spacecraft designers because of its detrimental effects such as electrostatic discharge in spacecraft and spacecraft subsystems. Space Environment Effect (SEE) program[40] is one of the tools available to model the plasma environment and spacecraft charging. In the SEE model we can specify the plasma parameters, spacecraft size, materials of different

parts and charging time, whereupon the program predicts potentials of finite number of elements of the spacecraft surface.

The transient response of a spacecraft in plasma is calculated by modeling the spacecraft – ambient plasma system as an equivalent electric circuit. The SEE model uses a simple three axis stabilized satellite with a single solar array wing as shown in Figure 2-8a and a simplified circuit model for this satellite shown in Figure 2-8b. In this model, we assume that the satellite is entirely covered with a perfect conductor, e.g. conducting thermal blankets (blue), and that the only insulators are the solar cell cover glasses (green). The circuit has only three nodes: 0 = Ground which is the magnetosphere potential, V_A = which is Spacecraft chassis potential, V_B = which is Cover glass potential.

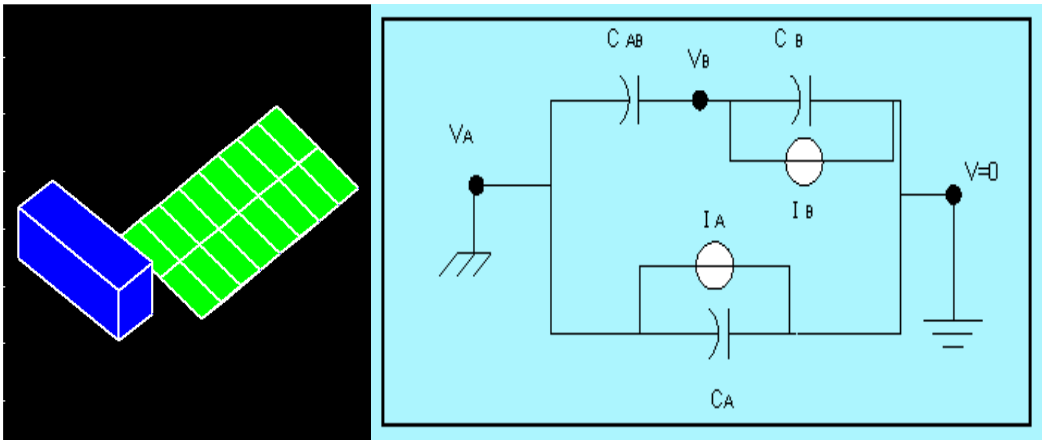

Figure 2-8. a) Simple Geometric Model and b) Equivalent Circuit for Spacecraft and Ambient Plasma Used by SEE

I_A and I_B are the currents from ambient plasma to the chassis of the spacecraft and solar array respectively. C_A is capacitance between spacecraft chassis surface and plasma. C_B is the capacitance between solar array and plasma. C_{AB} is capacitance between chassis and solar array. Typical values for these capacitances are $C_A \approx C_B \approx 4\pi\varepsilon_0 R \approx R \times 10^{-10}$ F. Where R (meters) is the effective spacecraft radius. C_{AB} is usually much larger as compared to C_A, and C_B.

We know that

Eqn. 2-19

$$\frac{dV}{dt} = \frac{I}{C}$$

Where V is the potential, I is the current and C is the capacitance. SEE program uses the same relation to calculate the changes in V_A, V_B and $(V_B - V_A)$ with respect to time as follows,

Eqn. 2-20

$$\frac{dV_A}{dt} \approx \frac{dV_B}{dt} \approx \frac{I_A}{C_A} \approx -R \times 10^4 \text{ V/s}$$

$$\frac{d(V_B - V_A)}{dt} \approx \frac{I_B - I_C}{C_{AB}} \approx 10 \text{ V/s}$$

As discussed in Section 2.1.5, an isolated spacecraft in plasma will assume an equilibrium (or floating or absolute) potential given by Eqn. 2-10, such that the net current to the vehicle is zero. This absolute potential can reach up to tens of thousands of volts depending upon plasma parameters but it is not, by itself, hazardous to spacecraft operations. In the simplest application of SEE program we can calculate the absolute potential of a spherical spacecraft made up of single material. If we use single material like Kapton or Teflon to build the entire spherical spacecraft of 1 m diameter, and if we select the ATS-6 Environment, the spacecraft shows absolute charging of tens of thousands of volts as shown in

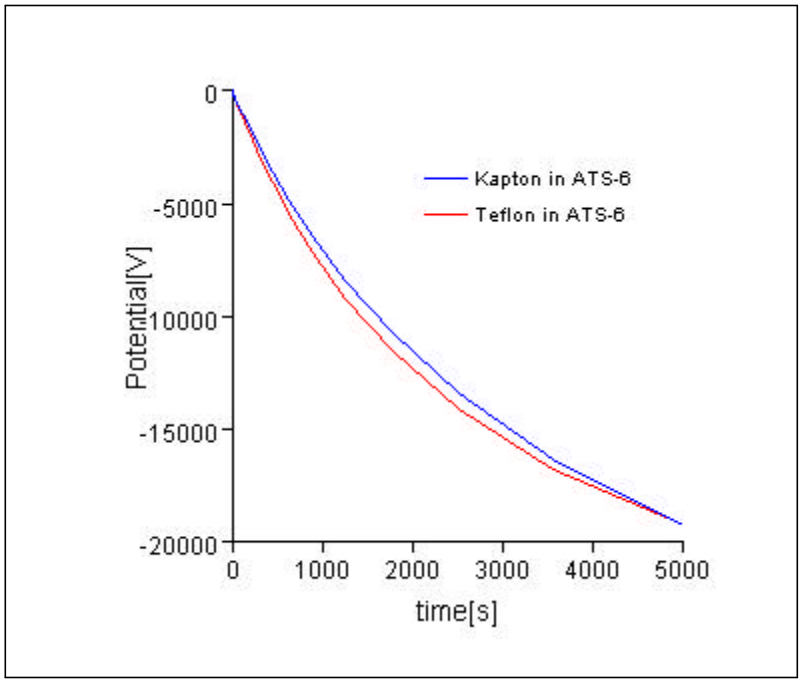

Figure 2-9. Potential Vs Time Plot for Spacecraft Using Kapton and Teflon as Materials and ATS-6 Plasma Environment.[40] (1 m Diameter)

Differential charging occurs when portions of the same spacecraft assume different potentials (voltages). It can occur because of more than one cause. Each exposed spacecraft surface will interact with the ambient plasma differently depending on the material composing the surface, whether that surface is in sunlight or shadow, and the flux of particles to that surface. When the breakdown threshold is exceeded between surfaces or within dielectrics an electrostatic discharge (ESD) can occur. ESD can couple

into spacecraft electronics and cause upsets ranging from logic switching to complete system failure.

In SEE program we can also select the complicated geometry for the typical communications satellite and different materials for its different parts as shown in Figure 2-10. In Figure 2-11, the potentials for different elements of spacecraft surface are shown in different colors.

Part	**Color**	**Material**
Chassis	Green	Kapton
Solar Arrays	Red	Solar Cells
Antenna	Blue	Teflon
Omni Antenna	Blue	Teflon

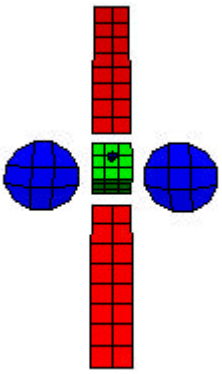

Figure 2-10. Materials Selected for Different Parts of Spacecraft[40]

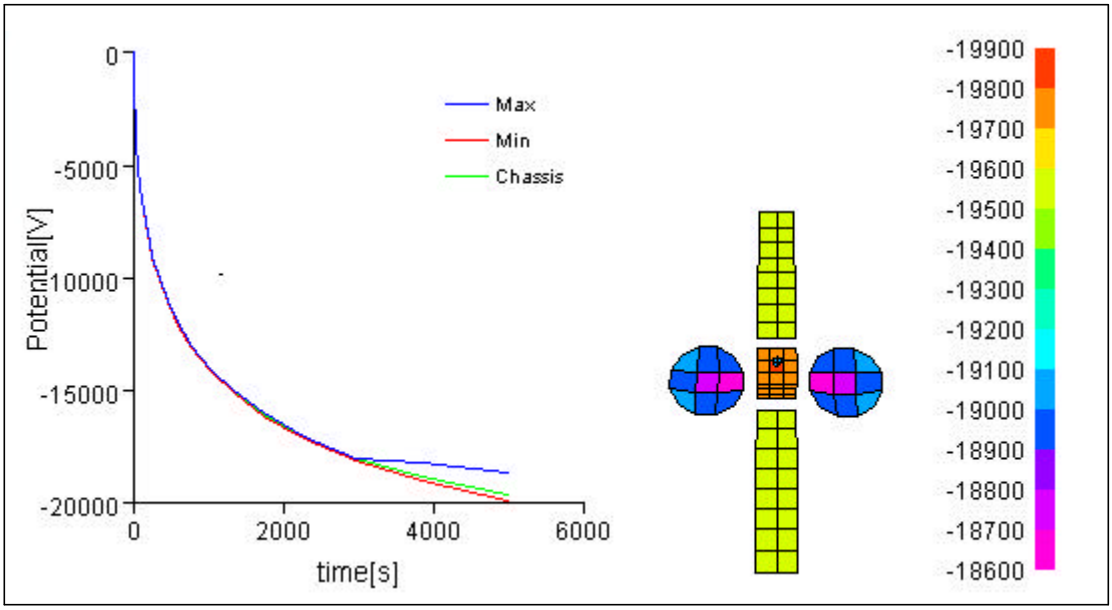

Figure 2-11. Max., Min and Chassis Potential Vs Time Plot For The Spacecraft[40]

[33] Hastings Daniel, Garrett Henry, "Spacecraft –Environment Interactions", Cambridge University Press, 1996, pp.44-71.

[34]Garrett H. B., and DeFrost, S. E. "An analytical simulation of the geosynchronous plasma environment", Planetary Space Science, 27:1101-09, 1979.

[35] Garrett H. B., Schwank, D. C., and DeFrost, S. E " A statistical analysis of the low energy geo-synchronous plasma environment–I. electrons, Planetary Space Science, 29:1021-44, 1981a.

[36] Garrett H. B., Schwank, D. C., and DeFrost, S. E " A statistical analysis of the low energy geo-synchronous plasma environment–I. protons, Planetary Space Science, 29:1045-60, 1981b.

[37] Mullen, E. G., Gussenhoven, M. S., and Hardy, D. A. SCATHA survey of high-voltage spacecraft charging in sunlight, "Journal of Geophysical Research", 91:1474-90, 1986.

[38] See, for instance, Gombosi, T.I., " Physics of The Space Environment", Cambridge University Press",1998.

[39] Chen, Francis. F., "Introduction to Plasma Physics and Controlled Fusion, Second Edition, Volume 1: Plasma Physics", Plenum Press, New York and London, 1974, pp. 8-10.

[40] Maxwell Technologies System Division, " Interactive Spacecraft Charging Handbook", Space Environment Effect Program, NASA Marshall Space Flight Center.

3. Dynamics of Charged Satellite Formations

In this section several formation geometries are introduced that are used throughout the report for a variety of analyses. First, methods for computing individual spacecraft charges to maintain dynamic equilibrium are presented, along with specific numerical examples. This is followed by comparisons of Coulomb control to conventional electric propulsion methods.

Similar to other work in spacecraft formation dynamics,[41,42] Hill's equations are used here. Since higher order effects may be of interest in the future, the dynamic equations are first developed without any linearizing assumptions, then reduced to Hill's equations using the conventional expansion of the gravitational terms. All the formations consist of a single combiner surrounded by collectors. It is assumed that the combiner has its own station keeping system, but the collectors do not. Thus the only external forces on the collectors are the Coulomb interactions between them and the combiner.

In the remainder of this section the formation geometries are presented with specific attention given to the nomenclature used in later sections. This is followed by the dynamic equation derivation leading to a compact set of equations for both Earth orbiting and Libration point fixed formations.

3.1. Formation Geometries

Four formations were considered in this study. Three of them

- 3 Satellites in a line (1 combiner, 2 collectors)
- 5 satellites in a plane (1 combiner, 4 collectors)
- 6 satellites in a plane (1 combiner, 5 collectors)

were assumed to have a combiner in a circular orbit (shown in Figure 3-1) with collector satellites positioned relative to it. The fourth case consisted of 5 satellites (1 combiner and 4 collectors) in a line located at a stable earth-sun Libration point. In the remainder of this section, the 4 formations are described in detail with specific attention given to the parameters defining their configuration.

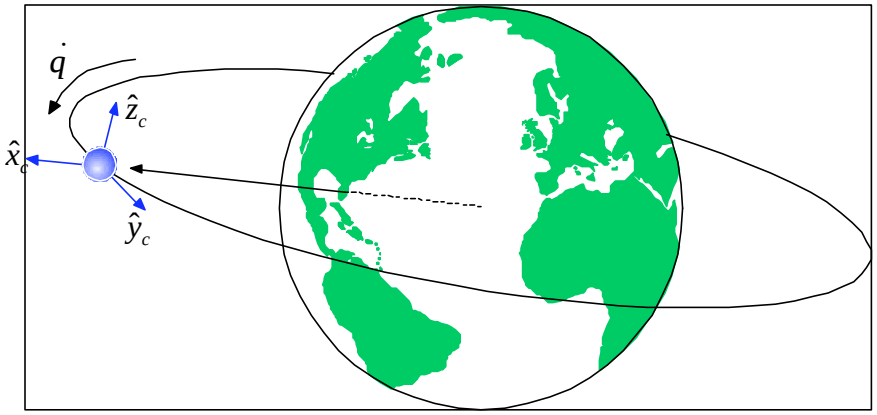

Figure 3-1. Combiner and its fixed frame, {c}, in a circular orbit.

3.1.1. Earth Orbiting Three Satellite – Geometry

Three different 3-satellite formations were considered. In each case the combiner (denoted with a 0 subscript) was assumed to maintain a circular orbit with radius r and true anomaly q. The combiner-fixed rotating reference frame, denoted {c} and shown in Figure 3-1, was used to describe collector motion relative to the combiner.

Spacecraft charges were analytically computed such that the 3 satellites formed a line shown in Figure 3-2 where M_i are spacecraft masses, q_i are spacecraft charges and L is the separation between the combiner (blue) and either collector (yellow). The distinguishing feature of the formations was their axis alignment.

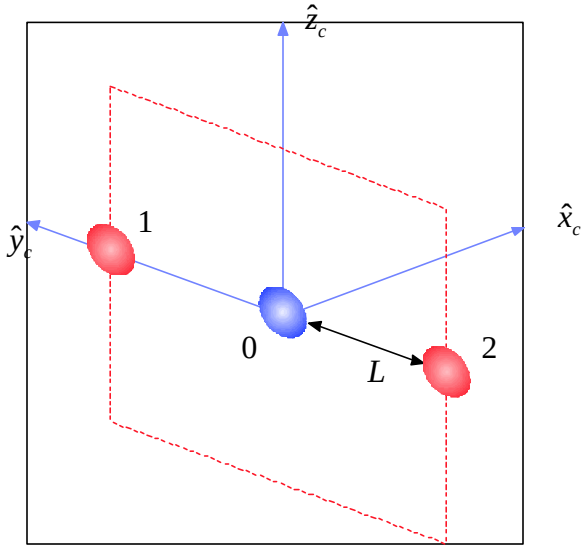

Figure 3-2. Three satellite formation.

Figure 3-3 shows the 3 cases examined with spacecraft aligned along the combiner fixed frame, x, y, and z axes. These ‘virtual tether` formations have little imaging use, but, provided insight into the solutions of the more complicated formations considered later.

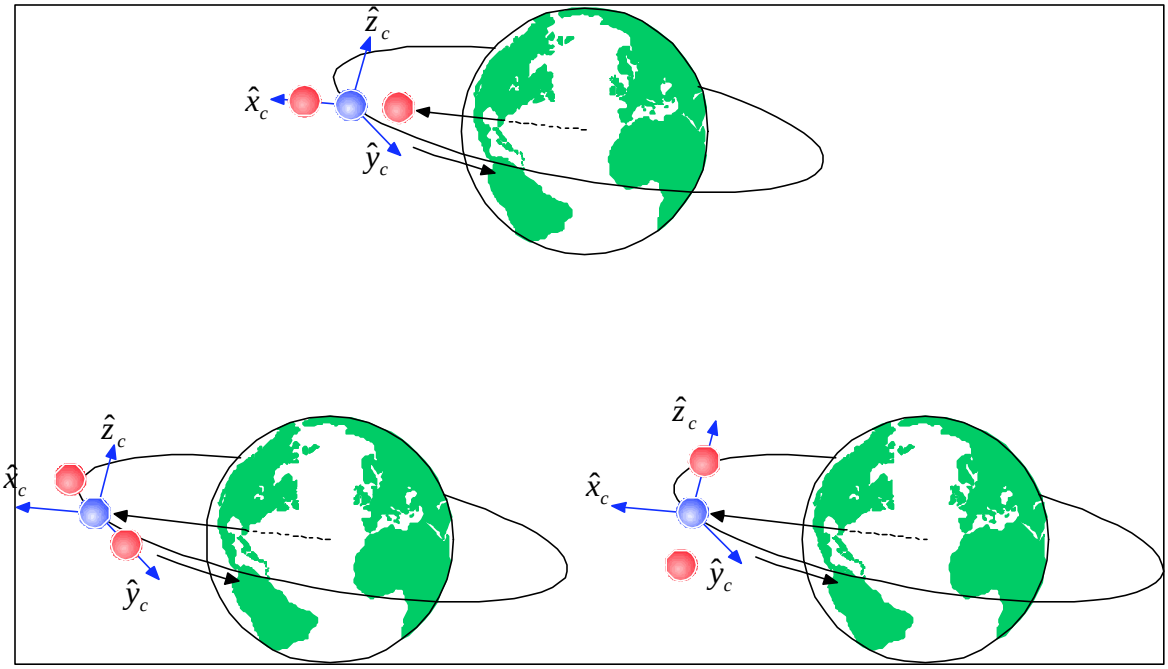

Figure 3-3. The three 3-satellite formations aligned along the x, y, and z {c} frame axes .

3.1.2. Earth Orbiting Five Satellite - Geometry

As in the previous formation, the combiner was assumed to have a circular orbit with radius r and true anomaly q shown in. Spacecraft charges were analytically determined such that the four collectors formed a square in the combiner fixed $\hat{y}_c - \hat{z}_c$ plane with side length $2L$ shown in Figure 3-4. Charges are again denoted q_i and masses as m_i. Although this formation could be used for imaging it is not optimal due to U-V plane overlap.

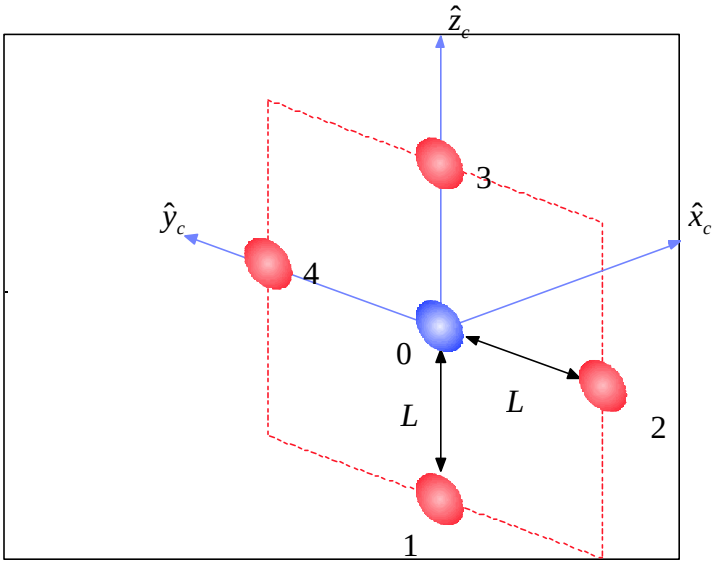

Figure 3-4. The five-satellite formation geometry.

3.1.3. Earth Orbiting Six Satellite - Geometry

Again the combiner was assumed to be in the circular orbit of with radius r and true anomaly ?̇. Spacecraft charges were computed numerically such that the 5 collectors were in a circle of radius L about the combiner, in its Y-Z plane. In addition, the goal was to maintain a pentagon formation, shown in Figure 3-5, as that is optimal from an imaging perspective.

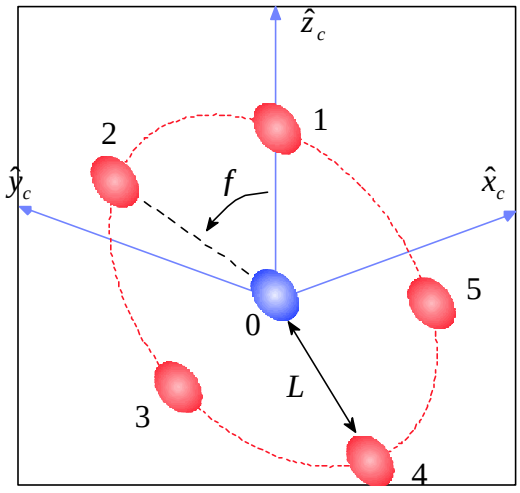

Figure 3-5. In-plane Pentagon Satellite Formation Configuration

3.1.4. *Libration Point Five Satellite – Geometry*

The five satellites were assumed to be at a stable Earth-Sun Libration point aligned as shown in Figure 3-6. Charges were analytically computed such that collectors `1` and `3` had a combiner separation of L_1 and collectors `2` and `4` had a separation of L_1+L_2. In addition, the system was assumed to rotate about the combiner fixed y-axis with angular rate $\dot{?}$.

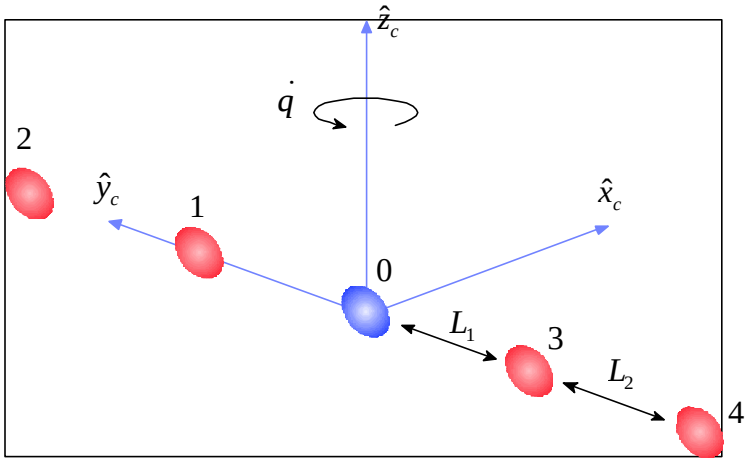

Figure 3-6. Rotating Five-satellites Formation Configuration

In the next following sections, the equations of motion for four different satellites formation flying configuration that discussed above are derived and described from Hill's equation.

3.2. *Dynamic Equations of the Formations*

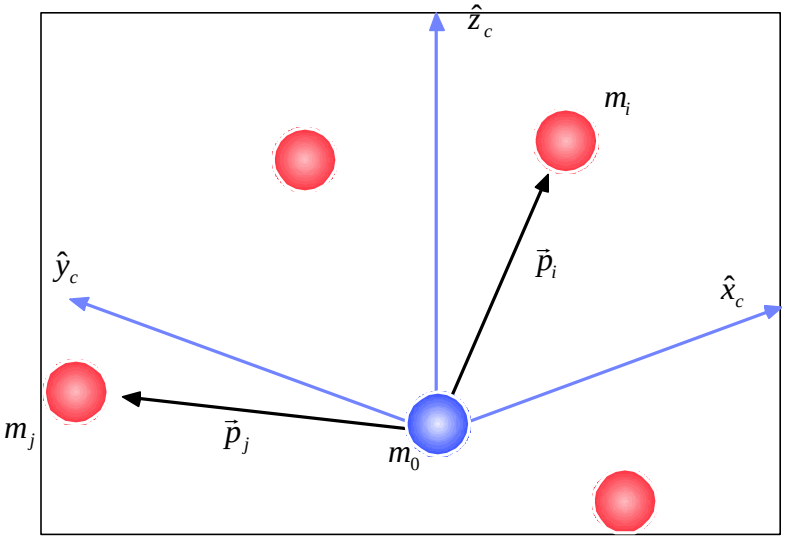

Figure 3-7 Assuming there are n collectors and 1 combiner, the position vector notation is illustrated for the ith and jth collectors.

Figure 3-7 shows the combiner in a circular orbit along with the ith and jth collector and will aid the development of the generic dynamic equations for n collectors. Lagrange's equations will be used where initially the full nonlinear equations are developed. After imposing linearizing assumptions, the Hill equations remain with Coulomb interaction forces between spacecraft.

The position vector from the origin of the combiner fixed frame to the ith collector is denoted $\vec{p}_i$ and has components x_i, y_i, and z_i. It should be noted that since the combiner motion is prescribed we have

Eqn. 3-1
$$x_0 = y_0 = z_0 = \dot{x}_0 = \dot{y}_0 = \dot{z}_0 = 0$$

The absolute velocity of the ith spacecraft is

Eqn. 3-2
$$\vec{p}_i = \begin{Bmatrix} \dot{x}_i - y_i\dot{q} \\ \dot{y}_i + \dot{q}\left(r + x_i\right) \\ \dot{z}_i \end{Bmatrix}$$

from which the kinetic energy is developed according to

Eqn. 3-3
$$T = \frac{1}{2}\sum_{i=0}^{n} m_i \dot{\vec{p}}_i^T \dot{\vec{p}}_i$$

The total potential energy is expressed as the sum of the gravitational and Coulomb potential energy

Eqn. 3-4
$$V = V_g + V_c$$

The gravitational component, V_g, is

Eqn. 3-5
$$V_g = -m\sum_{i=0}^{n} m_i \left[\left(r + x_i\right)^2 + y_i^2 + z_i^2 \right]^{-1/2}$$

where m is the gravitational constant. The Coulomb component, V_c, is

Eqn. 3-6
$$\begin{aligned} V_c &= k_c \sum_{i=0}^{n-1} q_i \sum_{j=i+1}^{n} q_j \left[\left(x_j - x_i\right)^2 + \left(y_j - y_i\right)^2 + \left(z_j - z_i\right)^2 \right]^{-1/2} \\ &= k_c \sum_{i=0}^{n-1} q_i \sum_{j=i+1}^{n} \frac{q_j}{\left|\vec{p}_i - \vec{p}_j\right|} \end{aligned}$$

where k_c is Coulomb's constant given by

Eqn. 3-7
$$k_c = \frac{1}{4pe_o} \approx 8.99\times10^9 \frac{Nm^2}{C^2}$$

and e_o is the electric permittivity of free space.

Applying Lagrange's equations yields the full nonlinear dynamic equations for the ith spacecraft

Eqn. 3-8
$$\begin{aligned} \ddot{x}_i - 2\Omega\dot{y}_i - (r + x_i)\Omega^2 + \frac{\mu(r + x_i)}{\left[\left(r + x_i\right)^2 + y_i^2 + z_i^2\right]^{3/2}} &= \frac{k_c}{m_i} \sum_{j=0}^{n} \frac{(x_i - x_j)}{\left|\vec{p}_i - \vec{p}_j\right|^3} q_i q_j \\ \ddot{y}_i - 2\Omega\dot{x}_i - y_i\Omega^2 + \frac{\mu y_i}{\left[\left(r + x_i\right)^2 + y_i^2 + z_i^2\right]^{3/2}} &= \frac{k}{m_i} \sum_{j=0}^{n} \frac{(y_j - y_i)}{\left|\vec{p}_i - \vec{p}_j\right|^3} q_i q_j \\ \ddot{z}_i + \frac{\mu z_i}{\left[\left(r + x_i\right)^2 + y_i^2 + z_i^2\right]^{3/2}} &= \frac{k}{m_i} \sum_{j=0}^{n} \frac{(z_j - z_i)}{\left|\vec{p}_i - \vec{p}_j\right|^3} q_i q_j \\ i = 1,\ldots,n \text{ and } i \neq j \end{aligned}$$

The gravity terms in Eqn. 3-8 can be linearized by first expressing them as

$$\frac{mm_i(r+x_i)}{\left[(r+x_i)^2+y_i^2+z_i^2\right]^{3/2}} = \frac{mm_i(r+x_i)}{r^3\left[1+\frac{2x_i}{r}+\frac{1}{r^2}(x_i^2+y_i^2+z_i^2)\right]^{3/2}}$$

Eqn. 3-9

$$\frac{mm_i y_i}{\left[(r+x_i)^2+y_i^2+z_i^2\right]^{3/2}} = \frac{mm_i y_i}{r^3\left[1+\frac{2x_i}{r}+\frac{1}{r^2}(x_i^2+y_i^2+z_i^2)\right]^{3/2}}$$

$$\frac{mm_i z_i}{\left[(r+x_i)^2+y_i^2+z_i^2\right]^{3/2}} = \frac{mm_i z_i}{r^3\left[1+\frac{2x_i}{r}+\frac{1}{r^2}(x_i^2+y_i^2+z_i^2)\right]^{3/2}}$$

and then expanding them in a binomial series

Eqn. -3-10

$$(1+z)^a = 1+za+\frac{2(a-1)}{2!}z^2+\frac{a(a-1)(a-2)}{3!}z^3$$

Substituting

Eqn. 3-11

$$a = -3/2$$

$$z = \frac{2x_i}{r}+\frac{x_i^2+y_i^2+z_i^2}{r^2}$$

into Eqn. -3-10, noting that the orbital radius of the combiner is much larger than the collector position vectors

Eqn. 3-12

$$r \gg \left|\vec{p}_i\right|$$

and keeping terms up through first order in x_i gives

$$\frac{mm_i(r+x_i)}{r^3\left[(r+x_i)^2+y_i^2+z_i^2\right]^{3/2}} \approx m_i\Omega^2(r+x_i)\left[1-\frac{3x_i}{r}\right] \approx m_i\Omega^2(r-2x_i)$$

Eqn. 3-13

$$\frac{mm_i y_i}{r^3\left[(r+x_i)^2+y_i^2+z_i^2\right]^{3/2}} \approx m_i\Omega^2 y_i\left[1-\frac{3x_i}{r}\right] \approx m_i\Omega^2 y_i$$

$$\frac{mm_i z_i}{r^3\left[(r+x_i)^2+y_i^2+z_i^2\right]^{3/2}} \approx m_i\Omega^2 z_i\left[1-\frac{3x_i}{r}\right] \approx m_i\Omega^2 z_i$$

where it is noted that $m = r^3\Omega^2$. Replacing the gravity terms in Eqn. 3-8 with those of Eqn. 3-13 and simplifying yields the final dynamic equations for the ith spacecraft, often called Hills equations

Eqn. 3-14

$$\ddot{x}_i - 2\Omega\dot{y}_i - 3\Omega^2 x_i = \frac{k_c}{m_i}\sum_{j=0}^{n}\frac{(x_i - x_j)}{\left|\vec{p}_i - \vec{p}_j\right|^3} q_i q_j$$

$$\ddot{y}_i + 2\Omega\dot{x}_i - y_i\Omega^2 = \frac{k}{m_i}\sum_{j=0}^{n}\frac{(y_j - y_i)}{\left|\vec{p}_i - \vec{p}_j\right|^3} q_i q_j$$

$$\ddot{z}_i + \Omega^2 z_i = \frac{k}{m_i}\sum_{j=0}^{n}\frac{(z_j - z_i)}{\left|\vec{p}_i - \vec{p}_j\right|^3} q_i q_j$$

$$i = 1,...,n \text{ and } i \neq j$$

The dynamic equations of the three Earth orbiting formations of Section 3.1.1 through Section 3.1.3 are obtained directly from Eqn. 3-14 by setting n equal to the number of collectors, or, 2, 3, and 4 respectively. The dynamic equations of the Libration point formation of Section 3.1.4 are readily obtained from Eqn. 3-8. For this case $m = 0$ and $r = 0$ from the Libration point assumption. The angular rate Ω is now the angular rate of the system about its center of mass instead of the angular rate of the combiner about the Earth. Finally, the combiner station keeping assumption is relaxed allowing it to have three degrees of freedom just like the collectors. Applying these conditions to Eqn. 3-8 yields the dynamic equations

Eqn. 3-15

$$\ddot{x}_i - 2\Omega\dot{y}_i - x_i\Omega^2 = \frac{k_c}{m_i}\sum_{j=0}^{n}\frac{(x_i - x_j)}{\left|\vec{p}_i - \vec{p}_j\right|^3} q_i q_j$$

$$\ddot{y}_i - 2\Omega\dot{x}_i - y_i\Omega^2 = \frac{k}{m_i}\sum_{j=0}^{n}\frac{(y_j - y_i)}{\left|\vec{p}_i - \vec{p}_j\right|^3} q_i q_j$$

$$\ddot{z}_i = \frac{k}{m_i}\sum_{j=0}^{n}\frac{(z_j - z_i)}{\left|\vec{p}_i - \vec{p}_j\right|^3} q_i q_j$$

$$i = 0,..., 4 \text{ and } i \neq j$$

3.3. Summary

The main result of this section was the formation descriptions and the dynamic equations of charged spacecraft, Eqn. 3-14 and Eqn. 3-15. These will be used extensively in Section 4 where equilibrium solutions for each formation are investigated.

[41] Kong, E.M.C, Miller, D.W, and Sedwick, R.J., "Exploiting Orbital Dynamics for Aperture Synthesis Using Distributed Satellite Systems: Applications to a Visible Earth Imager System," Proceedings of the AIAA/AAS Astrodynamics Specialist Conference, pp. 285-301.

[42] Sabol, C., Burns, R., McLaughlin, C.A., "Satellite Formation Flying Design and Evolution," Proceedings of the AIAA/AAS Astrodynamics Specialist Conference, pp. 265-283.

4. Equilibrium Solutions

Analytical and numerical methods were used to find equilibrium solutions for the 4 constellations introduced in Section 3. The three satellite (Section 3.1.1) and both five satellite (Section 3.1.2 and Section 3.1.4) formations were solved analytically. The six satellite (Section 3.1.3) formation was solved numerically due to the complexity of its equilibrium equations. In all cases the equilibrium equations were developed by setting the relative speeds and accelerations to zero in the dynamic equations of Eqn. 3-14 and Eqn. 3-15,

Eqn. 4-1

$$\dot{x}_i = \dot{y}_i = \dot{z}_i = 0$$
$$\ddot{x}_i = \ddot{y}_i = \ddot{z}_i = 0$$

For the Earth orbiting formations described by Eqn. 3-14, the equilibrium equations are

Eqn. 4-2

$$-3\Omega^2 x_i = \frac{k_c}{m_i}\sum_{j=0}^{n}\frac{(x_i - x_j)}{\left|\vec{p}_i - \vec{p}_j\right|^3} q_i q_j$$
$$-y_i\Omega^2 = \frac{k_c}{m_i}\sum_{j=0}^{n}\frac{(y_j - y_i)}{\left|\vec{p}_i - \vec{p}_j\right|^3} q_i q_j$$
$$\Omega^2 z_i = \frac{k_c}{m_i}\sum_{j=0}^{n}\frac{(z_j - z_i)}{\left|\vec{p}_i - \vec{p}_j\right|^3} q_i q_j$$
$$i = 1,...,n \text{ and } i \neq j$$

while for the Earth-Sun Libration point 5 satellite formation Eqn. 3-15) the equilibrium equations are

Eqn. 4-3

$$-x_i\Omega^2 = \frac{k_c}{m_i}\sum_{j=0}^{n}\frac{(x_i - x_j)}{\left|\vec{p}_i - \vec{p}_j\right|^3} q_i q_j$$
$$-y_i\Omega^2 = \frac{k_c}{m_i}\sum_{j=0}^{n}\frac{(y_j - y_i)}{\left|\vec{p}_i - \vec{p}_j\right|^3} q_i q_j$$
$$0 = \frac{k_c}{m_i}\sum_{j=0}^{n}\frac{(z_j - z_i)}{\left|\vec{p}_i - \vec{p}_j\right|^3} q_i q_j$$
$$i = 0,...,4 \text{ and } i \neq j$$

In the remainder of the section the equilibrium equations are explored for each formation. Specifically, the formation constraints are first imposed often resulting in simpler equilibrium equations. Equilibrium solutions are obtiained. In addition spacecraft charges, q_i, will be replaced with the more relevant spacecraft voltage according to the well known relationship

Eqn. 4-4
$$q_i = \frac{V_i r_i}{k_c}$$

where V_i is the spacecraft voltage and r_i is the spacecraft radius, assuming the spacecraft is spherical.

4.1. Earth-orbiting Three-satellite formation - Equilibrium

As described in Section 3.1.1, three different 3-satellite formations were considered categorized according to their axis alignment. The equilibrium equations for each case were developed by setting $n = 2$ in Eqn. 4-2, along with the appropriate values of x_i, y_i, and z_i based on axis alignment constraints. For each axis alignment case the specific equilibrium equations are developed and solved below.

4.1.1. X-Axis Aligned Equilibrium Solutions

Three spacecraft aligned along the combiner coordinate frame's x-axis as shown in Figure 3-3(a) require the following relative displacement constraints

Eqn. 4-5
$$\begin{aligned} x_1 &= L \\ x_2 &= -L \\ y_1 = y_2 &= z_1 = z_2 = 0 \end{aligned}$$

where L is the distance from the combiner to either collector. Forming all 6 of the equilibrium equations from Eqn. 4-2 and eliminating duplicate equations leaves only two equations.

Eqn. 4-6
$$\frac{k_c q_1 q_2}{4L^2} + \frac{k_c q_1 q_0}{L^2} + 3m_1 L\dot{?}^2 = 0$$

Eqn. 4-7
$$\frac{k_c q_1 q_2}{4L^2} + \frac{k_c q_2 q_0}{L^2} + 3m_2 L\dot{?}^2 = 0$$

If we further assume that the collectors have equal mass, $m = m_1 = m_2$ and introducing the normalized charges defined by

Eqn. 4-8
$$q_{0n} = \frac{q_0}{\sqrt{mL^3}} \qquad q_{1n} = \frac{q_1}{\sqrt{mL^3}} \qquad q_{2n} = \frac{q_2}{\sqrt{mL^3}}$$

allows Eqn. 4-6 and Eqn. 4-7 to be written without explicit mass and length dependencies

Eqn. 4-9

$$\frac{k_c q_{1n} q_{2n}}{4} + k_c q_{1n} q_{0n} + 3\dot{?}^2 = 0$$
$$\frac{k_c q_{1n} q_{2n}}{4} + k_c q_{2n} q_{0n} + 3\dot{?}^2 = 0$$

where the subscript n denotes a normalized quantity. If we further define the normalized spacecraft voltage

Eqn. 4-10

$$V_{in} = k_c q_{in}$$

the equilibrium equations of Eqn. 4-9 are

Eqn. 4-11

$$V_{1n} V_{2n} + 4V_{1n} V_{0n} + 12k_c \Omega^2 = 0$$
$$V_{1n} V_{2n} + 4V_{2n} V_{0n} + 12k_c \Omega^2 = 0$$

These are readily solved analytically. Given a suitable collector spacecraft voltage, V_{0n}, the two combiner voltages must be equal and are

Eqn. 4-12

$$V_{1n} = V_{2n} = V_{0n} \pm \sqrt{V_{0n}^2 - 3k_c \Omega^2}$$

where the collector voltage must satisfy the constraint

Eqn. 4-13

$$V_{0n}^2 - 3k_c \Omega^2 \geq 0$$

Knowing the actual collector mass, m, radius, r, separation, L, and the orbital angular rate Ω, the equilibrium collector voltage can be obtained from Eqn. 4-12 and the normalization relationship

Eqn. 4-14

$$V_{in} = \frac{V_i r_i}{\sqrt{mL^3}}$$

Where the quantity $V_i r_i$ is called the *reduced charge* of spacecraft i. The normalized collector voltages, obtained from Eqn. 4-12, are shown in Figure 4-1 as a function of the combiner voltage, V_{0n}. The rate Ω is for a geosynchronous orbit, $\Omega = 7.2915e-5$ rad/s.

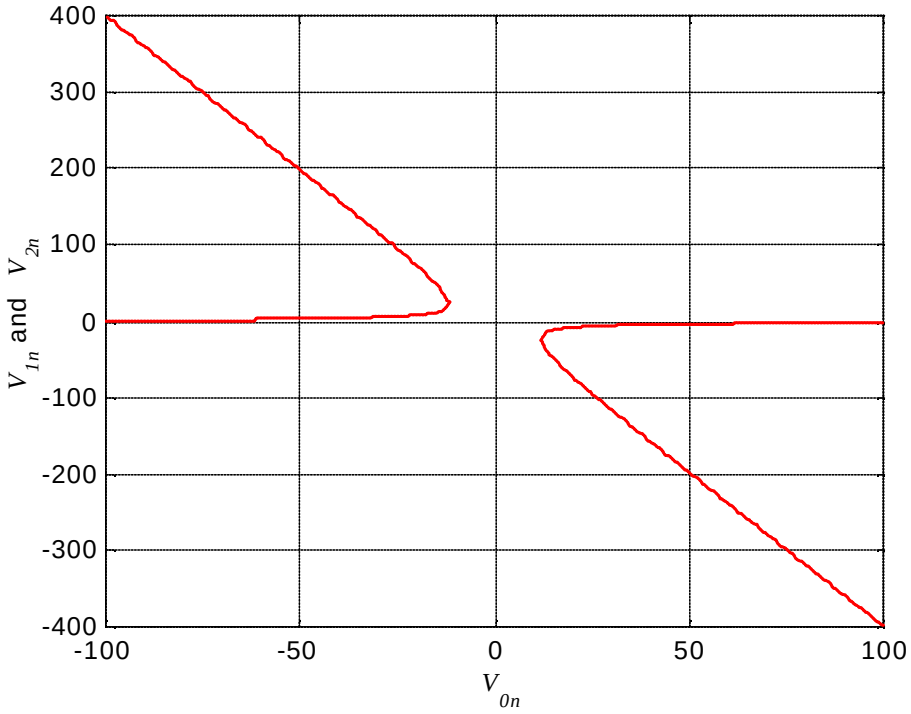

Figure 4-1 Normalized collector charges for a range of combiner charges for the 3-satellite, x-axis aligned formation.

Given any combiner charge, there exist two collector charges, one being much smaller in magnitude than the other. It is clear that the sign of the collector voltage must be opposite that of the combiner. Furthermore, the solutions on the negative V_{on} axis are the same as on the positive V_{0n} axis except for a difference in sign.

Better resolution on the solutions is obtained by examining them on a log-log plot as shown in Figure 4-2.

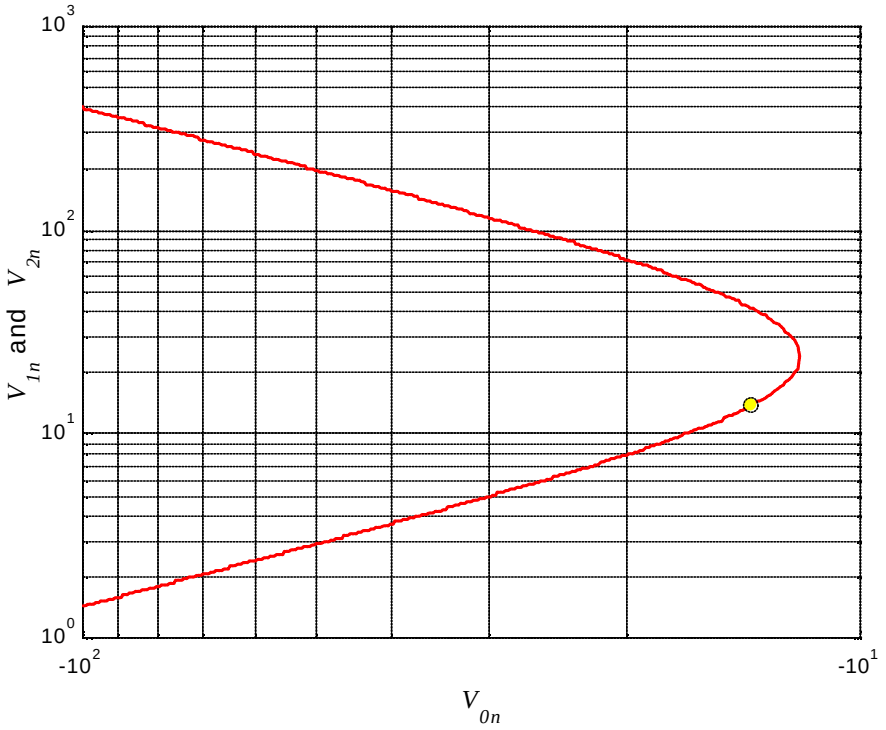

Figure 4-2 Collector equilibrium charges for negative combiner charges using a log-log scale. An "optimal" charge set is shown with the yellow dot.

If the combiner and collector have equal charging capability, then it may be prudent to find the lowest charge solution. This is obtained analytically by solving Eqn. 4-1 with the added constraint that $V_{1n} = -V_{0n}$, that is,

Eqn. 4-15
$$-V_{0n} = -2V_{on} - 2\sqrt{V_{on}^2 - 3k_c\Omega^2}$$

which gives

Eqn. 4-16
$$V_{0n} = 2\Omega\sqrt{k_c}$$

and is shown on Figure 4-2 as a yellow dot, and in normalized units is 13.8 for a geosynchronous orbit.

For a typical set of collector and spacing parameters

Eqn. 4-17
$$m = 150kg$$
$$L = 10m$$

the minimum collector charges would be

Eqn. 4-18
$$V_1 \cdot r = V_2 \cdot r = 2\Omega\sqrt{k_c} \cdot \sqrt{mL^3} = (13.8)(387.3) = 5.34kV \cdot m$$

where r is the collector radius.

4.1.2. Y-Axis Aligned Equilibrium Solutions

Here the three satellites are aligned along the combiner's y-axis as shown in Figure 3-3(b), the corresponding collector displacements are

Eqn. 4-19
$$y_1 = L$$
$$y_2 = -L$$
$$x_1 = x_2 = z_1 = z_2 = 0$$

where L is again the distance from the combiner to either collector.

Substituting Eqn. 4-19 into Eqn. 4-2 for $n = 2$, the unique equilibrium equations are simply

Eqn. 4-20
$$q_2 q_1 + 4q_0 q_1 = 0$$
$$q_1 q_2 + 4q_0 q_2 = 0$$

Since in this case there is no mass or separation dependency, charge normalization is not employed. In addition, there is no dependency on the combiner angular rate, Ω. The solution to Eqn. 4-20 is simply

Eqn. 4-21
$$q_1 = q_2 = -4q_0$$

or in terms of the collector voltages

Eqn. 4-22
$$V_1 = V_2 = -4V_0$$

where it is assumed that the radii of the collectors and the combiner are equal. This rather simple result is plotted in Figure 4-3 where it is noted that the trivial solution of setting all charges to zero and letting the formation free-fly is permitted.

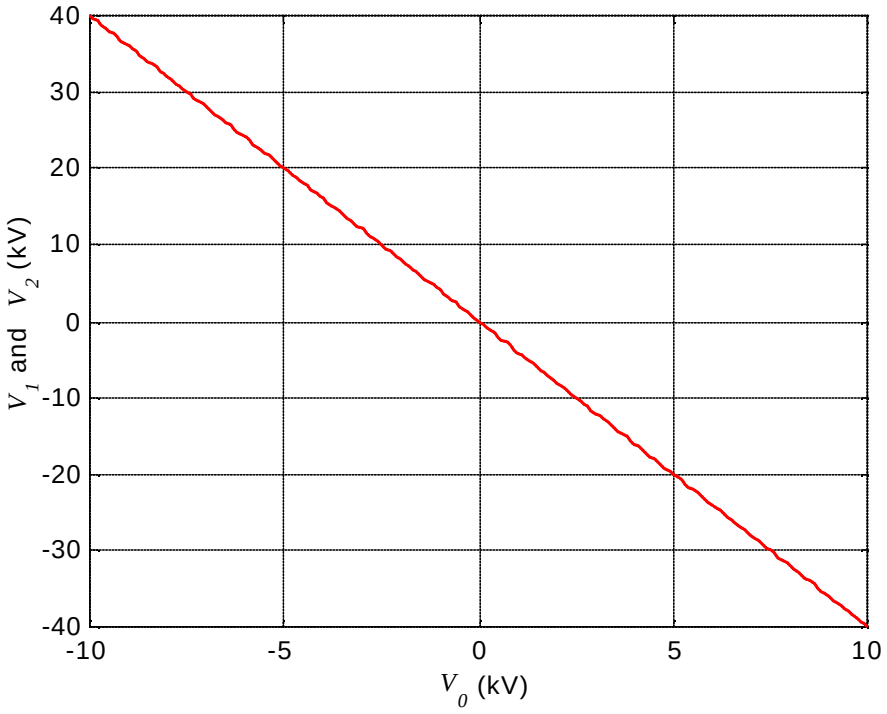

Figure 4-3 Collector voltages as a function of combiner voltage for the 3 satellite, y-axis aligned formation.

4.1.3. Z-Axis Aligned Equilibrium Solutions

Consider the 3 satellites aligned along the combiner's z-axis shown in Figure 3-3(c). The corresponding combiner displacements are

Eqn. 4-23

$$z_1 = L$$
$$z_2 = -L$$
$$x_1 = x_2 = y_1 = y_2 = 0$$

Substituting Eqn. 4-23 into Eqn. 4-2 and letting $n = 2$ yields only 2 unique equilibrium equations

Eqn. 4-24

$$\frac{k_c q_1 q_2}{4L^2} + \frac{k_c q_1 q_0}{L^2} - m_1 L \dot{?}^2 = 0$$
$$\frac{k_c q_1 q_2}{4L^2} + \frac{k_c q_2 q_0}{L^2} - m_2 L \dot{?}^2 = 0$$

which when normalized using Eqn. 4-8 and Eqn. 4-10 yield

Eqn. 4-25

$$V_{1n} V_{2n} + 4 V_{1n} V_{0n} - 4 k_c \Omega^2 = 0$$
$$V_{1n} V_{2n} + 4 V_{2n} V_{0n} - 4 k_c \Omega^2 = 0$$

assuming that the collector mass are equal as well as all spacecraft radii.

The solution to Eqn. 4-25 again requires that the two collectors have equal charge and is

Eqn. 4-26
$$V_{1n} = V_{2n} = -2V_{0n} \pm 2\sqrt{V_{0n}^2 + k_c \Omega^2}$$

Unlike the x-axis aligned case of Section 4.1.1 there is no constrain on the combiner charge. The normalized collector voltages are shown in Figure 4-4 for a range of combiner charges

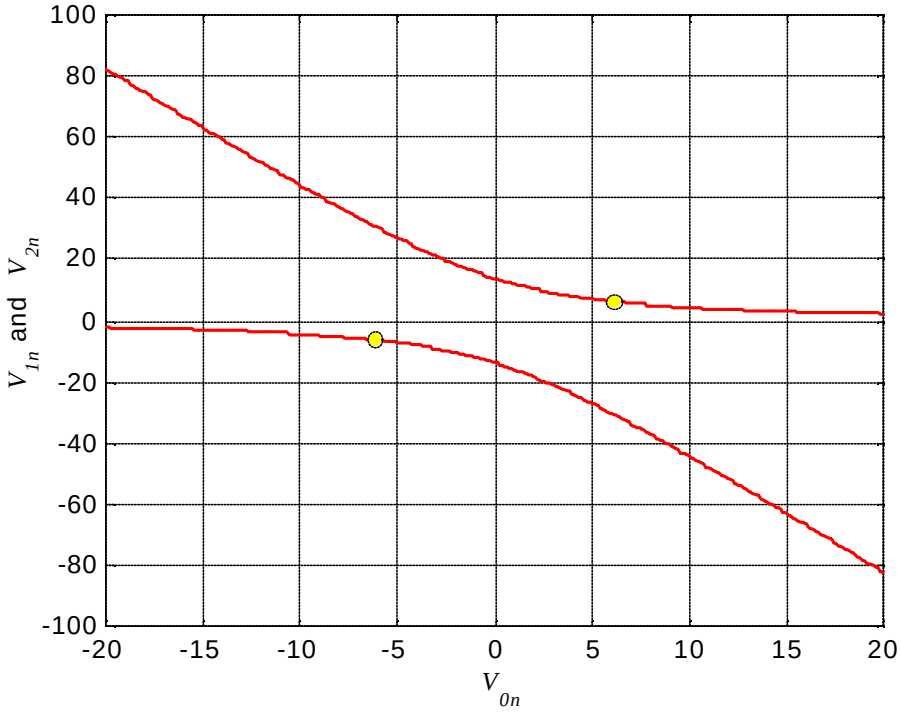

Figure 4-4 Normalized collector voltages for a range of combiner voltages for a geosynchronous orbit. The yellow dots indicate “optimal” voltages.

Similar to the x-axis aligned solution, there are two equilibrium voltages for any combiner voltage, one small and one large. However, the small charge solution is now of the same sign as the combiner, and the large charge solution of opposite sign. Assuming all the spacecraft have the same radius, an optimal normalized voltage can be computed by forcing the collector voltage to be equal to the combiner. This results in all spacecraft having the same voltage given by

Eqn. 4-27
$$V_{0n} = V_{1n} = V_{2n} = \pm\Omega\sqrt{\frac{4}{5}k_c}$$

and is 6.18 in voltage normalized units for geosynchronous orbit.

Using the same "typical" spacecraft and spacing parameters of Eqn. 4-17, the optimal spacecraft voltages, relative to their equal radii are

Eqn. 4-28 $$V_0 \cdot r = V_1 \cdot r = V_2 \cdot r = \pm\Omega\sqrt{\frac{4}{5}k_c} \cdot \sqrt{mL^3} = (6.18)(387.3) = 2.39kV \cdot m$$

4.2. Earth Orbiting Five Satellite Formation – Equilibrium

Consider the square, in-plane, 5-satellite formation shown in Figure 3-4. The relative position constraints

Eqn. 4-29
$$\begin{aligned} x_1 &= x_2 = x_3 = x_4 = 0 \\ y_1 &= y_3 = z_2 = z_4 = 0 \\ y_2 &= z_1 = -L \\ y_4 &= z_3 = L \end{aligned}$$

when substituted into the equilibrium equations (Eqn. 4-2) yields the following subset of unique necessary conditions for equilibrium.

Eqn. 4-30
$$\begin{aligned} & q_1 q_4 - q_1 q_2 = 0 \\ & \frac{k_c}{L^2}\left(q_0 q_1 + \frac{1}{4} q_1 q_3 + \frac{\sqrt{2}}{4} q_1 q_2 + \frac{\sqrt{2}}{4} q_1 q_4 \right) - mL\Omega^2 = 0 \\ & \frac{k_c}{L^2}\left(q_0 q_2 + \frac{1}{4} q_2 q_4 + \frac{\sqrt{2}}{4} q_1 q_2 + \frac{\sqrt{2}}{4} q_2 q_3 \right) = 0 \\ & -q_1 q_2 + q_2 q_3 = 0 \\ & q_3 q_4 - q_2 q_3 = 0 \\ & \frac{k_c}{L^2}\left(-q_0 q_3 - \frac{1}{4} q_1 q_3 - \frac{\sqrt{2}}{4} q_3 q_4 - \frac{\sqrt{2}}{4} q_2 q_3 \right) + mL\Omega^2 = 0 \\ & \frac{k_c}{L^2}\left(-q_0 q_4 - \frac{1}{4} q_2 q_4 - \frac{\sqrt{2}}{4} q_1 q_4 - \frac{\sqrt{2}}{4} q_3 q_4 \right) = 0 \\ & -q_1 q_4 + q_3 q_4 = 0 \end{aligned}$$

Two different analytical solutions were obtained. The first is trivial and consists of setting $q_2 = q_4 = 0$, resulting in the same z-axis aligned three satellite formation considered in Section 4.1.3. Applying this to Eqn. 4-30 results in

Eqn. 4-31
$$\begin{aligned} & \frac{k_c}{L^2}\left(q_0 q_1 + \frac{1}{4} q_1 q_3 \right) - mL\Omega^2 = 0 \\ & \frac{k_c}{L^2}\left(-q_0 q_3 - \frac{1}{4} q_1 q_3 \right) + mL\Omega^2 = 0 \end{aligned}$$

These are the same results of Eqn. 4-24 except, due to a collector numbering change between the 3 and 5 satellite formations, the subscripts of the 3 satellite system are

$$1 \rightarrow 3$$

$$2 \rightarrow 1$$

Thus, the solutions obtained for the z-axis aligned 3 satellite formation apply to this special case.

The second set of solutions assumes the following charge symmetry

Eqn. 4-32

$$q_1 = q_3$$
$$q_2 = q_4$$

resulting in only two unique equilibrium equations compared to 8 in the original set of Eqn. 4-30

Eqn. 4-33

$$\frac{k_c}{L^2}\left(q_0 q_3 + \frac{1}{4} q_3^2 + \frac{\sqrt{2}}{2} q_3 q_4 \right) - mL\Omega^2 = 0$$
$$\frac{k_c}{L^2}\left(q_0 q_4 + \frac{1}{4} q_4^2 + \frac{\sqrt{2}}{2} q_3 q_4 \right) = 0$$

Assuming a value of q_4, Eqn. 4-33 can be solved conditionally such that the q_1 and q_3 spacecraft charges have the form

Eqn. 4-34

$$q_1 = q_1(q_4)$$

Using these values of q_1, the combiner charge, q_0 can be expressed as

Eqn. 4-35

$$q_0 = q_0(q_1, q_4)$$

This procedure works equally well when the equilibrium equations are represented using the normalized voltages from Eqn. 4-8 and Eqn. 4-10,

Eqn. 4-36

$$4V_{0n}V_{3n} + V_{3n}^2 + 2\sqrt{2}V_{3n}V_{4n} - k_c\Omega^2 = 0$$
$$4V_{0n}V_{4n} + V_{4n}^2 + 2\sqrt{2}V_{3n}V_{4n} = 0$$

assuming all spacecraft are of equal radius.

The solutions for collector 1 and 3 normalized voltage are

Eqn. 4-37

$$V_{1n} = V_{3n} = \frac{1}{2}V_{4n} \pm \frac{1}{2}\sqrt{V_{4n}^2 - \frac{16}{2\sqrt{2}-1}k_c\Omega^2}$$

where V_{4n} (and similarly V_{2n}) must satisfy the constraint

Eqn. 4-38

$$V_{4n}^2 - \frac{16}{2\sqrt{2}-1}k_c\Omega \geq 0$$

Since V_{1n} and V_{3n} are known at this point, the combiner normalized voltage is readily computed from

Eqn. 4-39
$$V_{0n} = -\frac{1}{4}V_{4n} - \frac{\sqrt{2}}{2}V_{3n}$$

Figure 4-5 shows the two sets of V_{1n}, V_{3n} solutions to Eqn. 4-37, and the corresponding V_{0n} from Eqn. 4-39 for a range of V_{2n}, V_{4n} values satisfying the constraint of Eqn. 4-38 in a geosynchronous orbit. The red lines are the locus of solutions when V_{4n} is positive whereas the magenta lines are the solution loci for negative V_{4n}. Using the sum of the squared voltages as a cost function, an optimal charge set can be computed analytically as

Eqn. 4-40
$$V_{2n} = V_{4n} = \pm 4\Omega\sqrt{\frac{k_c}{2\sqrt{2}-1}}$$
$$V_{1n} = V_{3n} = \pm 2\Omega\sqrt{\frac{k_c}{2\sqrt{2}-1}}$$
$$V_{0n} = \mp\Omega\sqrt{\frac{k_c(3+2\sqrt{2})}{2\sqrt{2}-1}}$$

and are shown as yellow dots in Figure 4-5.

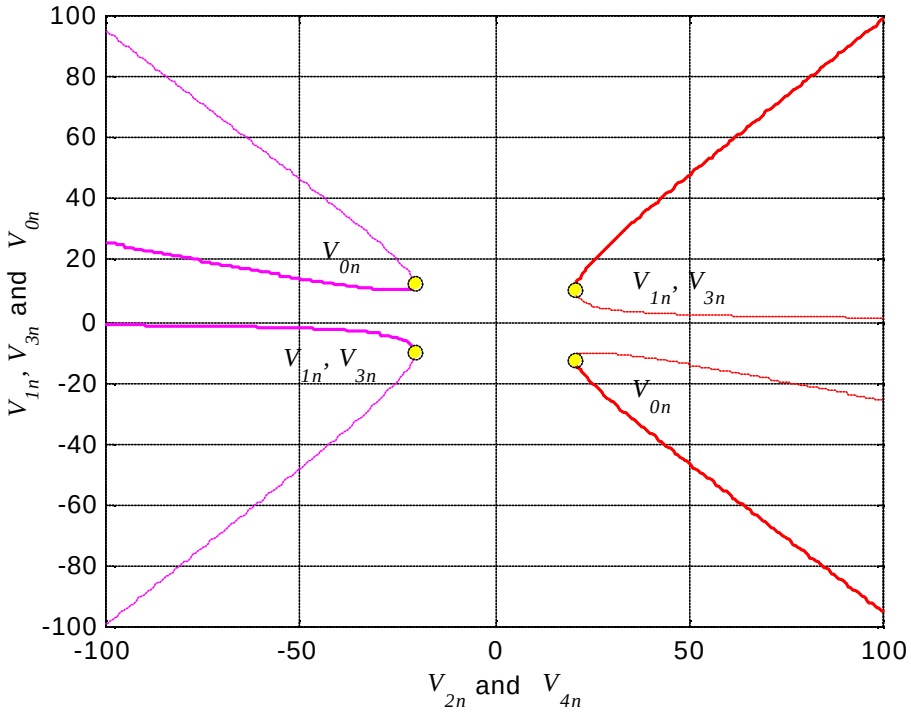

Figure 4-5 Normalized voltages of collectors 1 and 3, and the combiner for a range of acceptable collector 2 and 4 normalized voltages.

Using the "typical" spacecraft parameters of Eqn. 4-17, the actual spacecraft voltages, relative to their assumed equal radii, are

$$r \cdot V_2 = r \cdot V_4 = \pm 4\Omega \sqrt{\frac{k_c}{2\sqrt{2}-1}} \cdot \sqrt{mL^3} = \pm(20.45)(387.3) = \pm 7.92kV$$

Eqn. 4-41

$$r \cdot V_{1n} = r \cdot V_{3n} = \pm 2\Omega \sqrt{\frac{k_c}{2\sqrt{2}-1}} \cdot \sqrt{mL^3} = \pm(10.23)(387.3) = \pm 3.96kV$$

$$r \cdot V_{0n} = \mp\Omega \sqrt{\frac{k_c(3+2\sqrt{2})}{2\sqrt{2}-1}} \cdot \sqrt{mL^3} = \mp(12.34)(387.3) = \mp 4.78kV$$

4.3. Earth Orbiting Six Satellite Formation – Equilibrium

The equilibrium equations for the pentagon shaped formation, shown in Figure 3-5, were obtained by imposing the formation constraints

Eqn. 4-42

$$\begin{array}{lll} x_1 = 0 & y_1 = 0 & z_1 = L \\ x_2 = 0 & y_2 = L\sin(f) & z_2 = L\cos(f) \\ x_3 = 0 & y_3 = L\sin(2f) & z_3 = L\cos(2f) \\ x_4 = 0 & y_4 = L\sin(3f) & z_4 = L\cos(3f) \\ x_5 = 0 & y_5 = L\sin(4f) & z_5 = L\cos(5f) \end{array}$$

on Eqn. 4-2 where the central angle f is nominally 72°. Due to the lack of symmetry, the resulting 10 equilibrium conditions were too complicated to yield an analytical solution. Instead a numerical optimization approach was employed. The cost function J was defined as the sum of the squared residuals of Eqn. 4-2, that is

Eqn. 4-43

$$J = \sum_{i=1}^{5} (R_{yi}^2 + R_{zi}^2)$$

where

Eqn. 4-44

$$R_{yi} = \frac{k_c}{m_i} \sum_{j=0}^{5} \frac{(y_j - y_i)}{\left|\vec{p}_i - \vec{p}_j\right|^3} q_i q_j + y_i \Omega^2$$

$$R_{zi} = \frac{k_c}{m_i} \sum_{j=0}^{5} \frac{(z_j - z_i)}{\left|\vec{p}_i - \vec{p}_j\right|^3} q_i q_j - z_i \Omega^2$$

$$i = 1,...,5 \text{ and } i \neq j$$

where all the spacecraft masses were assumed to be equal.

The first approach was to fix the central angle at 72° and allow all 6 spacecraft charges to vary. MATLAB's sequential quadratic programming, constrained optimization code was then used to determine the "best" set of charges to minimize J. Unfortunately, there was inadequate degrees-of-freedom to permit a solution. The best value of J was only about 10% of the Ω^2 term in the residual equations. So, while a near-equilibrium solution could be found, there were not enough optimizable parameters to permit a solution.

The next approach was to increase the number of degrees-of-freedom by permitting near-pentagon formations. Specifically, the spacecraft were constrained to lie in a circle about the combiner, but were allowed to stray from the 72° central angle by 10%. The circle constraint maintained the integrity of the formation's imaging attributes while allowing the minimum cost function to be 3 orders of magnitude lower than the Ω^2 terms in the residuals. Although no proof is given to showing that these are true equilibrium solutions, it is likely.

Equilibrium *position* solutions for 4 different formation radii are shown in Figure 4-6 with the numerical values of the central angles given in Table 4-1. Again, the spacecraft radii were assumed equal, the orbit was geosynchronous, and the "typical" spacecraft parameters of Eqn. 4-17 were used. Normalization was not employed due to the spacecraft specific nature of the solution approach.

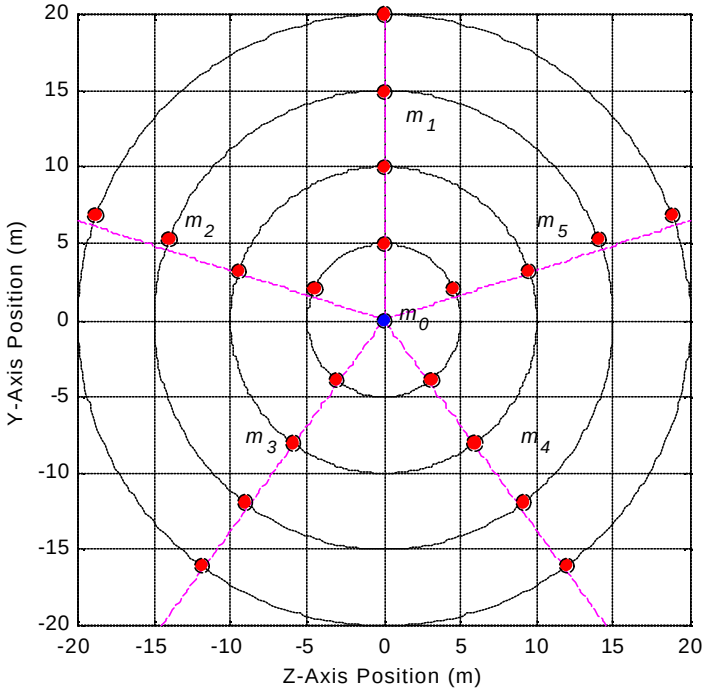

Figure 4-6 Equilibrium collector positions for 4 different radii from the combiner.

Distance	Central Angle			
L (m)	Phi 1 (72 deg)	Phi 2 (144 deg)	Phi 3 (216 deg)	Phi 4 (288 deg)
5	65.36	141.14	218.89	294.65
10	70.89	143.62	216.36	289.09
15	69.17	142.88	217.11	290.83
20	84.18	156.15	203.84	275.82

Table 4-1 Central angle results for 4 different radii.

The corresponding spacecraft specific voltages are plotted in Figure 4-7 with the numerical values given in Table 4-1. Examining the results indicates that collectors 2 and 5 and collectors 3 and 4 may require identical charge. However, this could not be shown analytically. Furthermore, when imposed as a constraint during optimization, this resulted in larger cost function solutions.

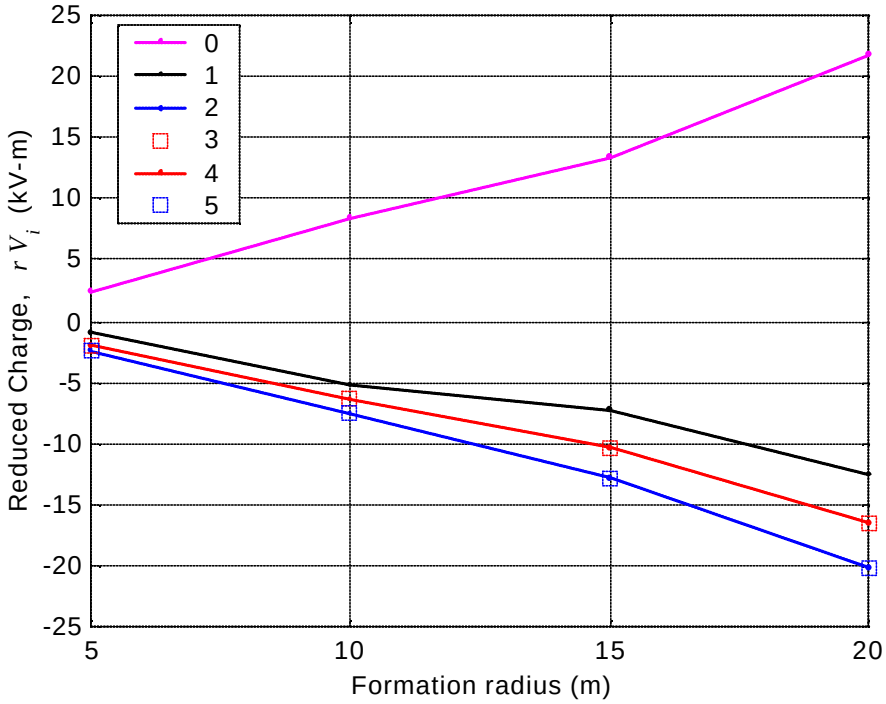

Figure 4-7 Spacecraft equilibrium reduced charges for 4 different formation radii.

Rad. (m)	Reduced Charge (m kV)					
	r V0	r V1	r V2	r V3	r V4	r V5
5	2.38	-1.00	-2.40	-1.99	-1.99	-2.40
10	8.47	-5.21	-7.56	-6.33	-6.33	-7.56
15	13.34	-7.19	-12.78	-10.35	-10.35	-12.78
20	1.18	-6.04	-25.55	-4.47	-4.47	-25.55

Table 4-2 Equilibrium solution spacecraft reduced charges for four different collector radii.

4.4. Libration Point Five Satellite Formation – Equilibrium

As discussed in Section 3, this case is different from those considered previously as the formation is not orbiting the Earth, but rather is at an Earth-Sun Libration point. The system of 5 spacecraft is shown in Figure 3-6 where it is assumed to rotate about the z-axis with angular rate Ω. The 15 equilibrium equations of Eqn. 4-3 are greatly simplified by enforcing the geometry constraints

Eqn. 4-45
$$\begin{aligned} x_1 &= L_1 \qquad x_2 = L_1 + L_2 \\ x_3 &= -L_1 \qquad x_4 = -L_1 - L_2 \\ y_1 &= y_2 = y_3 = y_4 = 0 \\ z_1 &= z_2 = z_3 = z_4 = 0 \end{aligned}$$

and imposing the symmetry requirements

Eqn. 4-46
$$\begin{aligned} m_1 &= m_3 \\ m_2 &= m_4 \\ q_1 &= q_3 \\ q_2 &= q_4 \end{aligned}$$

Only two unique equilibrium equations remain

Eqn. 4-47
$$\begin{aligned} &-m_1 L_1 \Omega^2 + \frac{k_c q_1 q_2}{L_2^2} - \frac{k_c q_0 q_1}{L_1^2} - \frac{k_c q_1^2}{4L_1^2} - \frac{2k_c q_1 q_2 L_1}{(2L_1 + L_2)^3} - \frac{k_c q_1 q_2 L_2}{(2L_1 + L_2)^3} \\ &-m_2 (L_1 + L_2)\Omega^2 - \frac{k_c q_1 q_2}{L_2^2} - \frac{k_c q_1 q_2}{(2L_1 + L_2)^2} - \frac{k_c q_2^2}{4(L_1 + L_2)^2} - \frac{k_c q_0 q_2}{(L_1 + L_2)^2} \end{aligned}$$

where L_1 is the distance between the combiner and collectors 1 and 3, and L_2 is the distance between collectors 1 and 2 (and also collectors 3 and 4). Both of these equations can be solved for $k_c q_0$, then equated yielding the single quadratic

Eqn. 4-48
$$a_2 q_2^2 + a_1 q_2 + a_0 = 0$$

where

$$a_2 = k_c q_1 \left(\frac{L_1^2}{L_2^2} - \frac{L_1^2}{(2L_1 + L_2)^2} + \frac{1}{4} \right)$$

Eqn. 4-49

$$a_1 = -m_1 L_1^3 \Omega^2 - k_c q_1^2 \left[\frac{(L_1 + L_2)^2}{L_2^2} + \frac{(L_1 + L_2)^2}{(2L_1 + L_2)^2} - \frac{1}{4} \right]$$

$$a_0 = m_2 (L_1 + L_2)^3 q_1 \Omega^2$$

Eqn. 4-48 can be solved for q_2 assuming a range of q_1 is known that satisfies the constraint

Eqn. 4-50

$$a_1^2 - 4a_2 a_0 \geq 0$$

For each q_1, q_2 pair, a unique q_0 can be obtained from either of the equilibrium conditions in Eqn. 4-47, such as

Eqn. 4-51

$$q_0 = \frac{L_1^2}{k_c} \left[\frac{-M_1 L_1 \dot{q}^2}{q_1} + \frac{k q_2}{L_2^2} - \frac{k q_1}{4L_1^2} - \frac{k q_2}{(2L_1 + L_2)^2} \right]$$

A specific example was considered with the following spacecraft and seperation parameters

Eqn. 4-52

$$m_0 = m_1 = m_3 = 150 kg$$
$$m_2 = m_4 = 150 kg$$
$$L_1 = 12.5 m$$
$$L_2 = 25 m$$

with all spacecraft radii being equal. Three different formation spin rates, Ω, were investigated

Eqn. 4-53

$$\Omega_1 = 0.5 \frac{rev}{hr} = \frac{p}{3600} \frac{rad}{\sec}$$
$$\Omega_2 = 0.05 \frac{rev}{hr} = \frac{.1p}{3600} \frac{rad}{\sec}$$
$$\Omega_3 = 0.005 \frac{rev}{hr} = \frac{.01p}{3600} \frac{rad}{\sec}$$

Specific spacecraft voltages are shown in Figure 4-8 (collectors 2 and 4) and Figure 4-9 (combiner) for a range of collector 1 and 3 voltages using the spin rate of Ω_1. An optimal solution was obtained resulting in the smallest charge across all spacecraft and is shown with yellow dots on the plots. The optimal spacecraft voltages for all spin rate cases are provided in

Table 4-3.

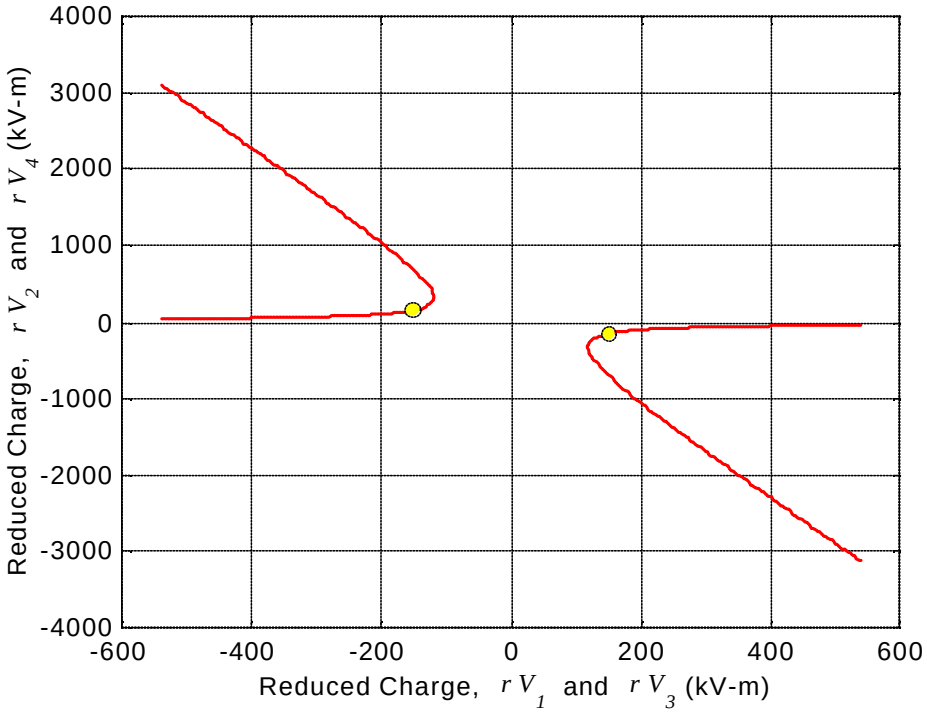

Figure 4-8 All sets of collector 2 and 4 reduced charges for a range of collector 1 and 3 charges. The yellow dot indicates the “optimal” solution resulting in the smallest charge across all spacecraft.

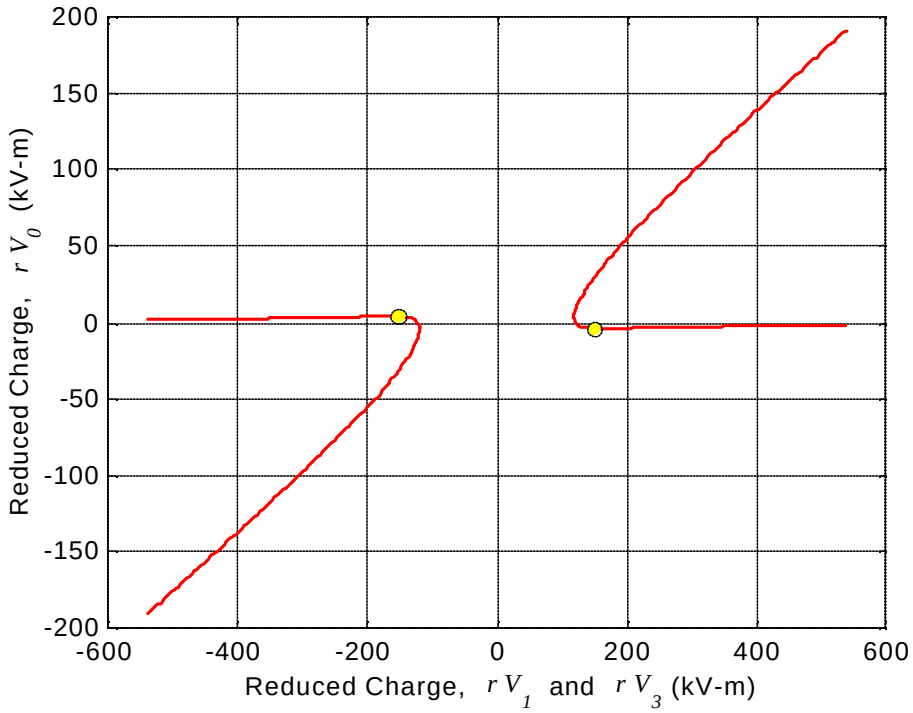

Figure 4-9 All sets of combiner reduced charges for a range of collector 1 and 3 charges. The yellow dot indicates the "optimal" solution resulting in the smallest charge across all spacecraft.

Spin Rate	Reduced Charge (m kV)				
(rad/s)	r V0	r V1	r V2	r V3	r V4
8.73E-06	3.73E-02	-1.52E+00	1.52E+00	-1.52E+00	1.52E+00
8.73E-05	3.73E-01	-1.52E+01	1.52E+01	-1.52E+01	1.52E+01
8.73E-04	3.73E+00	-1.52E+02	1.52E+02	-1.52E+02	1.52E+02

Table 4-3 Optimal reduced charges for all spacecraft using three different spin rates.

It is noted that for the "optimal" solutions obtained the condition

Eqn. 4-54
$$V_2 = -V_1$$

is required, resulting in a linear relationship between the spacecraft charges and the spin rate as observed in

Table 4-3. This will not be the case for other solutions.

4.5. Summary

Equilibrium spacecraft charges were computed for several formation examples. In theory, once the formation is placed in an equilibrium configuration, it should remain there. If the equilibrium state is stable, then the formation will return to it given small external perturbations.

For small numbers of spacecraft (up to 5) analytical solutions were readily obtained. A numerical optimization approach was developed for determining equilibrium solutions for formations with n spacecraft illustrated by the 6-satellite, pentagon-like formation of Section 4.3. Future work should address the equilibrium point stability question including active charge control for ensuring stability. One approach would be to modify the optimality criteria used for selecting a particular solution from the solution loci to include the relative stability metric.

5. Performance Evaluation of a Coulomb System

The purpose of this section is to evaluate some fundamental performance metrics of a Coulomb control system on a spacecraft formation. Aspects such as control force, input power, required consumable mass, and environment interaction will be calculated first for a simple two-spacecraft system, then later extended to a multiple-vehicle formation.

5.1. Two Body Analysis

Consider two spherical spacecraft having radii of r_{sc1}, r_{sc2}, separated by a distance of d from each other in a vacuum. Each vehicle uses some amount of active on-board power P, to generate a charge of q_{sc1} and q_{sc2} respectively. The spacecraft will then interact according to Coulomb's Law.

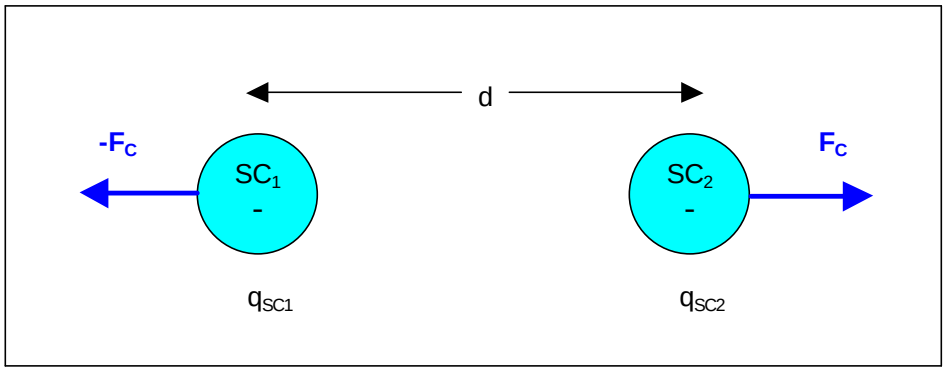

Figure 5-1. Schematic of two-vehicle interaction

We can express Coulomb's Law[43] as an equation giving the magnitude of the electric force between point charges.

Eqn. 5-1

$$F_o = \frac{1}{4 p e_0} \frac{| q_{SC1} \| q_{SC2} |}{d^2}$$

Where ε_0 the permittivity of free space, q_{SC1}, q_{SC2} are point charges at the centers of the spacecraft.

The potential of the spacecraft surface due to the internal charge can be easily evaluated from Gauss's law according to

Eqn. 5-2

$$V_{SC} = \frac{1}{4 p e_0} \frac{q_{SC}}{r_{SC}} .$$

By combining Eqn. 5-1 and Eqn. 5-2 we can write the magnitude of electric force between two spacecraft in vacuum as ,

Eqn. 5-3
$$F_0 = 4 \pi \varepsilon_0 \frac{r_{SC1} r_{SC2} | V_{SC1} \| V_{SC2} |}{d^2}.$$

For vehicles immersed in plasma, we must modify the vacuum force F_o, to account for the shielding effect of the free charges according to Eqn. 2-8 as follows,

Eqn. 5-4
$$F_c = F_0 e^{-d/\lambda_d} .$$

Combining Eqn. 5-3 with Eqn. 5-4 we get,

Eqn. 5-5
$$F_c = 4 \pi \varepsilon_0 e^{-d/\lambda_d} \frac{r_{SC1} r_{SC2} | V_{SC1} \| V_{SC2} |}{d^2}.$$

Where λ_d is the Debye length.

5.1.1. Power Required for Coulomb Force

As discussed previously in Section 2, an isolated spacecraft will assume an equilibrium potential (voltage) such that the net environmental current due to plasma and photoelectron emission is zero. It is possible to change the vehicle potential by emitting charge from the spacecraft. For example, if it is desired to drive the spacecraft potential lower than equilibrium (more negative), the emission of positive charge from the vehicle will cause a net surplus of on-board electrons and a lowering of the potential. In order to emit such a current, the charges must be ejected from the vehicle with sufficient kinetic energy to escape the spacecraft potential well. Thus, if the vehicle as at a (negative) potential $-V_{SC}$, then ions must be emitted from a source operating at a power supply voltage, V_{PS}, greater than $\|-V_{SC}|$. This is illustrated schematically in Figure 5-2.

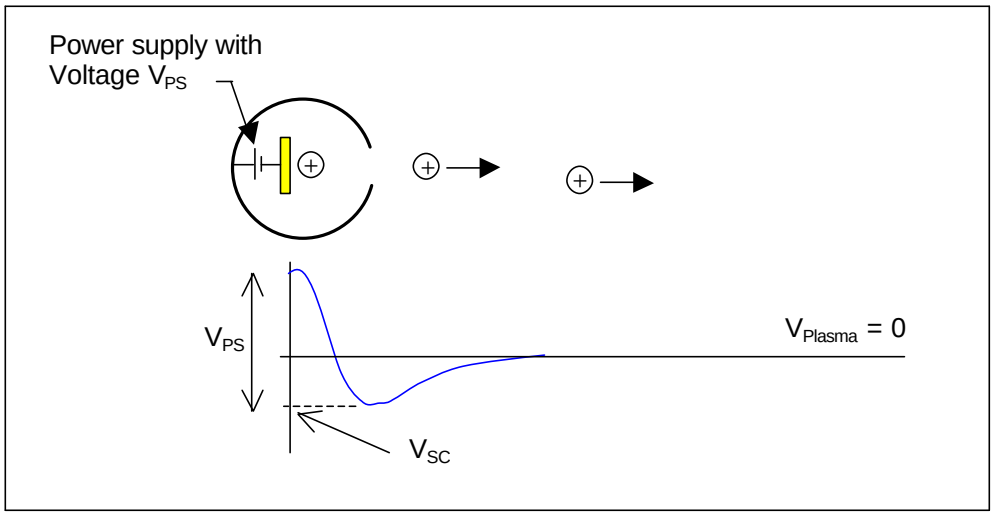

Figure 5-2. Schematic showing required voltages for charge emission from spacecraft. V_{PS} is the voltage of the on-board power supply. Top portion of figure represents ion emission system within spherical spacecraft, while bottom portion shows an aligned plot of electric potential on vertical axis with distance on horizontal axis.

While V_{PS} is greater than $|-V_{SC}|$ ions are able to escape the spacecraft, the net current to the spacecraft is *not* zero, and the potential of the vehicle will change. Once the spacecraft reaches a potential where $V_{SC} = -V_{PS}$, the emitted ions have insufficient energy to escape the spacecraft (they can't climb the potential hill) and the current is returned. This is demonstrated in Figure 5-3.

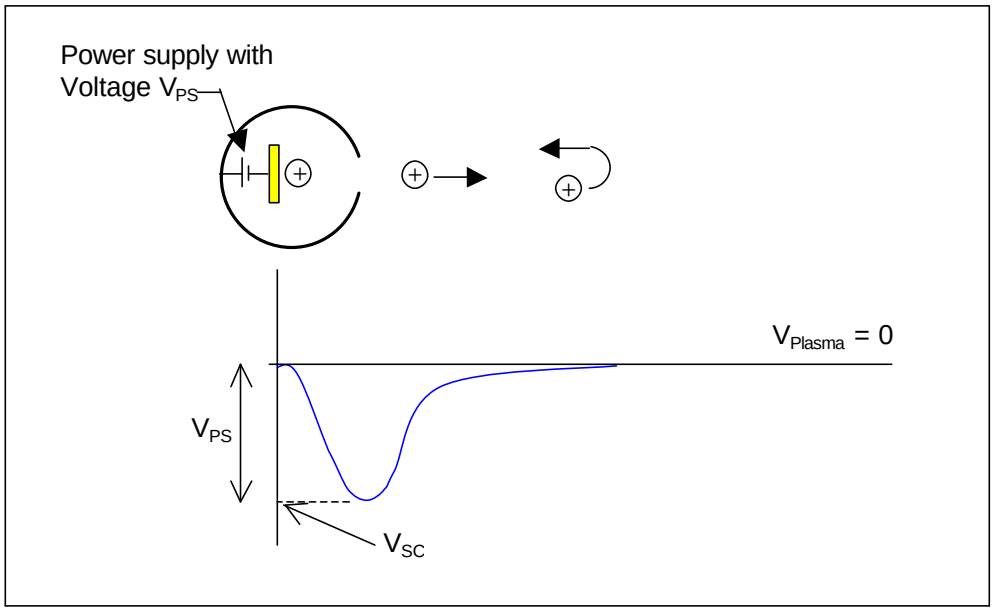

Figure 5-3. Vehicle potential will stabilize when V_{SC} reaches the value of $-V_{PS}$. Top portion of figure represents ion emission system within spherical spacecraft, while bottom portion shows an aligned plot of electric potential on vertical axis with distance on horizontal axis.

The spacecraft potential will thus stabilize at $V_{SC} = -V_{PS}$. At this increased negative potential, the vehicle will attract a larger amount of ion plasma current from the environment. If the increased ion current from the plasma reaches the spacecraft, the vehicle potential will increase slightly (become more positive), allowing some of the emitted ion current to escape the vehicle and restore the potential to the more negative value. Thus the emitted ion current, I_e, must be at least as large as the environmental ion current, $I_{environ}$, to maintain the vehicle at the steady state potential. If I_e were less than $I_{environ}$, the vehicle power supply would be insufficient to maintain the spacecraft potential at $V_{SC} = -V_{PS}$. The above discussion could easily be extended to include electron emission raising the vehicle potential to some positive value.

Basic concepts can be used to calculate the power required to maintain the spacecraft at some steady state potential. To maintain the spacecraft at a voltage of $|V_{SC}|$, current must be emitted in the amount of $|I_e| = 4\pi r^2 |J_p|$, where J_p is the current density to the vehicle from the plasma, using a power supply having voltage of at least $|V_{PS}| = |V_{SC}|$. Quantitatively,

Eqn. 5-6
$$P = | V_{SC} I_e | .$$

For a two-spacecraft system with each vehicle using Power P, the total system power is just the sum of the individual power to each vehicle. Combining Eqn. 5-6 with Eqn. 5-5 gives,

Eqn. 5-7
$$F_C = 4\pi\varepsilon_0 \, e^{-d/\lambda_d} \, \frac{r_{SC1} r_{SC2} P^2}{d^2 I_{e1} I_{e2}} .$$

Eqn. 5-7 shows how to determine the required system power to maintain a steady-state Coulomb force in a given plasma environment. Since the space environment is constantly changing due to solar events and other phenomena, we must calculate the transient response characteristics of the Coulomb control force. To simplify the analysis we will eliminate the solar array from the equivalent circuit in SEE program and assume that the spacecraft (i.e. just chassis) is just a sphere of radius r m. The circuit diagram is shown in Figure 5-4. Thus we have eliminated the node, which was at potential V_B i.e. cover glass potential and in turn the capacitances C_B and C_{AB}, current I_B in the SEE program model. Now we have only two nodes: ground, which is at plasma potential V_p (i.e. V = 0 in SEE program model) and spacecraft chassis, which is at potential V_{SC} (i.e. V_A in SEE program model). C (i.e. C_A in SEE program model) is capacitance of the spacecraft. It is given by

Eqn. 5-8
$$C = 4\pi\varepsilon_0 r$$

where r is the radius of the spacecraft. I (i.e. I_A in SEE program model) is the resultant net current to the spacecraft. It is the sum of ion current, electron current, photoelectron current and control current (or emission current). It is given by

Eqn. 5-9

$$I = 4 \pi r^2 J_p + I_e$$

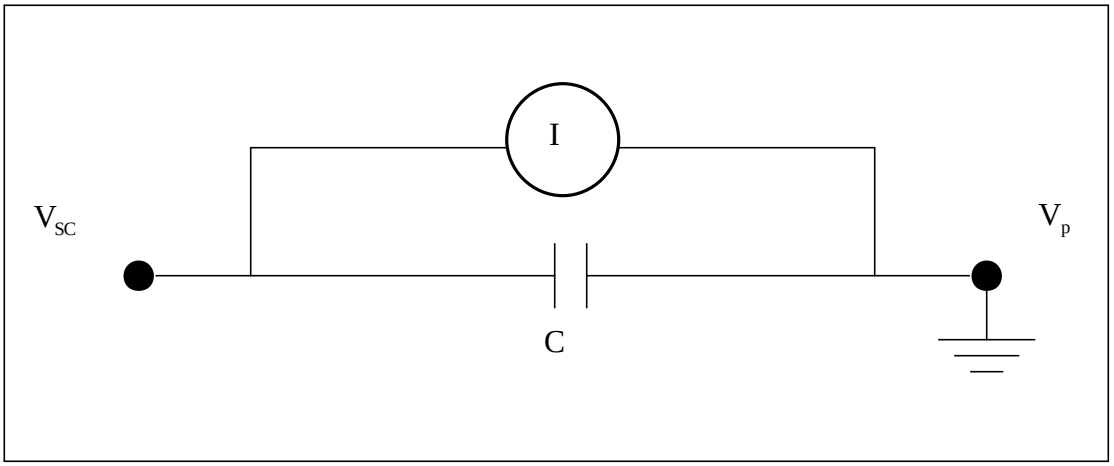

Figure 5-4. Equivalent circuit model for spacecraft and surrounding plasma

If this sum is zero, then the net current is zero; there won't be any change in the spacecraft potential because

Eqn. 5-10

$$\frac{dV_{SC}}{dt} = \frac{4 \pi r^2 J_p + I_e}{C} \quad .$$

So if we adjust $I_{control}$ such that dV/dt is not zero, we can change the potential of the spacecraft and thus dither the control force. From the above circuit, Eqn. 2-17, and Eqn. 2-18, we can write the governing equation for the spacecraft potential:

Eqn. 5-11

If $V_{SC} < 0$,

$$\frac{dV_{sc}}{dt} = \frac{I}{C} = \frac{I_e + 4 \pi r^2 J_p}{4 \pi \varepsilon_0 r}$$

$$= \frac{I_e + 4 \pi r^2 \left\{ J_{e0} \exp\left[\frac{-e|V_{sc}|}{k_B T_e} \right] - J_{i0} \left[1 + \frac{e|V_{sc}|}{k_B T_i} \right] - J_{pe0} \right\}}{4 \pi \varepsilon_0 r}$$

Eqn. 5-12 If $V_{SC} > 0$,

$$\frac{dV_{sc}}{dt} = \frac{I}{C} = \frac{I_e + 4\pi r^2 J_p}{4\pi \varepsilon_0 r}$$

$$= \frac{I_e + 4\pi r^2 \left\{ J_{e0}\left[1 + \frac{eV_{sc}}{k_B T_e}\right] - J_{i0}\exp\left[\frac{-eV_{sc}}{k_B T_i}\right] - J_{pe0}\exp\left[\frac{-eV_{sc}}{k_B T_{pe}}\right]\left[1 + \frac{eV_{SC}}{k_B T_{pe}}\right]\right\}}{4\pi \varepsilon_0 r}$$

Where J_{e0}, J_{i0} and J_{pe0} can be calculated from Eqn. 2-13, Eqn. 2-14, and Eqn. 2-15 respectively. We can solve this equation numerically to calculate the transient charging response of the spacecraft. If V_f is the desired final voltage, then the emission current must be emitted with energy at least equal to V_f. Once the vehicle reaches $V_{sc}=V_f$ the emission current will be extinguished and the potential will stabilize. Thus, the emission current can be written in terms of the emission power supply voltage $I_e=P_{ps}/V_f$. Consider a simple spherical spacecraft of radius 0.5 m, with V_f=6kV and exposed to average GEO plasma. A typical photoelectron current J_{pe0} is on the order of 10 μA/m^2 and temperature of photoelectrons on the order of spacecraft material work function (around 4.5 eV for most materials). The spacecraft potential V_{SC} is plotted against time at various levels of power P_{PS} of the emission system assuming the initial potential to be zero as shown in Figure 5-5. It can be seen that for only 200 mW of system power the vehicle can be charged to a potential of 6 kV within 8 msec. Faster charging times are enabled with a larger power investment.

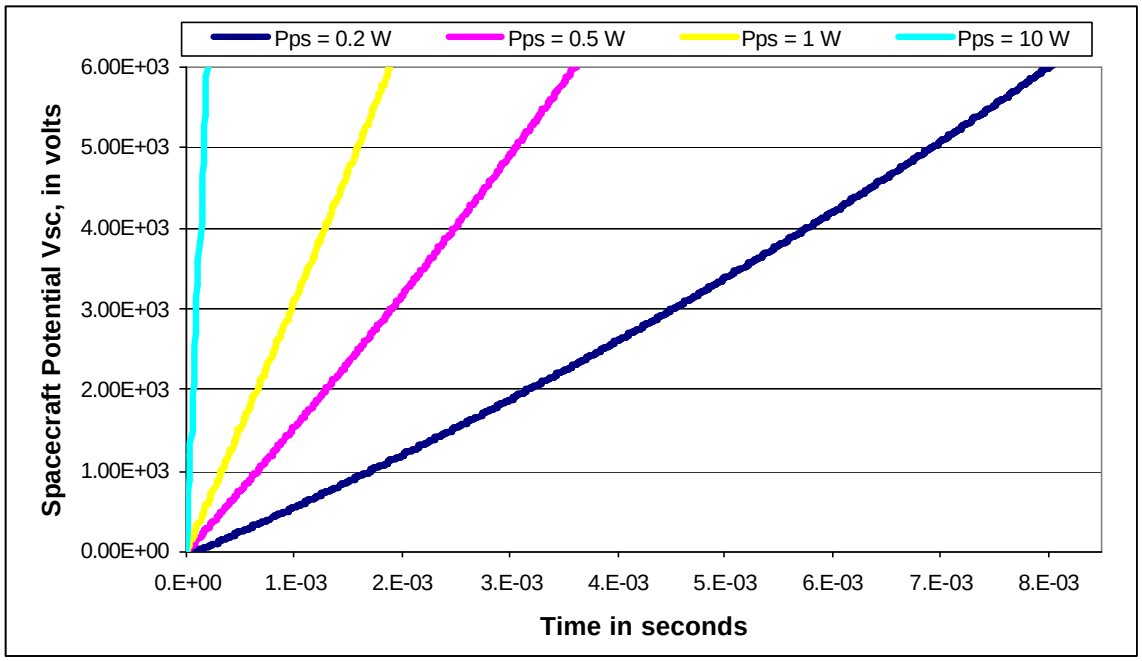

Figure 5-5. Plot of spacecraft potential V_{SC} against time, at different levels of power of the ion emitting gun P_{PS}.

5.1.2. Mass Flow Rate For Coulomb Control System

Coulomb control is fundamentally a propellantless concept. However, vehicle charge control will require some amount of consumables. For instance, driving the spacecraft charge negative requires the active emission of positive charge. This is accomplished by a beam of gaseous ions.

Mass flow rate is then the mass of gaseous ions expelled out per unit time to maintain potential of the SC. As electrons have negligible mass we can say that mass flow rate of electrons is negligible and thus driving the potential positive requires zero mass flow. If I_e is the emission current constituting ions, m_{ion} is the mass of ion, and q_{ion} is the charge, then mass flow rate is given by,

Eqn. 5-13

$$\dot{m} = \frac{I_e m_{ion}}{q_{ion}}.$$

Since the only purpose of the ion emission is to carry charge form the vehicle, it makes sense to use the least massive ions that are practical.

For the two spacecraft combination, propellant mass flow rate will be the sum of mass flow rates for individual spacecraft.

Eqn. 5-14

$$\dot{m}_{Total} = \dot{m}_{SC1} + \dot{m}_{SC2} = \frac{I_{e1}\, m_{ion}}{q_{ion}} + \frac{I_{e2}\, m_{ion}}{q_{ion}}$$

$$\dot{m}_{Total} = \frac{m_{ion}}{q_{ion}}\left(I_{e1} + I_{e2}\right).$$

5.1.3. Specific Impulse of a Coulomb System

A common performance parameter used for propulsion systems is specific impulse I_{sp} This parameter compares the thrust derived from a system to the required propellant mass flow rate.[44] Although I_{sp} is traditionally used as a parameter to evaluate momentum transfer (rocket) systems, we can use the formal definition to compare the Coulomb system. For a Coulomb control system the specific impulse I_{sp} is given by

Eqn. 5-15

$$I_{sp} = \frac{F}{\dot{m}_{Total} g_0}$$

Since Coulomb force calculations are meaningless for a single vehicle, we will treat the system as two separate vehicles, each subject to a force of F_c given by Eqn. 5-7, so that the sum of the forces experienced by all spacecraft in the formation is $F=2F_c$.

Eqn. 5-16

$$I_{sp} = \frac{8\, p\, e_0\, e^{-d/?_d}\, q_{ion}}{g_0\, m_{ion}} \frac{r_{SC1}\, r_{SC2}\, P^2}{d^2\, I_{e1}\, I_{e2}\, (I_{e1} + I_{e2})}$$

Where g_0 is the gravitational constant. If $r_{sc1} = r_{sc2} = r_{sc}$, and $I = I_{e1} = I_{e2}$, then Eqn. 5-16 becomes,

Eqn. 5-17

$$I_{sp} = \frac{4\, p\, e_0 e^{-d/?_d} q_{ion}}{g_0 m_{ion}} \frac{r^2{}_{SC} P^2}{d^2 I_e{}^3}.$$

Note that, unlike a rocket system, the definition of I_{sp} of a coulomb system is meaningless for a single vehicle. For a formation of two spacecraft, Eqn. 5-17 indicates that the specific impulse of the formation is a function of the radii of the spacecraft, power supplied to the ion (electron) gun, the separation between the two spacecraft, the emission currents of both vehicles, and the mass of the charge carriers, m_{ion}.

Consider a two-spacecraft formation with identical 0.5-m-radius vehicles in the average GEO plasma environment charged to the same negative potential. In order to reach and maintain this negative potential, the vehicles must emit an ion current. Consequently, the spacecraft will attract ion saturation current from the plasma, so I_e must be equal to I_{i0} for steady state. It is apparent that light ions will provide the most efficient I_{sp}, so assume that the emitted species is H^+. Calculated values of specific impulse for each vehicle in the formation is shown in Figure 5-6 for various system input power levels. For 1 mW systems with vehicle separation on the order of 20 m, I_{sp} values of 10^4 seconds are obtained, with values increasing to 10^{10} sec for just 1 W of power. It should be noted that for a positive vehicle potential the emitted species would be electrons and, thus, the calculated values of I_{sp} would be a factor of 2,000 greater.

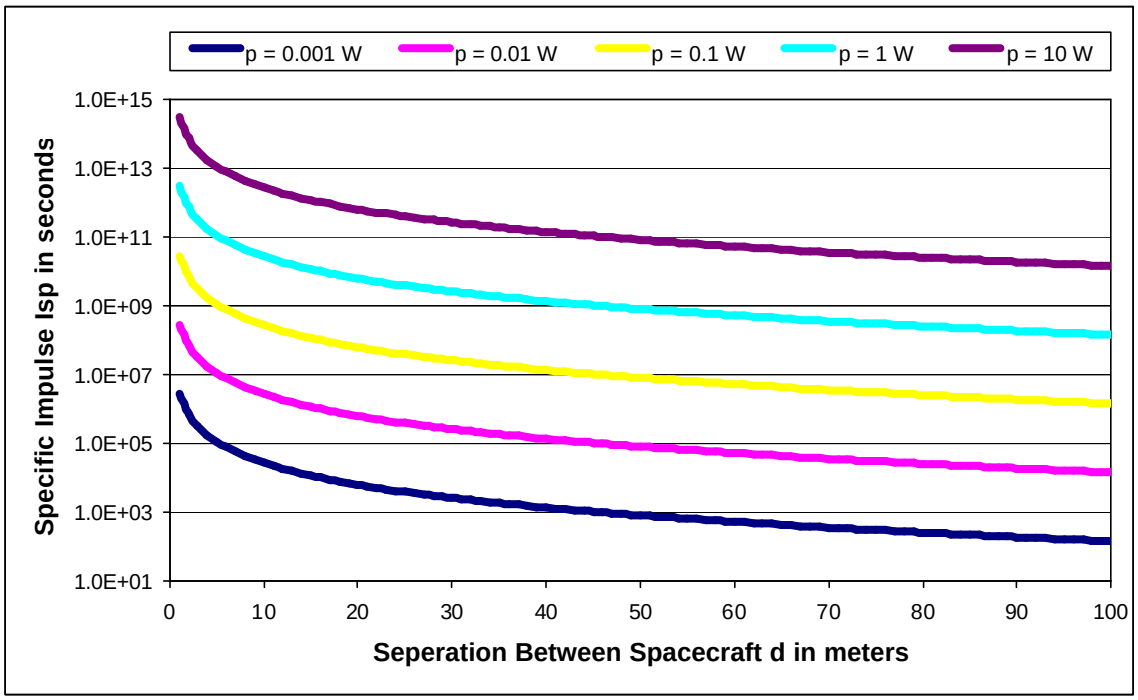

Figure 5-6. Graph of specific impulse for a 2 spacecraft formation as a function of spacecraft separation at different values of input power.

5.1.4. Emission Current Jet Force

Generating usable net charge on a spacecraft for Coulomb force requires the emission of current. In principle, the charge will be carried away from the vehicle by particles with non-zero mass. Such mass ejection will result in a momentum jet force on the vehicle as in a traditional electric propulsion thruster. In the case of electron emission, the mass of the charge carriers is insignificant and the resulting jet force is negligible. Ion emission, however, may produce a significant reaction force. It is instructive to consider how the Coulomb force between spacecraft compares with the momentum reaction on the vehicle induced by the beam of ion current.

The reactive thrust force of an ejected mass flow is computed as

Eqn. 5-18 $$F_J = \dot{m} u_e ,$$

where $\dot{m}$ is the ejected mass flow rate and u_e is the exhaust velocity at which the mass is emitted. Assuming steady state Coulomb force generation, the ions will be electrostatically accelerated through a potential of V_{SC}, such that

Eqn. 5-19 $$u_e = \sqrt{\frac{2 q_{ion} V_{SC}}{m_{ion}}} .$$

With this simplification and recognizing that the mass flow is related to the emission current via Eqn. 5-13, the momentum jet force of the emitted ion current is

Eqn. 5-20 $$F_J = I_e \sqrt{\frac{2 m_{ion} V_{SC}}{q_{ion}}} .$$

The jet force can also be written in terms of the input power to the emission system as

Eqn. 5-21 $$F_J = \sqrt{\frac{2 m_{ion} P I_e}{q_{ion}}} .$$

We can compare the magnitude of the jet reaction force with the induced Coulomb force between two vehicles. Assume identical spacecraft charged to the same value of V_{SC}. From Eqn. 5-7 and Eqn. 5-21 we can write the ratio of F_C/F_J (taking F_c as the total Coulomb force on both vehicles) in terms of the input power as

Eqn. 5-22 $$\frac{F_C}{F_J} = 4\sqrt{2}\, p\, e_0 \sqrt{\frac{q_{ion}}{m_{ion}}} \frac{r_{SC1}\, r_{SC2}\, P^{3/2}\, e^{\frac{-d}{?_d}}}{I_{e1}\, I_{e2}\, (I_{e1} + I_{e2})\, d^2} .$$

If $r_{sc1} = r_{sc2} = r_{sc}$, and $I = I_{e1} = I_{e2}$ then Eqn. 5-22 becomes,

Eqn. 5-23 $$\frac{F_C}{F_J} = 2\sqrt{2}\, p\, e_0 \sqrt{\frac{q_{ion}}{m_{ion}}} \frac{r_{SC}^{\,2}\, P^{3/2}\, e^{\frac{-d}{?_d}}}{I_e^{\,3}\, d^2} .$$

For a formation of two spacecraft, we find that the F_C/F_J ratio is a function of the radii of the spacecraft, power supplied to the ion (electron) gun, the separation between the two spacecraft and the emission currents of both of them. Similar to the calculations

for specific impulse, if we consider formation of two identical spacecraft in GEO having same radii of 0.5 m, charged to same high negative voltage V_{SC} and provided with same power P for each of them, they will draw same ion saturation current from the ambient plasma. So the (ion) emission current I_e will be also same. Figure 5-7 shows the ratio of Coulomb to jet force assuming hydrogen ion emission in average GEO plasma.

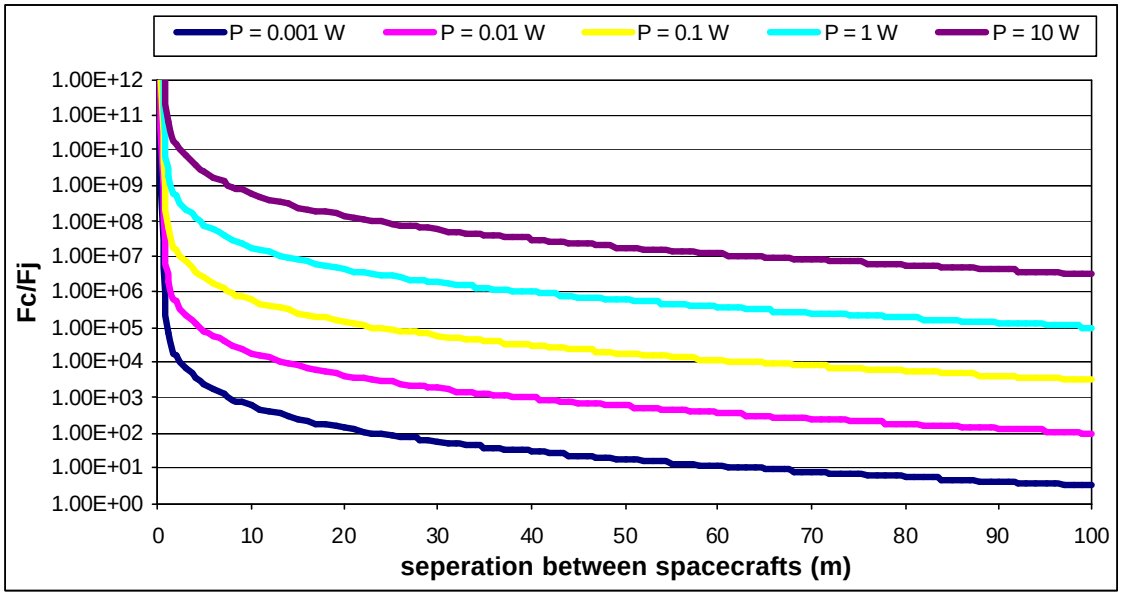

Figure 5-7. Graph of F_C / F_J Vs separation between spacecraft for 2 spacecraft formation at different levels of system power.

It can be seen that for separations up to 100 m and system power greater than 1 mW the Coulomb force is considerably higher than the jet force. This implies two conclusions: 1) the Coulomb force is a much wiser use of power than a mass-emitting EP thruster, and 2) the directional jet force will not be a significant perturbation to the Coulomb control system.

5.2. Multi-body Analysis

In this section we will see how to calculate the various parameters in section 5.1 for a general case with more than two spacecraft. Suppose we have n number of spacecraft. Let's assume that q_i are the charges on the spacecraft, r_i are the radii of the spacecraft, $d_{i,j}$ is the distance from spacecraft$_i$ to spacecraft$_j$, V_i are the voltages of the spacecraft; $\hat{d}_{i,j}$ is the unit vector along the line joining the centers of spacecraft$_i$ and spacecraft$_j$, directed from spacecraft$_j$ to spaceraft$_i$.

For steady state operation, the emission current from each vehicle must balance the environmental current to maintain desired potential:

Eqn. 5-24
$$I_{(e)\,i} = I_{(environ)\,i}$$

The total power required for the entire system to maintain steady state is,

Eqn. 5-25
$$P_{(input)Total} = \sum_{i=1}^{n} P_{(input)i} = \sum_{i=1}^{n} |\, V_{(SC)\,i} \,|\, I_{(e)\,i}$$

The sum of coulomb forces F_i , acting on any spacecraft SC_i in the formation can be written as the vector sum,

Eqn. 5-26
$$F_i = F_{i,1} + F_{i,2} + \ldots\ldots\ldots + F_{i,n} = \sum_{\substack{j=1 \\ j\neq i}}^{n} F_{i,j}$$
$$= \frac{q_i}{4\,p\,e_0} \sum_{\substack{j=1 \\ j\neq i}}^{n} \frac{q_j}{d^2_{\,i,j}} \hat{d}_{i,j} e^{\frac{-d_{i,j}}{?_d}}$$

Total coulomb force F_C in the formation will be sum of all such F_i's,

Eqn. 5-27
$$F_C = \sum_{i=1}^{n} |\, F_i \,| = \frac{1}{4p\varepsilon_0} \sum_{i=1}^{n} \left| q_i \sum_{\substack{j=1 \\ j\neq i}}^{n} \frac{q_j}{d^2_{\,i,j}} \hat{d}_{i,j} e^{\frac{-d_{i,j}}{?_d}} \right| .$$

5.2.1. Total Mass Flow Rate For Coulomb Control System

As an upper bound for calculating the amount of consumables needed, we will assume all vehicles must emit ions. If emitting ions mass flow rate of any spacecraft F_i is given by Eqn. 5-13. For a formation, total mass flow rate for the coulomb control system,

Eqn. 5-28
$$\dot{m}_{Total} = \sum_{i=1}^{n} \dot{m}_i = \frac{m_{ion}}{q_{ion}} \sum_{i=1}^{n} I_{\,(e)\,i}$$

5.2.2. Specific Impulse of The Entire Coulomb System

Referring to Eqn. 5-27 and Eqn. 5-28, the specific impulse of entire coulomb formation, $I_{(sp)Total}$ will be,

Eqn. 5-29

$$I_{(sp)Total} = \frac{\sum_{i=1}^{n} |F_i|}{g_0 \sum_{i=1}^{n} \dot{m}_i}$$

$$I_{(sp)Total} = \frac{q_{ion}}{g_0 \, m_{ion} \, 4\pi e_0} \frac{\sum_{i=1}^{n} \left| q_i \sum_{\substack{j=1 \\ j \neq i}}^{n} \frac{q_j}{d^2_{i,j}} \hat{d}_{i,j} e^{\frac{-d_{i,j}}{\lambda_d}} \right|}{\sum_{i=1}^{n} I_{(e)i}}$$

5.3. Propulsion System Mass

In order to evaluate the utility of a Coulomb control system for a given mission, we must calculate the propulsion system mass required. System mass can be broken down into two categories: inert mass due to electrical power supplies, and propellant mass due to ion beam gas supply (if needed).

Inert mass of the Coulomb Control System is mass of power supply; electron, ion guns etc. We assume that inert mass of Coulomb control system m_{inert} is proportional to the power P of power supply.

Eqn. 5-30

$$m_{inert} \propto P$$
$$\therefore m_{inert} = \beta P$$

Where β is the constant of proportionality. It is the ratio of the mass of the coulomb control system I_{inert} to the input power required and it is measured in kg/W. ß is known as the specific mass of the coulomb control system. Eqn. 5-25 gives us the power required $P_{(input)\,Total}$, to keep the spacecraft voltages at steady state. So the inert mass of the coulomb formation is given by

Eqn. 5-31

$$m_{inert} = bP_{(input)Total} = b\sum_{i=1}^{n} P_{(input)i} = b\sum_{i=1}^{n} |V_{(SC)i}| \, I_{(e)i}$$

If τ is the mission lifetime, then from Eqn. 5-28 the total mass of fuel (propellant) required m_{fuel}, becomes,

Eqn. 5-32

$$m_{fuel} = \tau \, \dot{m}_{(fuel)Total} = \tau \sum_{i=1}^{n} \dot{m}_{(fuel)i} = \frac{\tau \, m_{ion}}{q_{ion}} \sum_{i=1}^{n} I_{(e)i}$$

Total mass of Coulomb control propulsion system m_{prop}, is the sum of inert mass of the coulomb control system and mass of fuel required over mission lifetime τ. Thus, we can write,

$$
\begin{aligned}
m_{prop} &= m_{inert} + m_{fuel} \\
&= b\sum_{i=1}^{n} |\, V_{(SC)\,i} \,|\, I_{(e)i} + \frac{t\ m_{ion}}{q_{ion}} \sum_{i=1}^{n} I_{(e)i} \\
&= \sum_{i=1}^{n} \left\{ I_{(e)\,i} \left[b \,|\, V_{(SC)\,i} \,| + \frac{t\ m_{ion}}{q_{ion}} \right] \right\} \\
&= \sum_{i=1}^{n} \left\{ I_{(e)\,i} \left[\frac{b \,|\, q_i \,|}{4\pi e_0 r_i} + \frac{t\ m_{ion}}{q_{ion}} \right] \right\}
\end{aligned}
$$

Eqn. 5-33

[43] See, for instance, Serwey, R. A., Beichner, R.J., "Physics for Scientists and Engineers with Modern Physics", Saunders College Publishing, 2000, pp 714.

[44] Ronald W. Humble, Gary N. Henry, Wiley J. Larson, "Space Propulsion Analysis And Design, revised", Space Technology Series, 1995, pp10.

6. Comparative Mission Analyses

The purpose of this chapter is to compare the performance of a Coulomb control system with more traditional EP thrusters under consideration for formation flying missions. The formations discussed in this study, namely three-spacecraft, five-spacecraft, and six-spacecraft Earth orbiting along with five-spacecraft rotating formation at a libration point will be analyzed Performance parameters such as total propulsion system mass, input power, and specific impulse will be compared.

6.1. Conventional EP Systems

The most likely thruster candidates for planned formation flying missions are micro pulsed-plasma thrusters (MicroPPT), Colloid thrusters, and Field-emission Electric Propulsion (FEEP) thrusters. A brief overview of the operating principles for each technology will be presented.

6.1.1. Micro Pulsed Plasma Thruster

MicroPPT is essentially an electromagnetic accelerator, which uses solid Teflon (Polytetrafluoroethylene-PTEE) bars as propellant. It is a pulsed thruster with characteristically very short pulse width of the order of tens of microseconds. The minimum amount of impulse that can be imparted to a spacecraft in one pulse (the impulse bit) can be as small as 2 micronewton-seconds. MicroPPTs can be characterized by I_{sp} = 500 sec, η = 2.6%, and power-specific mass of β = 0.37 kg/W.[45,46]

The most common types of PPTs are breech-fed, side-fed, and co-axial versions. Here we will focus on simple and more general breech-fed type, as shown in Figure 6-1. In order to fire a PPT, a capacitor is discharged, creating a large potential across the space between an anode and a cathode. This potential causes a surface breakdown (which is initiated at a semiconducting spark plug surface) on the face of a solid bar of Teflon propellant, ablating it and allowing an arc to pass through the outer, gaseous layer, ionizing it. This large current carrying arc induces a magnetic field around itself. So the Lorentz force ($I \times B$) acting on the ions upstream of the arc accelerates them downstream. In addition, there is a gas dynamic effect caused by the heating of the ablated Teflon by the arc.[47]

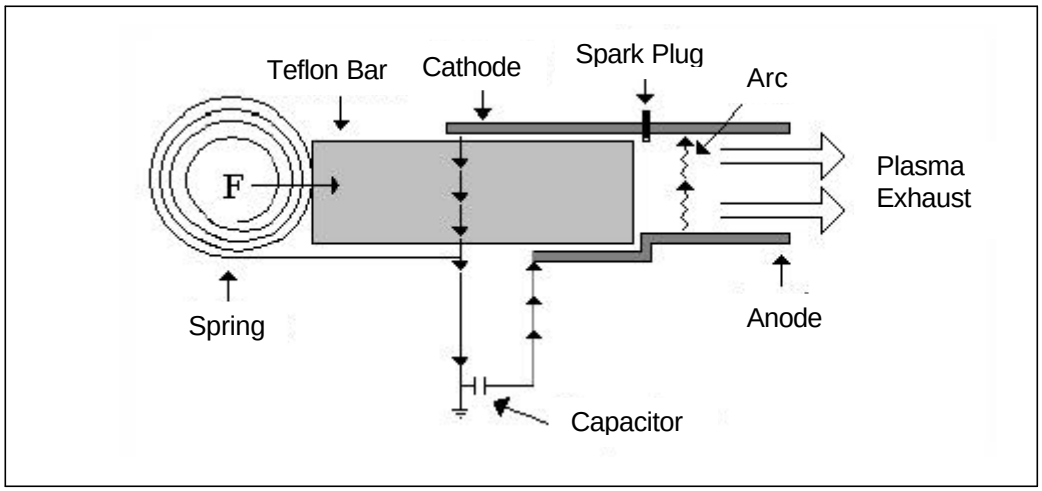

Figure 6-1. Breech-fed pulsed plasma thruster schematic.[47]

6.1.2. Colloid Thruster

A colloid thruster extracts charged droplets (and/or free ions) from an electrolytic liquid using strong electric fields. Common examples of propellant mixtures include combinations of formamide or glycerol as solvents and sodium iodide (NaI) or lithium chloride (LiCl) as solutes. Figure 6-2 shows a schematic of a single needle colloid emitter's main elements.

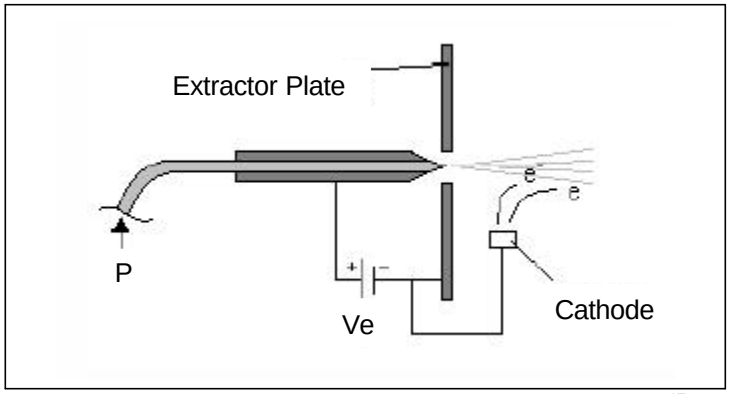

Figure 6-2. Single-needle colloid thruster schematic.[47]

The lightest gray shading represents the propellant, while the annular extracting plate and conducting needle are shown in a darker gray. A power supply is used to establish a voltage difference V_e between the extractor and needle creating an electrostatic attraction force on the surface of the fluid meniscus that forms at the needle exit. This force, balanced with the fluid surface tension and possible back pressure on the fluid results in the formation of a cone that emits a jet of droplets at its vertex. Then, these droplets are accelerated through the potential V_e to a high speed. Colloid thruster

performance can be characterized by I_{sp} = 1,000 sec, efficiency η = 65%, and power-specific mass β = 0.216 kg/W.[45]

6.1.3. Field Emission Electric Propulsion Thruster (FEEP)

Similar to the colloid thruster, the FEEP device extracts charged particles from a liquid propellant. The difference is in the propellant used and operating voltage range. Instead of electrolytic fluid, FEEP uses liquid phase metal, like cesium or indium because of their low ionization potential, high atomic weight and low melting point. Ions are directly extracted by field emission and subsequently accelerated down the electric potential. In order to overcome the ionization potential they need to be operated at higher voltages than the colloid thrusters.

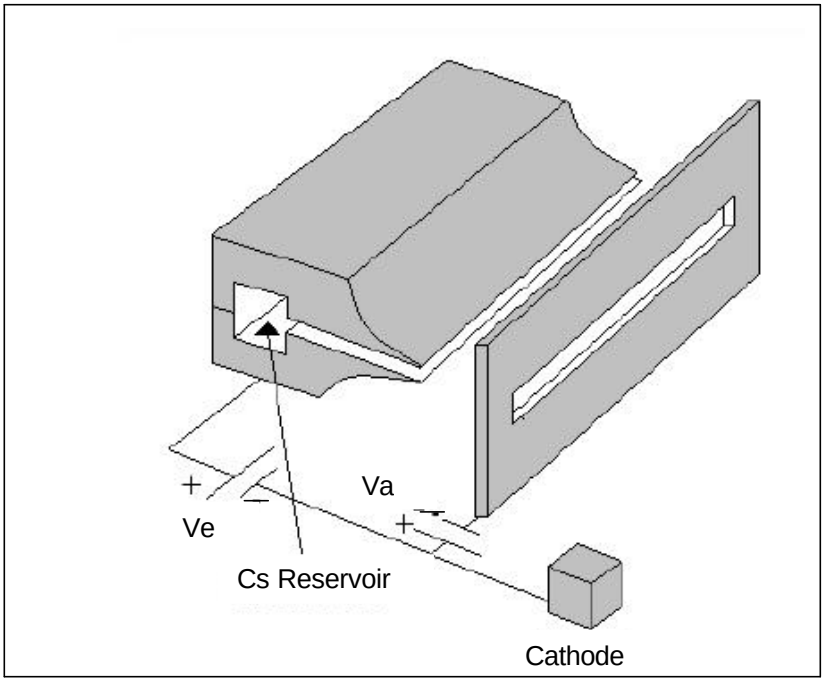

Figure 6-3. Schematic of Cesium FEEP thruster.[47]

The cesium FEEP thruster shown in Figure 6-3 consists of a slit shaped emitter which contains a propellant reservoir. Generally the slit is 1-2 microns high and 1 mm to several cm long. The extractor plate is biased at a negative potential of several kilovolts. The distance between the emitter and the extractor is greatly exaggerated for clarity. A neutralizer is also necessary since the beam consists only of ions.[47] The FEEP technology can be characterized with performance parameters of I_{sp} = 10,000 sec, efficiency η = 65%, and power-specific mass β = 0.11 kg/W.[45]

6.1.4. Mission Parameter Calculations for Thruster Technologies

Using traditional thruster performance parameters we can calculate propulsion system design metrics for the EP technologies. Of particular importance to any mission is the input power required by the system, the propellant mass, and the inert mass (consisting of power supplies, thruster hardware, etc.) necessary to maintain a formation. Considering n spacecraft in a formation, each using an EP thruster to maintain formation by exerting a thrust force T_i, the total thrust T_{Total} for the formation is,

Eqn. 6-1
$$T_{Total} = \sum_{i=1}^{n} | T_i |$$

The input power P_{input} can be calculated knowing the force required of each thruster, the efficiency of the thruster in converting electrical power to kinetic thrust power, and the specific impulse of the device. For the entire formation, the total power is

Eqn. 6-2
$$P_{(input)Total} = \sum_{i=1}^{n} P_{(input)i} = \sum_{i=1}^{n} \frac{| T_i | g I_{(sp)i}}{h_i}$$

where g is the gravitational constant, $I_{(sp)i}$ is the specific impulse of individual thruster, η_i is the efficiency of individual thrusters.

The inert mass of the thruster system m_{inert} is proportional to the power P of power supply.

Eqn. 6-3
$$m_{inert} \propto P$$
$$\therefore m_{inert} = ßP$$

Where β is a constant of proportionality known as the power-specific mass measured in kg/W. Eqn. 6-2 gives us the power required $P_{(input)\ Total}$ for the formation, so the inert mass of the thruster system is given by,

Eqn. 6-4
$$m_{inert} = bP_{(input)Total} = b \sum_{i=1}^{n} P_{(input)i} = bg \sum_{i=1}^{n} \frac{| T_i | I_{(sp)i}}{h_i}$$

If the mission lifetime is t, total impulse I_{Total} in the formation becomes,

Eqn. 6-5
$$I_{Total} = t\, T_{Total}$$
$$= \sum_{i=1}^{n} t | T_i |$$

The total mass of fuel required for the formation m_{fuel} for lifetime t will be,

Eqn. 6-6

$$m_{fuel} = \frac{I_{Total}}{g_0 I_{sp}} = \frac{t}{g_0} \sum_{i=1}^{n} \frac{|T_i|}{I_{(sp)i}}$$

The total mass m_{prop} for the electric thruster system will be sum of mass of fuel m_{fuel} and inert mass m_{inert},

Eqn. 6-7

$$m_{prop} = \sum_{i=1}^{n} |T_i| \left(\frac{bgI_{(sp)i}}{h_i} + \frac{t}{gI_{(sp)i}} \right)$$

6.2. Comparative Mission Trade Study

Six basic formation geometries were considered in this study (see Section 3), namely, three variations on three-satellite linear formations, one configuration consisting of five satellites in a plane, one configuration of five satellites in a pentagon formation with a center vehicle, and one rotating linear set of five spacecraft. For each of these formations, the required absolute potential (electric charge) to maintain a static formation using Coulomb control was computed. We can use these solutions to compare the performance of the Coulomb system with the three canonical EP thrusters described in Section 6.1. For this section of the report, we will consider all spacecraft to be 1-m-dia spheres with mass 150 kg (except the five-spacecraft rotating formation – see Section 4) operating for a mission time τ = 10 years.

Using Hill's equations to predict the required equilibrium formation forces and the performance characteristics of the three EP technologies, the relations Eqn. 6-2, Eqn. 6-4, and Eqn. 6-6 can be used to calculate the input power needed by the EP system, the inert mass required for the mission, and the propellant mass.

For the Coulomb system comparison, the fuel mass can easily be calculated from Eqn. 5-32 if the required emission current, I_e, is known. The emission current is chosen to balance the environmental current (net vehicle current equals zero) in order to maintain a steady potential on the spacecraft. The required vehicle potential for a given formation is found from the solution methods of Section 4. Since very general solutions were found for most cases, the "charge optimal" solutions represented by the yellow marker dots on the plots of equilibrium solutions were used to compute mission parameters (for instance, see Figure 4-2 for three-spacecraft case 'a'). Using the required vehicle potential, the net environmental current from the plasma is computed according to Eqn. 2-17 and Eqn. 2-18 assuming average GEO plasma conditions as outlined in Table 2-1, a photoelectron current density J_{pe0} = 10 μA/m^2, and a photoelectron temperature on the order of 5eV.

With the required emission current for each vehicle, $I_{(e)i}$, and vehicle potential, $V_{(sc)i}$, known, the system input power for each vehicle using Coulomb control is simply

$P_i = I_{(e)i} V_{(sc)i}$. In order to calculate the inert mass of the Coulomb system, it is necessary to know the value of the power-specific mass, β, in kg/W. Since the Coulomb technology does not yet exist, this number had to be estimated. Based on the similarity of the Coulomb system to the basic principles of electrostatic emission, such as that used in the Colloid thruster and FEEP, a value of β was chosen to be the average of the Colloid and the FEEP technologies, namely $\beta_{Coulomb}$ = 0.165 kg/W. As the Coulomb system does not need to convert electrical power to kinetic thrust power, the efficiency parameter η is not applicable. Although there will be some power loss in the controlling electronics, the amount is believed to be very small and thus an efficiency of unity is applied when calculating the Coulomb input power.

6.2.1. Earth Orbiting Three Spacecraft Formation

In order to investigate the dynamics of a Coulomb formation, very simple three-spacecraft geometries were studied. Three different combinations were specified depending upon the axis along which the spacecraft are aligned (see Section 3). In case a, the spacecraft are aligned along X axis as shown in Figure 6-4. The combiner spacecraft SC_0 is at the center of the Hill's coordinate frame and follows constant equatorial circular orbit. The collectors, i.e. SC_1 and SC_2, are along the X axis at a distance L=10 m from the combiner.

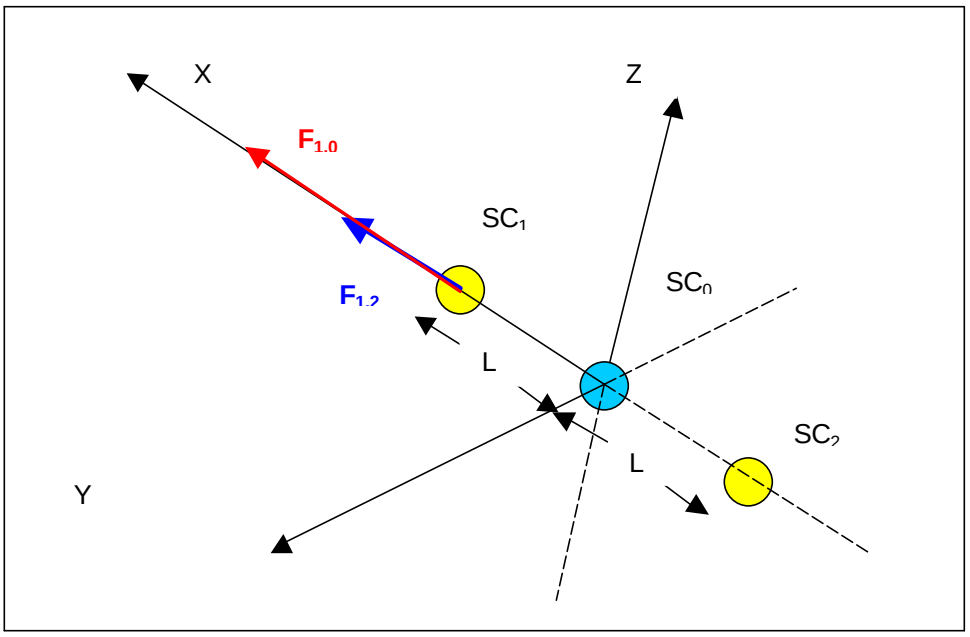

Figure 6-4. Coulomb forces acting on SC_1 in the 3 satellite formation aligned along x axis with respect to Earth. (Diagram not drawn to scale)

The Coulomb performance metrics are listed in Table 6-1 for each spacecraft in the formation case 'a'. Mission parameters of the entire formation using Coulomb control are compared to those using three canonical EP technologies in Table 6-2.

Graphical comparison between the total propulsion system mass as well as required input power is presented in Figure 6-5 and Figure 6-6.

As determined in Section 4, the three-spacecraft case 'b' permitted trivial solutions where the vehicles remained uncharged and no formation control force was required. However, an identical mission analysis is presented for the three-spacecraft case 'c' in Table 6-3, Table 6-4, and Figure 6-7 and Figure 6-8.

Parameters	**Numerical Values For Spacecraft**		
	SC_0	**SC_1**	**SC_2**
1.Charge q_i C	-2.97×10^{-7}	2.97×10^{-7}	2.97×10^{-7}
2.Radius r_i m	0.50	0.50	0.50
3.Emission Current Ie A	3.03×10^{-5}	-2.04×10^{-5}	-2.04×10^{-5}
4.Surface Voltage V_{SC} V	-5.34×10^{3}	5.34×10^{3}	5.34×10^{3}
5.Input Power P_{input} W	1.62×10^{-1}	1.09×10^{-1}	1.09×10^{-1}
6.Propellant Mass Flow Rate $\dot{m}$ kg/s	3.16×10^{-13}	1.16×10^{-16}	1.16×10^{-16}
7.Net Control Force F_i N	0.00	5.67×10^{-6}	5.67×10^{-6}

Table 6-1. Vehicle parameters calculated for the 3-spacecraft formation - Case 'a'.

Parameters	**Coulomb Control**	**MicroPPT**	**Colloid Thrusters**	**FEEP**
1.Specific Impulse Isp s	3.65×10^{6}	5×10^{2}	1×10^{3}	1×10^{4}
2.Efficiency ? %	N/A	2.6×10^{-2}	6.5×10^{-1}	6.5×10^{-1}
3.Fuel Mass for 10 Years m_{fuel} kg	9.99×10^{-5}	7.29×10^{-1}	3.64×10^{-1}	3.64×10^{-2}
4.Input Power P_{input} W	3.79×10^{-1}	2.14	1.71×10^{-1}	1.71
5.Specific Mass ß kg/W	1.65×10^{-1}	3.70×10^{-1}	2.16×10^{-1}	1.13×10^{-1}
6.Inert Mass m_{inert} kg	6.26×10^{-2}	7.92×10^{-1}	3.70×10^{-2}	1.92×10^{-1}
7.Total Mass m_{Total} kg	6.26×10^{-2}	1.52	4.01×10^{-1}	2.29×10^{-1}

Table 6-2. Comparison between Coulomb control system and three EP technologies for the 3-spacecraft formation - Case 'a'.

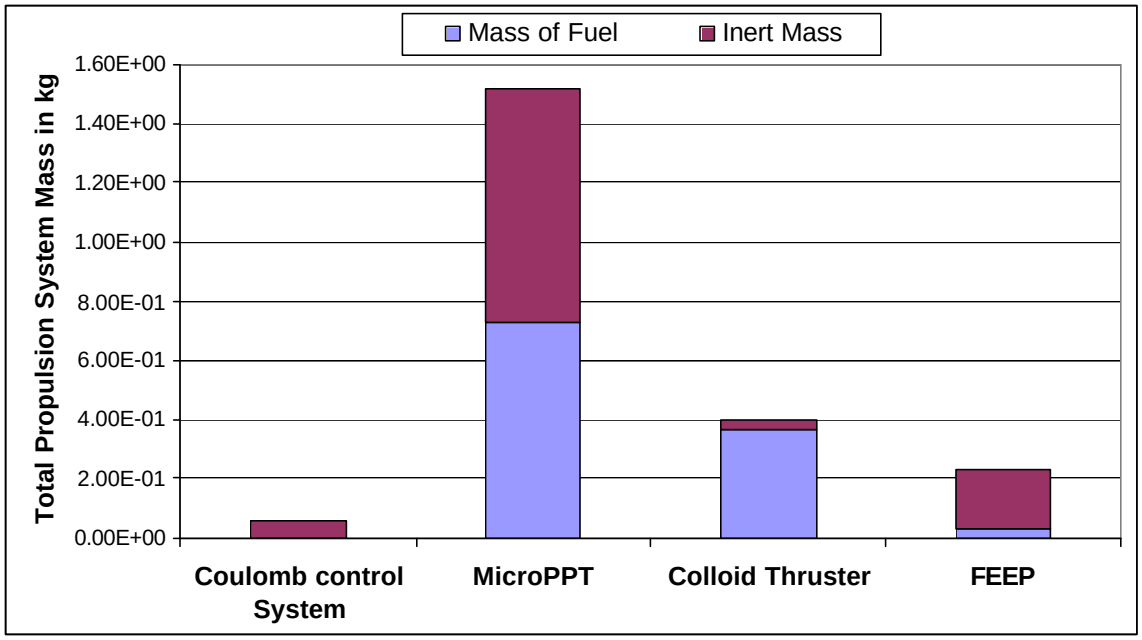

Figure 6-5. Total propulsion system mass for Coulomb control system and three EP technologies (3 spacecraft formation Case 'a').

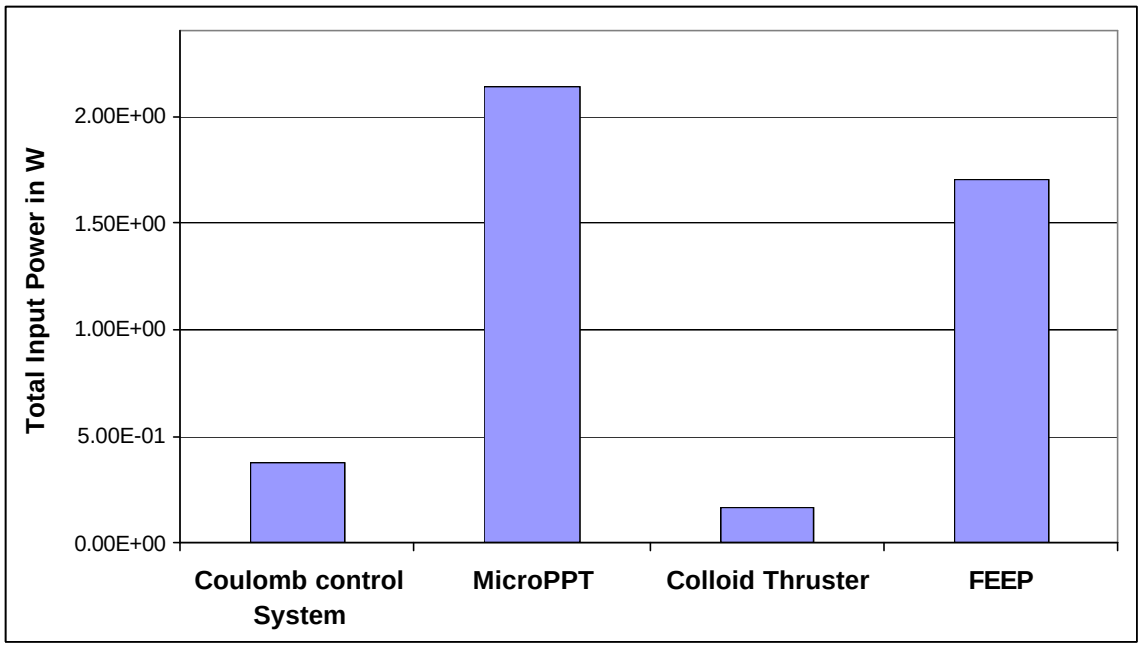

Figure 6-6. Total input power required to maintain formation for Coulomb control and three EP technologies (3 spacecraft formation Case 'a').

Parameters	Numerical Values For Spacecraft		
	SC_0	SC_1	SC_2
1.Charge q_i C	1.33×10^{-7}	1.33×10^{-7}	1.33×10^{-7}
2.Radius r_i m	0.50	0.50	0.50
3.Emission Current Ie A	-1.13×10^{-5}	-1.13×10^{-5}	-1.13×10^{-5}
4.Surface Voltage V_{SC} V	2.39×10^{3}	2.39×10^{3}	2.39×10^{3}
5.Input Power P_{input} W	2.69×10^{-2}	2.69×10^{-2}	2.69×10^{-2}
6.Propellant Mass Flow Rate $\dot{m}$ kg/s	6.40×10^{-17}	6.40×10^{-17}	6.40×10^{-17}
7.Net Control Force F_i N	0.00	1.82×10^{-6}	1.82×10^{-6}

Table 6-3. Vehicle parameters calculated for the 3-spacecraft formation Case 'c'.

Parameters	Coulomb Control	MicroPPT	Colloid Thrusters	FEEP
1.Specific Impulse Isp s	1.94×10^{9}	5×10^{2}	1×10^{3}	1×10^{4}
2.Efficiency ? %	N/A	2.6×10^{-2}	6.5×10^{-1}	6.5×10^{-1}
3.Fuel Mass for 10 Years m_{fuel} kg	6.05×10^{-8}	2.35×10^{-1}	1.17×10^{-1}	1.17×10^{-2}
4.Input Power P_{input} W	8.07×10^{-2}	6.88×10^{-1}	5.51×10^{-2}	5.51×10^{-1}
5.Specific Mass ß kg/W	1.65×10^{-1}	3.70×10^{-1}	2.16×10^{-1}	1.13×10^{-1}
6.Inert Mass m_{inert} kg	1.33×10^{-2}	2.55×10^{-1}	1.19×10^{-2}	6.20×10^{-2}
7.Total Mass m_{Total} kg	1.33×10^{-2}	4.90×10^{-1}	1.29×10^{-1}	7.37×10^{-2}

Table 6-4. Comparison between Coulomb control system and three EP technologies for the 3-spacecraft formation - Case 'c'.

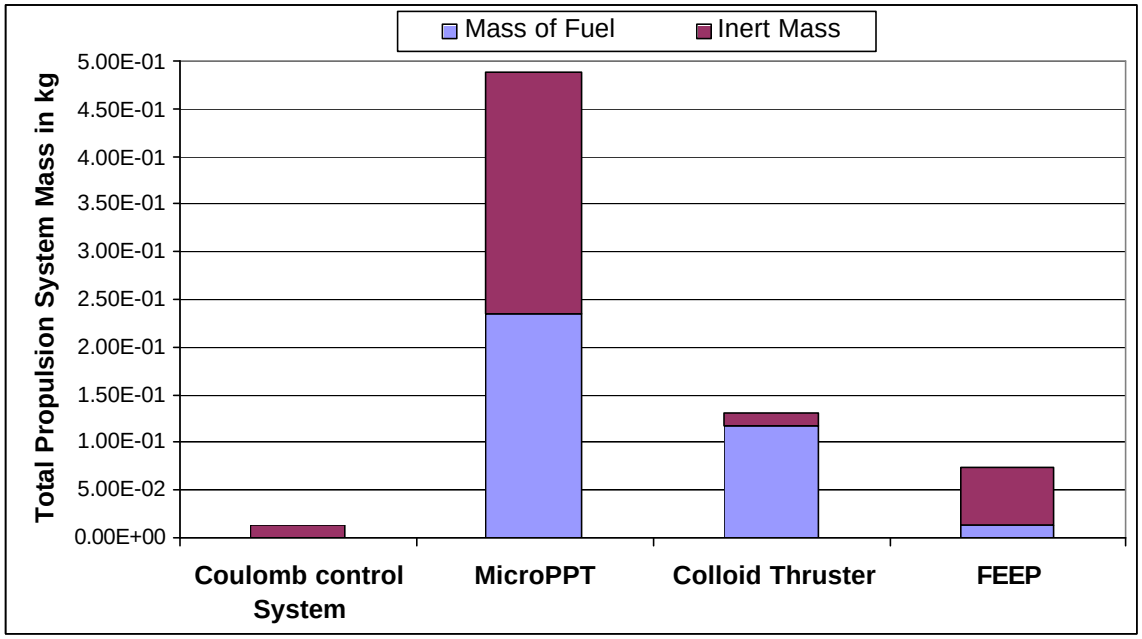

Figure 6-7. Total propulsion system mass for Coulomb control system and three EP technologies (3 Spacecraft Formation – Case 'c').

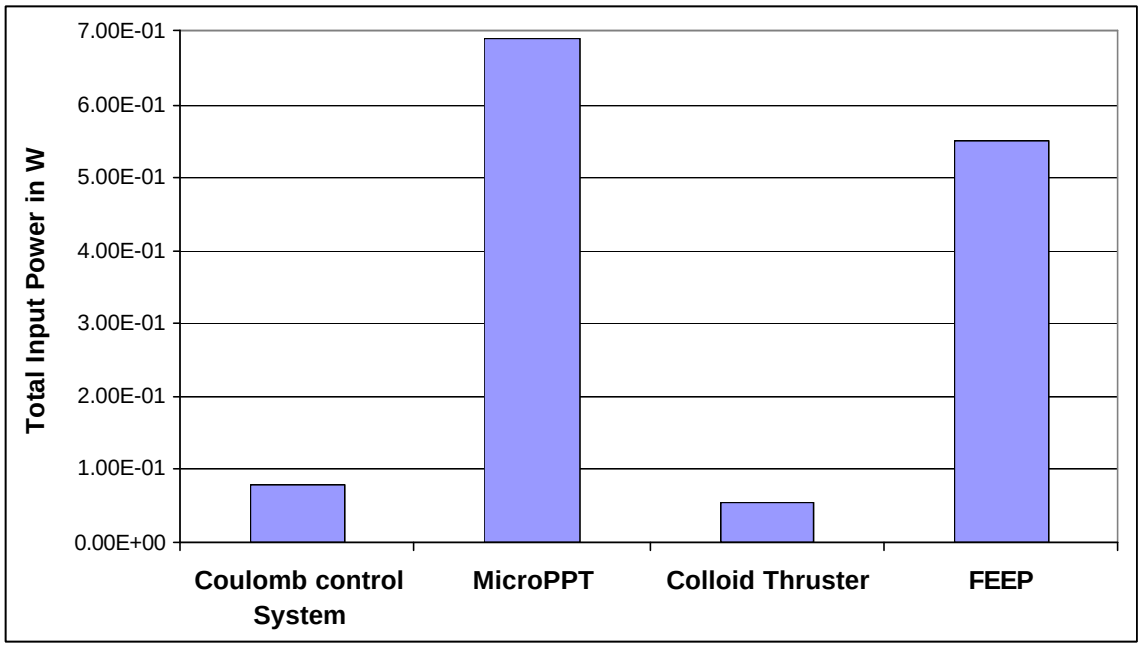

Figure 6-8. Total input power required to maintain formation for Coulomb control and three EP technologies (3 Spacecraft Formation – Case 'c').

6.2.2. Earth Orbiting Five Spacecraft Formation

In an incremental step towards considering practical interferometry formations, a five-spacecraft formation comprised of four collectors and one central combiner was studied and is shown schematically in Figure 6-9. Using techniques identical to those of Section 6.2.1, the Coulomb vehicle parameters for all five spacecraft have been calculated and presented in Table 6-5. Table 6-6 compares the formation performance characteristics using Coulomb control and three canonical EP technologies. The total system input power and propellant masses are compared in Figure 6-10 and Figure 6-11.

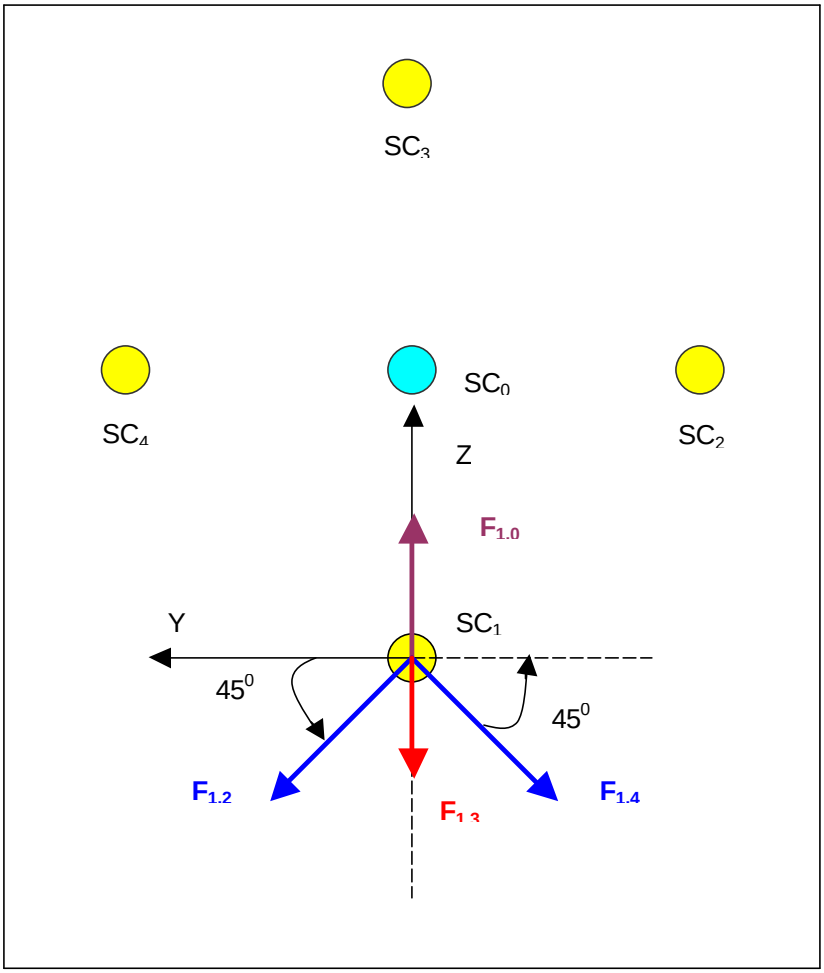

Figure 6-9. Coulomb forces exerted on SC_1 by other 4 spacecraft in five-vehicle Earth-orbiting formation (diagram not drawn to the scale).

Parameters	**Numerical Values For Spacecraft**				
	SC_0	**SC_1**	**SC_2**	**SC_3**	**SC_4**
q_i C	5.32×10^{-7}	-4.40×10^{-7}	-8.81×10^{-7}	-4.40×10^{-7}	-8.81×10^{-7}
r_i m	5.0000×10^{-1}	5.0000×10^{-1}	5.0000×10^{-1}	5.0000×10^{-1}	5.0000×10^{-1}
I_e A	-3.34×10^{-5}	3.07×10^{-5}	3.14×10^{-5}	3.07×10^{-5}	3.14×10^{-5}
$V_{(SC)i}$ V	9.56×10^{3}	-7.92×10^{3}	-1.58×10^{4}	-7.92×10^{3}	-1.58×10^{4}
$P_{(input)i}$ W	3.19×10^{-1}	2.43×10^{-1}	4.98×10^{-1}	2.43×10^{-1}	4.98×10^{-1}
$\dot{m}_i$ kg/s	1.90×10^{-16}	3.20×10^{-13}	3.28×10^{-13}	3.20×10^{-13}	3.28×10^{-13}
F_i N	0.00	7.98×10^{-6}	8.98×10^{-9}	7.98×10^{-6}	8.98×10^{-9}

Table 6-5. Vehicle parameters calculated for the five-spacecraft Earth-orbiting formation.

Parameters	Coulomb Control	MicroPPT	Colloid Thrusters	FEEP
1.Specific Impulse Isp s	1.26×10^{6}	5×10^{2}	1×10^{3}	1×10^{4}
2.Efficiency ? %	N/A	2.6×10^{-2}	6.5×10^{-1}	6.5×10^{-1}
3.Fuel Mass for 10 Years m_{fuel} kg	4.09×10^{-4}	1.03	5.13×10^{-1}	5.13×10^{-2}
4.Input Power P_{input} W	1.80	3.02	2.41×10^{-1}	2.41
5.Specific Mass ß kg/W	1.65×10^{-1}	3.70×10^{-1}	2.16×10^{-1}	1.13×10^{-1}
6.Inert Mass m_{inert} kg	2.97×10^{-1}	1.12	5.21×10^{-2}	2.71×10^{-1}
7.Total Mass m_{Total} kg	2.98×10^{-1}	2.14	5.66×10^{-1}	3.23×10^{-1}

Table 6-6. Comparison between Coulomb control system and three EP technologies for five-spacecraft Earth-orbiting formation.

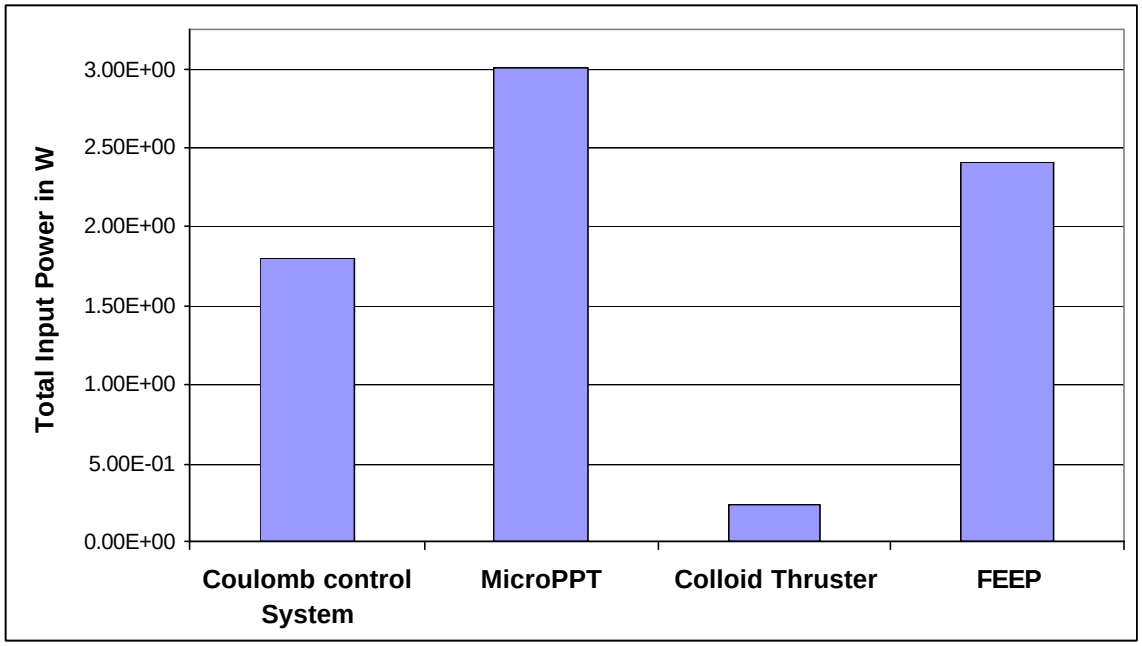

Figure 6-10. Total propulsion system input power required for five-spacecraft formation (Square In-Planer) using Coulomb control and EP systems.

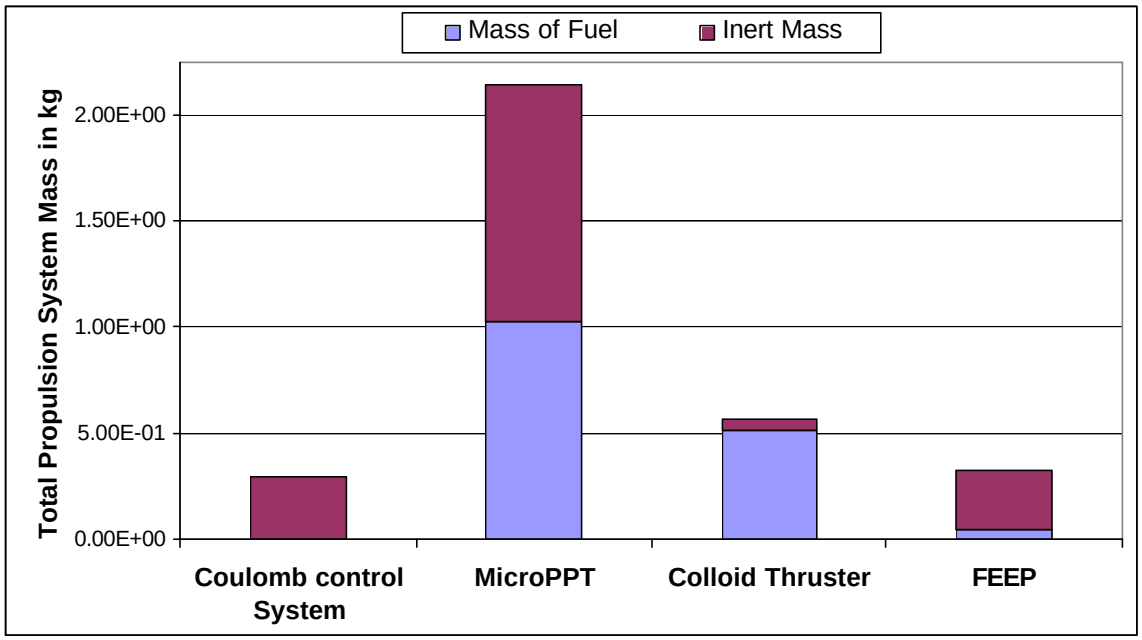

Figure 6-11. Total propulsion system mass for five-spacecraft formation (Square In-Planer) using Coulomb control and EP systems.

6.2.3. Earth Orbiting Six Spacecraft Formation

The dynamics of a realistic interferometry formation, namely that of a five-vehicle Cornwell array with a central combiner, was studied. Using the "optimal" equilibrium formation potentials (charges) calculated in the numerical solution along with the average GEO plasma conditions, the Coulomb vehicle parameters have been calculated and are presented in Table 6-7, with Table 6-8 comparing the Coulomb control system with three canonical EP technologies for the same formation. A graphical comparison of total system power and propulsion system mass is presented in Figure 6-12 and Figure 6-13.

Parameters	Numerical Values For Spacecrafts					
	SC_0	SC_1	SC_2	SC_3	SC_4	SC_5
q_i C	9.42	-5.80×10^{-7}	-8.41×10^{-7}	-7.04×10^{-7}	-7.04×10^{-7}	-8.41×10^{-7}
r_i m	5.00×10^{-1}	5.00×10^{-1}	5.00×10^{-1}	5.00×10^{-1}	5.00×10^{-1}	5.00×10^{-1}
I_e A	-5.61×10^{-5}	3.10×10^{-5}	3.14×10^{-5}	3.12×10^{-5}	3.12×10^{-5}	3.14×10^{-5}
$V_{(SC)i}$ V	1.69×10^{4}	-1.04×10^{4}	-1.51×10^{4}	-1.27×10^{4}	-1.27×10^{4}	-1.51×10^{4}
$P_{(input)i}$ W	9.51×10^{-1}	3.23×10^{-1}	4.74×10^{-1}	3.95×10^{-1}	3.95×10^{-1}	4.74×10^{-1}
$\dot{m}_i$ kg/s	3.19×10^{-16}	3.24×10^{-13}	3.28×10^{-13}	3.26×10^{-13}	3.26×10^{-13}	3.28×10^{-13}
F_i N	3.10×10^{-6}	5.39×10^{-6}	8.59×10^{-6}	4.80×10^{-6}	4.81×10^{-6}	8.59×10^{-6}

Table 6-7. Vehicle parameters calculated for the five-spacecraft Cornwell array with central combiner.

Parameters	Coulomb Control	MicroPPT	Colloid Thrusters	FEEP
1.Specific Impulse Isp s	2.21×10^{6}	5×10^{2}	1×10^{3}	1×10^{4}
2.Efficiency ? %	N/A	2.6×10^{-2}	6.5×10^{-1}	6.5×10^{-1}
3.Fuel Mass for 10 Years m_{fuel} kg	5.14×10^{-4}	2.27	1.13	1.13×10^{-1}
4.Input Power P_{input} W	3.01	6.66	5.33×10^{-1}	5.33
5.Specific Mass ß kg/W	1.65×10^{-1}	3.70×10^{-1}	2.16×10^{-1}	1.13×10^{-1}
6.Inert Mass m_{inert} kg	4.97×10^{-1}	2.47	1.15×10^{-1}	5.99×10^{-1}
7.Total Mass m_{Total} kg	4.98×10^{-1}	4.73	1.25	7.13×10^{-1}

Table 6-8. . Comparison between Coulomb control system and three EP technologies for five-spacecraft Cornwell array with central combiner.

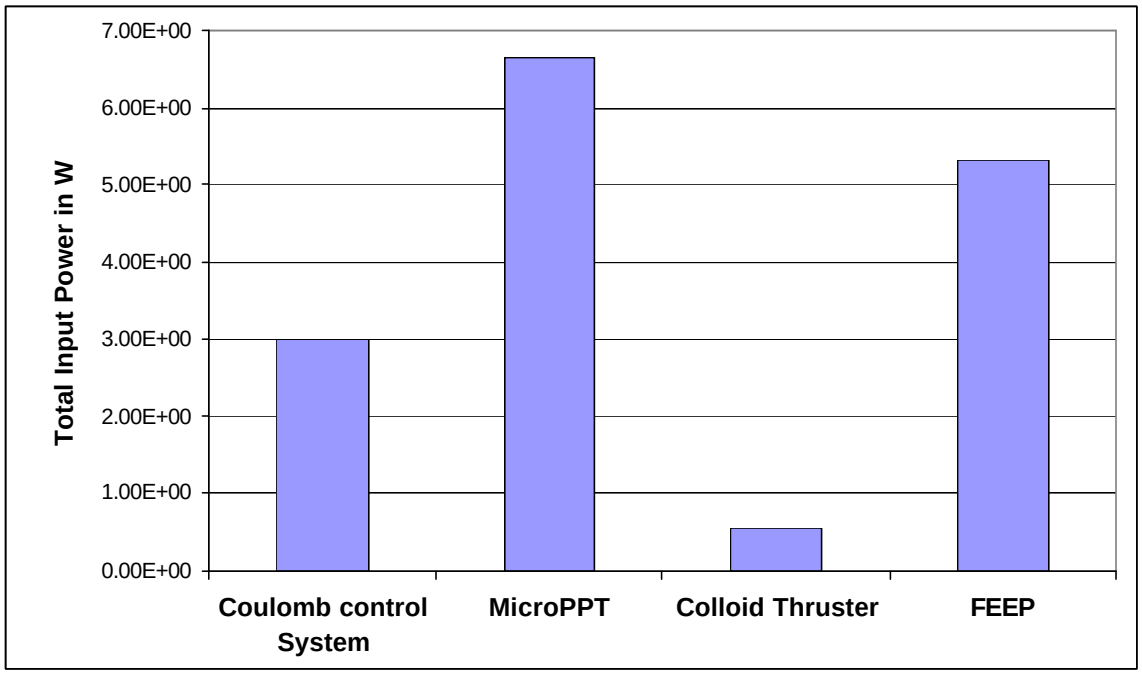

Figure 6-12. Total propulsion system input power for formation calculated for five-spacecraft Cornwell array with central combiner.

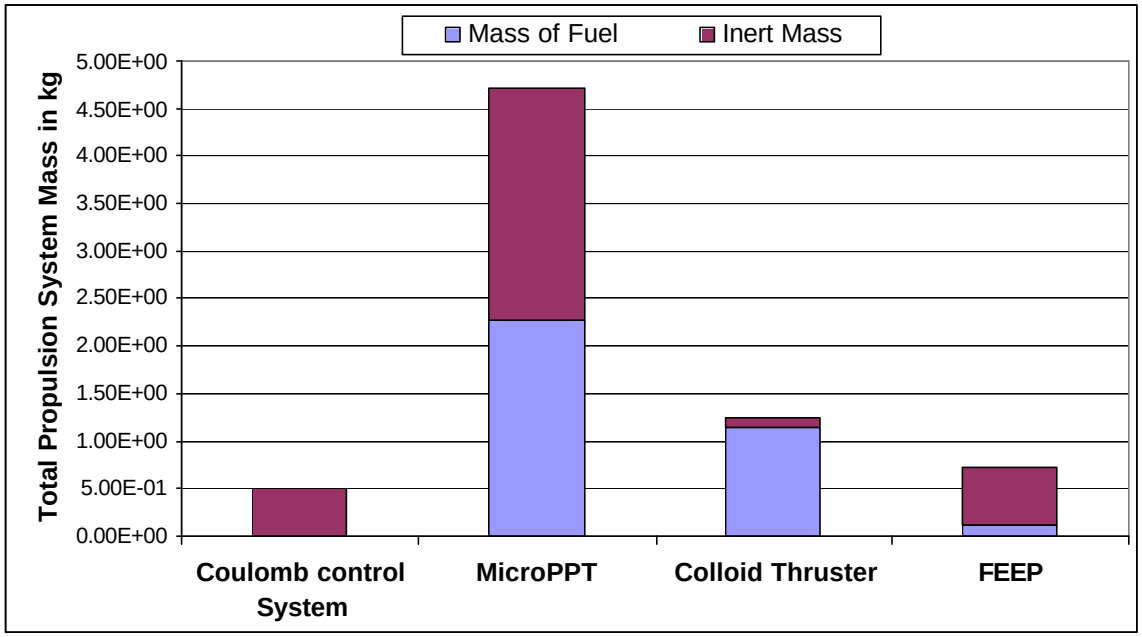

Figure 6-13. Total propulsion system mass required to maintain formation for five-vehicle Cornwell array with central combiner.

6.2.4. *Five-vehicle rotating linear array (TPF)*

The rotating array was chosen for its similarity to the geometric configuration of the Terrestrial Planet Finder Mission, for which considerable design analyses have been performed. The TPF formation is assumed to operate outside of a significant gravity well in conditions resembling those found at one of the Earth-Sun Lagrange points. Formation forces are required to hold the collector vehicles in a circular orbit about the central combiner. In Section 3 equilibrium solutions were found for three different rotation rates: 200 hrs/revolution, 20 hrs/revolution, and 2 hrs/revolution. Since the slowest rotation rate considered is impractical for a real mission, the two larger rotation rates are analyzed in this section. Vehicle parameters and system comparisons can be found in Table 6-9, Table 6-10, Figure 6-14, and Figure 6-15 for the 20 hrs/revolution rate, with Table 6-11, Table 6-12, Figure 6-16, and Figure 6-17 representing the 2 hrs/revolution rate.

Parameters	**Numerical Values For Spacecraft**				
	SC_0	**SC_1**	**SC_2**	**SC_3**	**SC_4**
q_i C	4.15×10^{-8}	-1.69×10^{-6}	1.69×10^{-6}	-1.69×10^{-6}	1.69×10^{-6}
r_i m	0.50	0.50	0.50	0.50	0.50
I_e A	-6.18×10^{-6}	3.20×10^{-5}	-9.75×10^{-5}	3.20×10^{-5}	-9.75×10^{-5}
$V_{(SC)i}$ V	7.46×10^{2}	-3.03×10^{4}	3.03×10^{4}	-3.03×10^{4}	3.03×10^{4}
$P_{(input)i}$ W	4.61×10^{-3}	9.72×10^{-1}	2.96	9.72×10^{-1}	2.96
$\dot{m}_i$ kg/s	3.51×10^{-17}	3.34×10^{-13}	5.54×10^{-16}	3.34×10^{-13}	5.54×10^{-16}
F_i N	0.00	5.78×10^{-5}	3.85×10^{-5}	5.78×10^{-5}	3.85×10^{-5}

Table 6-9. Vehicle parameters calculated for TPF-like rotating five spacecraft linear formation with rotation rate of 0.1×(p/3600) rev/sec.

Parameters	**Coulomb Control**	**MicroPPT**	**Colloid Thrusters**	**FEEP**
1.Specific Impulse Isp s	2.93×10^{7}	5×10^{2}	1×10^{3}	1×10^{4}
2.Efficiency ? %	N/A	2.6×10^{-2}	6.5×10^{-1}	6.5×10^{-1}
3.Fuel Mass for 10 Years m_{fuel} kg	2.11×10^{-4}	1.24×10^{1}	6.19	6.19×10^{-1}
4.Input Power P_{input} W	7.86	3.63×10^{1}	2.91	2.91×10^{1}
5.Specific Mass ß kg/W	1.65×10^{-1}	3.70×10^{-1}	2.16×10^{-1}	1.13×10^{-1}
6.Inert Mass m_{inert} kg	1.30	1.35×10^{1}	6.29×10^{-1}	3.27
7.Total Mass m_{Total} kg	1.30	2.58×10^{1}	6.82	3.89

Table 6-10. Comparison Between Coulomb Control System and Electric Propulsion Systems for TPF-like rotating five spacecraft linear formation with rotation rate of 0.1×(p/3600) rev/sec.

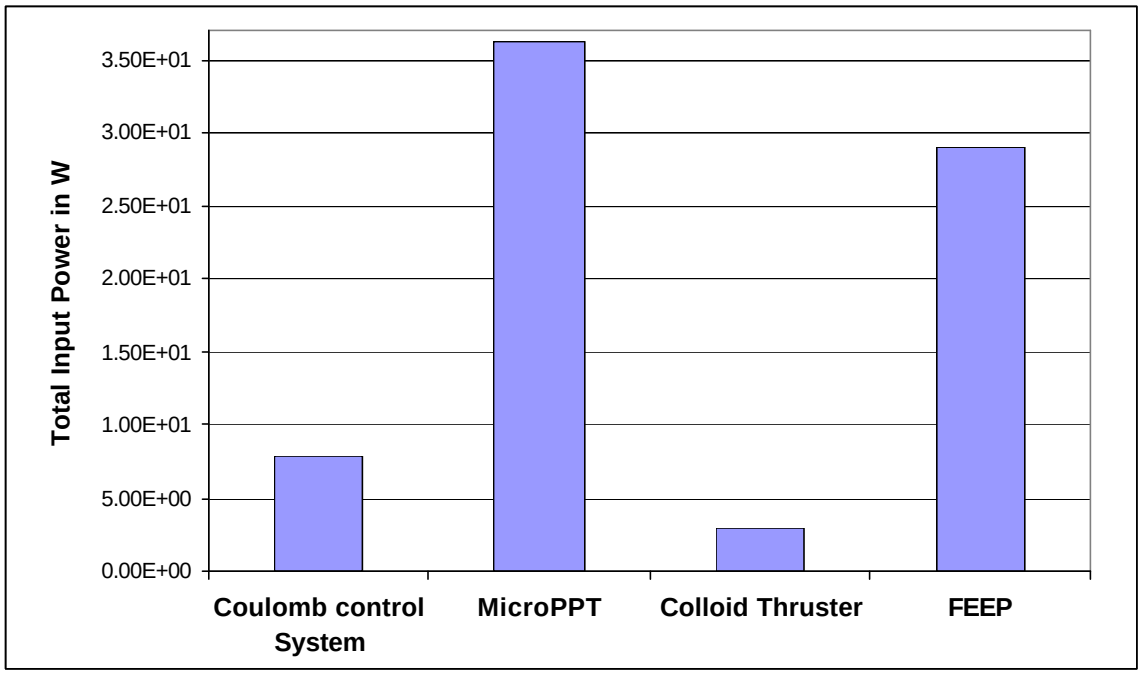

Figure 6-14. Total propulsion system input power for TPF-like rotating five spacecraft linear formation with rotation rate of 0.1×(p/3600) rev/sec.

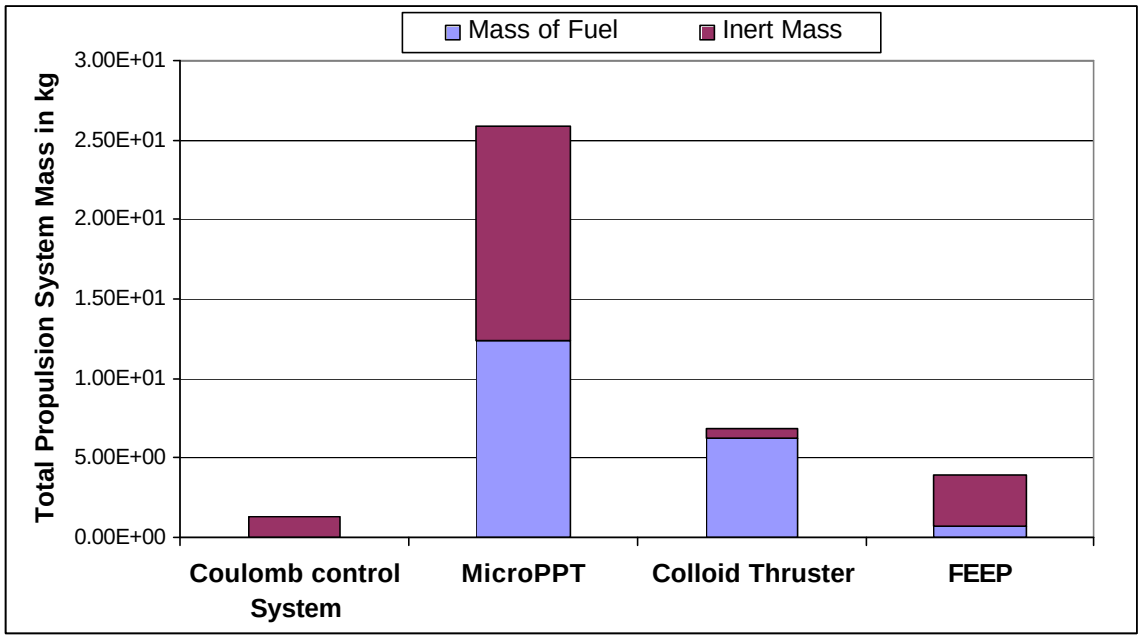

Figure 6-15. Total propulsion system mass required to maintain TPF-like rotating five-spacecraft linear array with rotation rate of 0.1×(p/3600) rev/sec.

Parameters	Numerical Values For Spacecraft				
	SC_0	SC_1	SC_2	SC_3	SC_4
q_i C	4.15×10^{-7}	-1.69×10^{-5}	1.69×10^{-5}	-1.69×10^{-5}	1.69×10^{-5}
r_i m	0.50	0.50	0.50	0.50	0.50
I_e A	-2.69×10^{-5}	3.74×10^{-5}	-9.39×10^{-4}	3.74×10^{-5}	-9.39×10^{-4}
$V_{(SC)i}$ V	7.46×10^{3}	-3.03×10^{5}	3.03×10^{5}	-3.03×10^{5}	3.03×10^{5}
$P_{(input)i}$ W	2.01×10^{-1}	1.13×10^{1}	2.85×10^{2}	1.13×10^{1}	2.85×10^{2}
$\dot{m}_i$ kg/s	1.53×10^{-16}	3.90×10^{-13}	5.34×10^{-15}	3.90×10^{-13}	5.34×10^{-15}
F_i N	0.00	5.78×10^{-3}	3.85×10^{-3}	5.78×10^{-3}	3.85×10^{-3}

Table 6-11. Vehicle parameters calculated for TPF-like rotating five spacecraft linear formation with rotation rate of 1×(p/3600) rev/sec.

Parameters	Coulomb Control	MicroPPT	Colloid Thrusters	FEEP
1.Specific Impulse Isp s	2.48×10^{9}	5×10^{2}	1×10^{3}	1×10^{4}
2.Efficiency ? %	N/A	2.6×10^{-2}	6.5×10^{-1}	6.5×10^{-1}
3.Fuel Mass for 10 Years m_{fuel} kg	2.49×10^{-4}	1.24×10^{3}	6.19×10^{2}	6.19×10^{1}
4.Input Power P_{input} W	5.93×10^{2}	3.63×10^{3}	2.91×10^{2}	2.91×10^{3}
5.Specific Mass ß kg/W	1.65×10^{-1}	3.70×10^{-1}	2.16×10^{-1}	1.13×10^{-1}
6.Inert Mass m_{inert} kg	9.78×10^{1}	1.35×10^{3}	6.28×10^{1}	3.27×10^{2}
7.Total Mass m_{Total} kg	9.78×10^{1}	2.58×10^{3}	6.82×10^{2}	3.89×10^{2}

Table 6-12. Comparison Between Coulomb Control System and Electric Propulsion Systems for TPF-like rotating five spacecraft linear formation with rotation rate of 1×(p/3600) rev/sec.

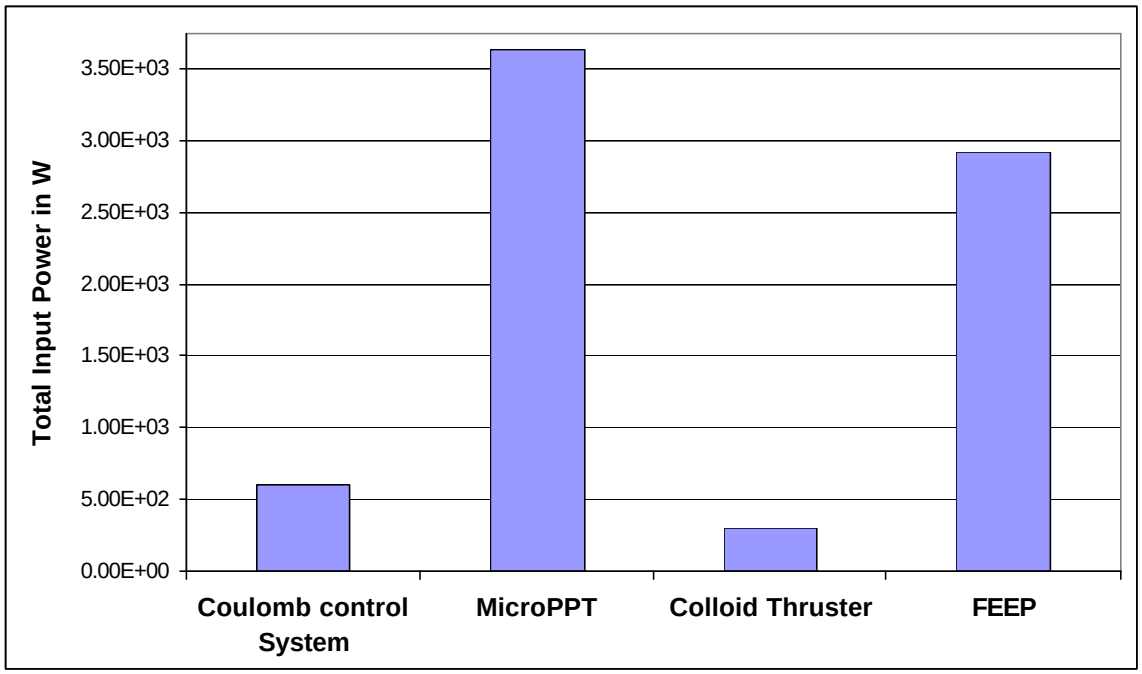

Figure 6-16. Total propulsion system input power for TPF-like rotating five spacecraft linear formation with rotation rate of 1×(p/3600) rev/sec.

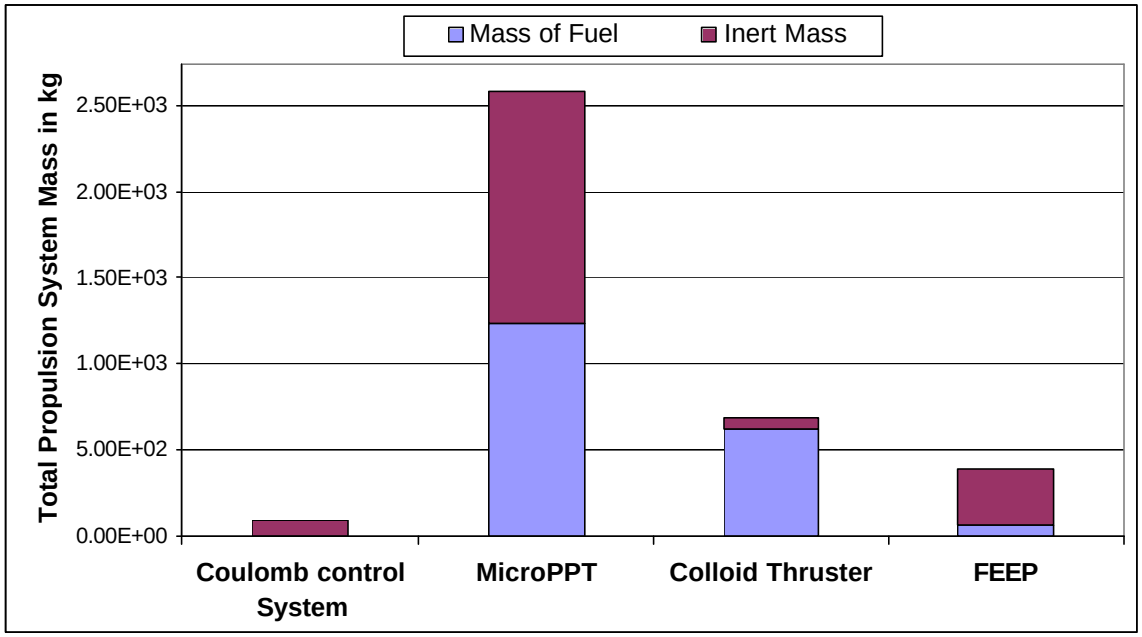

Figure 6-17. Total propulsion system mass required to maintain TPF-like rotating five-spacecraft linear array with rotation rate of 1×(p/3600) rev/sec.

[45] M. Martinez-Sanchez, Pollard J. E., "Spacecraft Electric Propulsion – An Overview", Journal of Propulsion and Power, Vol. 14, No. 5, September-October 1998, pp.688-699.

[46] Rayburn C., Campbell R., Hoskins W., Cassady R., "AIAA 2000-3256, Development of a Micro Pulsed Plasma Thruster for the Dawgstar Nanosatellite.", 36th Joint Propulsion Conference & Exhibit, 16-29 July 2000, Huntsville, Alabama.

[47] Jeffery G. Reichbach, Raymond J. Sedwick, Manuel Martinez-Sanchez, "Micropropulsion System Selection for Precision Flying Satellites",SERC #1-01, January 2001.

7. Conclusions

7.1. Coulomb Control: Strengths and Weaknesses

The Coulomb control concept appears very promising form the results of Phase I investigations. When reconciled with future NASA mission needs, Coulomb control seems to lend itself best to sparse-aperture imaging using separated spacecraft interferometry for rapidly changing targets (full, instantaneous u-v coverage). For the close formations necessary to achieve full, instantaneous u-v coverage, the Coulomb concept is capable of generating control forces which easily exceed the gravity perturbations that must be overcome to maintain a static formation of vehicles occupying non-Keplerian orbital slots. In summary, three aspects of Coulomb control can be stated as strengths of the concept:

1. A Coulomb control system will greatly reduce the propulsion system mass necessary to maintain close formations when compared to other thrusting technologies
2. A spacecraft formation flying under Coulomb control will not produce a local contaminating environment due to caustic propellant exhaust
3. The continuous and rapid nature with which the control force can be varied between vehicles should allow greater precision in close formations

The Coulomb forces can be generated with as little as a few milli-Watts of spacecraft power, producing specific impulse values as large as 10^{13} seconds. Hence, the Coulomb control concept is nearly propellantless. Furthermore, the Coulomb control forces can be rapidly dithered over a continuous range on a time scale of milliseconds using spacecraft power much less than 1 Watt. Concept development requires no new devices or technology. In fact, vehicle charge control such as that proposed in this study has been demonstrated in the 1970's on spacecraft such as SCATHA. The revolutionary nature of the concept relies on an innovative integration of existing technologies and simple physical principles.

In an effort to compare the Coulomb control system with traditional EP thrusters for close formation flying, four representative formation geometries were analyzed in the context of a 10-year mission with representative small spacecraft. For all formations considered, the total propulsion system mass was less for Coulomb control than for competing EP systems, with the required input power competitive or less for each mission. The propulsion system mass comparison is summarized in Table 7-1. This table shows the percentage of the EP propulsion system mass that can be saved using a Coulomb system according to

Eqn. 7-1
$$Savings = \frac{m_{EP} - m_{Coul}}{m_{EP}} \times 100\%$$

where m_{Coul} is the total propulsion system mass using Coulomb control and m_{EP} is the total propulsion system mass using the EP thruster.

Formation Geometry	Savings over Micro PPT	Savings over Colloid thruster	Savings over FEEP thruster
3-spacecraft case 'a'	96%	84%	73%
3-spacecraft case 'c'	97%	90%	82%
5-spacecraft Earth orbiting	86%	48%	8%
6-spacecraft Earth orbiting (Cornwell)	90%	60%	30%
5-spacecraft rotating (20 hrs/rev)	95%	81%	67%
5-spacecraft rotating (2 hrs/rev)	96%	86%	75%

Table 7-1. Propulsion system mass savings incurred using Coulomb control system in place of traditional EP thrusters for formation-keeping.

Traditional EP systems considered for close formation flying are either pulsed or of limited throttleability. Thus, formation control systems utilizing such thrusters will operate according to a "thrust-coast-thrust" sequence in an effort to maintain position. The Coulomb force is continuously adjustable on a rapid time scale. Such continual dithering will work well in a robust active-feedback control system and should enable much smaller position errors than competing thrusters.

Although many facets of the Coulomb concept are attractive, it is not without its faults. As identified thus far, two main weaknesses are found for a Coulomb control system:

1. A Coulomb control system is limited to close formation flying in plasma environments characterized by Debye lengths greater than inter-vehicle separation.
2. Generating usable control forces requires charging spacecraft to intimidating absolute voltages. Great care must be taken in vehicle design to prevent differential charging and instrument damage due to electrostatic discharge.

Many formation missions currently under consideration are planned for low-earth orbit (LEO) environments. As demonstrated in Section 2, the Debye length in LEO is on the order of centimeters and, thus, is far too small to permit a Coulomb formation. There are, however, many missions of interest for astronomical imaging where it would be beneficial to place the inteferometry formation in much higher orbits where the Debye length is amenable to generating control forces. For instance, a visible GEO Earth imager with resolution of 1 m at the earth's surface could be performed using a formation such as the six-spacecraft Cornwell geometry considered here. Additionally, the five-spacecraft rotating array emulating the TPF mission is slated for either Earth-trailing heliocentric orbit or a halo orbit about L2. Such conditions would allow integration of a Coulomb control system. Even for such formations, however, the Coulomb control forces become negligible for separations much greater than, say, 50 m. It is apparent that more traditional thrusters would be necessary for formation keeping over larger distances.

Contemporary spacecraft designers shudder to think about purposely charging a spacecraft to multi-kilovolt potentials. Although absolute charging alone is not hazardous, techniques must be used to ensure even charging over the vehicle. Historical data has shown that electrostatic discharges induced by differential vehicle charging can cripple on-board systems. Many spacecraft, including the International Space Station, are equipped with charge emission systems with the sole purpose of dispersing excess vehicle charge to maintain a potential close to zero and, thus, avoid both absolute and differential charging. Permitting a spacecraft to attain large absolute voltage, while minimizing differential charging, is a task that must be addressed at the vehicle design stage. Methods including multiple conductive ground paths and careful material selection can be used to mitigate differential charging. Such methods are beyond the scope of this proof-of-concept research and have not been addressed here. Vehicle design implications will undoubtedly be formidable. The deleterious effects of differential spacecraft charging have left a deep impression on the spacecraft design industry through a few catastrophic failures. Applying the Coulomb control concept to practical vehicles will involve much more than retro-fitting a charge-control subsystem on a traditionally designed satellite, however, the benefits suggested in this Phase I research may justify research into mitigating differential charging while allowing absolute charging.

7.2. Integrating Coulomb Control

In analyzing the strengths and weaknesses of Coulomb control and traditional EP thrusters, it becomes apparent that where one technology is least attractive, the other technology excels. For example, thrusters are well-suited to formation-keeping over large spacecraft separations where Coulomb control is of limited use and position tolerances may be greater. In turn, a Coulomb system is very well suited for fine formation control in tight swarms, where the contamination and "thrust-coast-thrust" nature of EP devices makes them a poor choice. A synergistic control system utilizing both Coulomb control and EP thrusters would seem to provide excellent performance. The thrusters would allow both large-baseline interferometry and coarse corrections to disturbances in the formation, while a hand-off to the Coulomb system would allow fine station-keeping in tight arrays.

7.3. Concept Development Cost

Although it is difficult to accurately estimate the cost of developing a new concept such as Coulomb control, an attempt will be made here to provide rough guidelines. The subsystems involved in the proposed concept are not new technologies. In fact, electron and ion emitters have routinely been used on spacecraft and in the laboratory for vehicle charge control. The novelty of the formation-controlling concept proposed in this document lies in the innovative integration of existing technologies. Since no major new technologies must be developed prior to a proof-of-concept flight

experiment, it seems reasonable that the demonstration mission cost can be estimated based on existing space mission design guidelines.

7.3.1. Mission Cost Model

Each spacecraft within the formation can be envisioned as two separate subsystems: a payload to perform the interferometry mission and a spacecraft bus containing guidance, navigation, control, telemetry, and other vital functions. With this rough delineation in vehicle hardware, the total mission cost can be divided into the four categories payload cost, spacecraft bus cost, launch cost, and mission operations cost. These four categories are shown graphically in Figure 7-1.

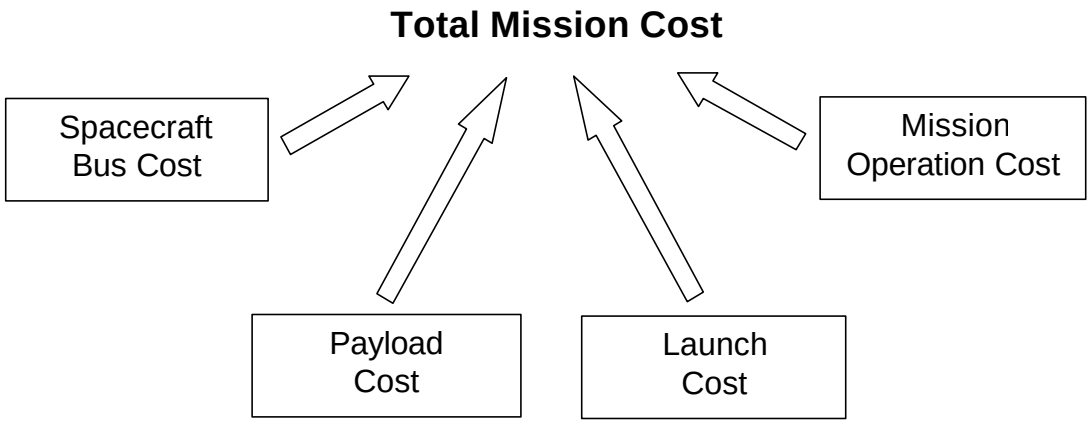

Figure 7-1. Categories considered in development mission cost estimate.

7.3.2. Payload Cost

No historical cost database exists for separated spacecraft interferometry payloads since space-qualified optics for interferometery have never been flown. The payload costs estimated for this report come from a NASA Deep Space 3 (DS3) costing workshop held in March, 1997, and reported in Ref. 48. Based on bids from various companies, the workshop concluded that a single space-qualified interferometer collector payload would cost $8.45M and a space-qualified combiner for a two-collector interferometer would cost $16.9M. For lack of better method, the combiner cost figure is assumed to scale with the number of collectors in a multi-collector array according to $8.45M-per-collector.

In the DS3 workshop, the operational requirements of the optics payloads were estimated. It was assumed that a single collector payload would require 35W of power, and weigh in at 23 kg. A combiner was assumed to require 135W of power and constitute a mass of 58 kg. Each spacecraft was assumed to weigh approximately 150 kg,

implying a bus mass around 100 kg. These requirements will be used to estimate the launch mass and spacecraft bus requirements.

7.3.3. Spacecraft Bus Cost

The cost of the spacecraft bus, including designing, manufacturing, integrating, and testing each bus, can be estimated from historical databases known as cost estimation relationships (CERs). The two most commonly used CERs are the U.S. Air Force's Unmanned Spacecraft Cost Model (USCM) and the Aerospace Corporation's Small Satellite Cost Model (SSCM). The SSCM is valid for satellites approximately 500 kg or less and is based on 1990's technology.[49] Such a small satellite model is ideal for evaluating a separated spacecraft interferometry array.

Over twenty separate CERs exist in the SCCM. Using the CERs, independent estimates of total bus cost can be made from subsystem requirements. For instance, a total bus cost estimate can be obtained from the solar array area required of the payload, while a separate estimate can be obtained from the number of on-board thrusters required. With the preliminary mission definitions included in this document, the most relevant CERs applicable concern the spacecraft bus mass and end-of-life (EOL) power required of the vehicles. The two CERs are shown in Table 7-2.

Independent Variable (x)	**Applicable Range**	**CER for Total Bus Cost (FY94$M)**	**Standard Error (s) (FY94$M)**
Bus dry mass (kg)	20-400	$C=0.704+0.0235x^{1.261}$	3.33
EOL Power (W)	5-440	$C=0.507+1.55x^{0.452}$	6.20

Table 7-2. Cost estimating relationships used to calculate spacecraft bus cost.

Assuming a 100 kg spacecraft bus dry mass yields a bus cost estimate of $8.5M. An independent estimate can be made from the EOL power required. Assuming the vehicle will need at least 135W of power at completion of the mission, the bus cost is estimated at $14.7M. These two estimates can be combined into a weighted average based on their standard errors according to

Eqn. 7-2

$$Cost = \frac{C_1 / s_1^2 + C_2 / s_2^2}{1/s_1^2 + 1/s_2^2}$$

Which yields a bus cost estimate of FY94$9.6M.

7.3.4. Launch Cost

The launch cost of a given mission is almost exclusively dependent upon the spacecraft mass. It is certain that a Coulomb control development mission would be flown as a U.S. government science payload, thus only U.S. domestic launch vehicles are considered in this analysis. The launch cost of each of the formations considered in this study will be estimated separately.

The three-spacecraft formation consists of two collectors and one combiner vehicle. The total mass of the system will then be 1) two collector payloads at 23 kg, 2) one combiner payload at 58 kg, and 3) three spacecraft busses at 100 kg for a total system payload of 404 kg. The launch cost to GEO is estimated from a NASA online cost calculating tool.[50] The most likely vehicle for such a mission is found to be a Taurus, which is capable of delivering 514 kg to GTO at a launch cost of $21M-$26M (FY94).

The five-spacecraft Earth orbiting array has also been analyzed in the context of GEO orbit deployment. The total mass for the five-vehicle formation will be 1) four collector payloads at 23 kg, 2) one combiner payload at 58 kg, and 3) five spacecraft busses at 100 kg equaling 650 kg throw mass. The most likely U.S. launcher for this payload is the Taurus XL/S Star 37FM with 736 kg capability to GTO at a launch cost of $23M-$26M (FY94).

The six-spacecraft (five-aperture Cornwell array) formation in GEO orbit will require 1) five collector payloads at 23 kg, 2) one combiner payload at 58 kg, and 3) six spacecraft busses at 100 kg for a total launch mass of 773 kg. Inspecting the available U.S. launch vehicles leads to selection of the Delta II Model 7920, with 1,240 kg capability to GTO at a launch cost of $49M-$60M (FY94).

The five-spacecraft rotating array was chosen to resemble the NASA TPF mission. This mission is not intended for Earth orbit, instead it is aimed at operation at the stable Earth-Sun Lagrange point (L2). The total mass for this mission is assumed to be identical to that of the five-spacecraft Earth orbiting formation, namely 650kg. Launch cost for this mission has been estimated using information from the Boeing corporation on the Delta II family capabilities.[51] For launch to a halo orbit about L2, it is found that the Model 7325 is capable of placing 687 kg into the appropriate orbit for a launch cost of roughly $44M.

7.3.5. Operations Cost

The operations cost for the proposed missions is estimated from results of the DS3 costing workshop of March 1997. For the three-vehicle DS3 mission, it was estimated that three hours-per-day of tracking time through the NASA Deep Space Network would be required to support the mission, costing $4.2M over a six-month mission. It seems reasonable to extrapolate this figure to a value of $233k-per spacecraft-per month operating cost. With this guiding figure, the operating costs associated with the formations under consideration here are presented in Table 7-3.

Formation Geometry	Estimated Operating Cost for 6-month Mission
3-spacecraft Earth orbiting	$4.2M
5-spacecraft Earth orbiting	$7M
6-spacecraft Earth orbiting	$8.4M
5-spacecraft rotating at L2 point	$7M

Table 7-3. Estimated mission operation cost for formations under study in this report.

7.3.6. Total Estimated Mission Costs

Although of limited accuracy, the sub-system cost estimates for payload, spacecraft bus, launch, and operations can be used to estimate the total cost of each of the formations considered in this study. Estimates assume a six-month mission duration for evaluation of the Coulomb concept. Total mission costs are detailed in

Formation Geometry	Payload Cost (M)	Spacecraft Bus Cost (M)	Launch Cost (M)	Operations Cost (M)	Total Cost (M)
3-spacecraft Earth orbiting	$33.8	$28.8	$26	$4.2	$92.8
5-spacecraft Earth orbiting	$42.3	$48	$26	$7	$123.3
6-spacecraft Earth orbiting	$50.7	$57.6	$60	$8.4	$176.7
5-spacecraft rotating at L2 point	$42.3	$48	$44	$7	$141.3

Table 7-4. Estimated total mission costs for formation geometries under consideration in this study.

[48] Jilla, C.D., Separated Spacecraft Interferometry-System Architecture Design and Optimization, Master's Thesis, Dept. of Aeronautics and Astronautics, Massachusetts Institute of Technology, Feb. 1999.

[49] Bearden, D.A., Reducing Space Mission Cost, Editors J.R. Wertz and W.J. Larson, *Chapter 8.2: The Aerospace Corporation Small Satellite Cost Model*, Microcosm Press, Torrance, CA, 1996.

[50] http://www.jsc.nasa.gov/bu2/models.htm

[51] Boeing. Delta II Family of Launch Vehicles. Boeing Informational Brochure. 1997.